Department of Civil Engineering

University of Cape Town

October 2008

DYNAMIC MODELING AND VIBRATION CONTROL OF HIGH-VOLTAGE OVERHEAD TRANSMISSION LINES.

BY

JAMESON JOSEPH MTANGA

SUPERVISOR: PROF A. ZINGONI

A Thesis submitted to the University of Cape Town in partial fulfillment of the requirements for the degree of Master of Science in Engineering.

DECLARATION

I know the meaning of plagiarism and declare that this thesis is my own unaided work, both in conception and execution, and that apart from the normal guidance of my supervisors; I have received no assistance except from the one acknowledged.

Name: Jameson. J. Mtanga

Signature: _____

Year: October 2008

ACKNOWLEDGEMENTS

Firstly, I would like to give thanks and Praise to God, for the strength and wisdom to carry out this work.

I also would like to extend my heartfelt gratitude to my supervisors, Prof. Alphose Zingoni and Ass. Prof. Pilate Moyo, for their continued guidance and support.

Appreciation is also extended to my colleagues in the Structural Mechanics Research group, as well as all the staff in the Department of Civil Engineering for their support and companionship throughout the course of the study.

Consistent advice on numerical modeling from my colleague Mr Sifiso P. Nhleko is greatly recognized.

Further appreciation is given to Mr Pravesh Moodley from the Vibration and Research Centre at the University of KwaZulu Natal (VRTC-UKZN) for his support with most of the literature and with a tour around their conductor testing facility.

Lastly, but not least I would like to thank my family and my fellow brethren at Forward in Faith Ministries International-Cape Town City Assembly for their spiritual support. This thesis would not appear without their consistent encouragement, love and peace.

ABSTRACT

The problem of the dynamic behavior of overhead power transmission lines under wind and other excitations is an important one, since it allows an optimal design and positioning of vibration dampers for the cables. Excessive sway and oscillation of power lines need to be avoided, as they can lead to damage of the lines and power interruptions. The relatively high flexibility of the cables, coupled with the large spans and large sags involved, make the dynamic response of the system highly nonlinear.

In this study, we numerically investigate the damped free-vibration response of systems of cables of particularly large spans (120, 200 and 400m). For each span, spacers which act as damper devices are placed along the cable. The stiffness of the system is very much a function of the pre-tensioning (and hence the sag) given to the cables. To take into account the effect of this on the system vibration response, five different sag to span ratios are considered in this study, mainly at 15, 20 25, 30 and 40% of the Ultimate cable Tensile Strength (UTS). For each case, the first five (5) natural frequencies and mode shapes are computed, for three different spacer stiffness levels and damping coefficients. The results of the investigation are compared with findings from literature.

A cost function is developed to obtain the number of viscoelastic passive dampers needed to achieve maximum reduction of the cost function due to an excitation force and thereby obtaining the optimal placement. For a system of optimally placed spacers the overall reduction of 60% of the cost function is generally noted for the structure, this also was in agreement with the findings obtained from the numerical analysis. It is also noted from the parametric study conducted that as the stiffness of the spacer device is increased, the damping capabilities are reduced. The results obtained show a general increase in the frequency of vibration as the tension in the conductor is increased. Thus, for optimum spacer placement along the line, the results obtained are useful to the transmission line design engineer for the specific spans considered.

TABLE OF CONTENTS

DECLARATION ..... **I**
ACKNOWLEDGEMENTS ..... **II**
ABSTRACT ..... **III**
LIST OF FIGURES ..... **VII**
LIST OF TABLES ..... **X**
NOMENCLETURE ..... **XI**
1.0 INTRODUCTION: **1**
2.0 LITERATURE REVIEW: **3**
2.1 Wind Induced Vibrations 3
2.1.1 Types of Excitations 3
2.1.2 Effects of wind on transmission structures 5
2.1.3 Trends in Design Practice 9
2.2 Vibration dampers 10
2.2.1 Types of dampers 11
2.2.1.1 Spiral vibration dampers 12
2.2.1.2 Multi frequency Stockbridge vibration dampers 13
2.2.1.3 Torsional Damper Detuners 13
2.2.1.4 Spacer dampers and rigid spacers 14
2.3 Use of vibration indicators and analysers 15
2.3.1 Technology Research and Investigation Vibration Activity Indicator (TRIVAI) 15
2.3.2 Pavica device 16
2.3.3 Fibre optic Bragg grating Sensors 16
2.4 Current Practices in damper usage 17
2.5 Cable Dynamics-A Historical Review 19
2.5.1 Modeling of overhead cables 21
2.5.1.1 Analytical modeling of overhead cables 21
2.5.1.2 Finite Element modeling of overhead cables 27
2.5.1.3 An Experimental modeling of overhead cables 34
2.6 Existing Problems 42
2.7 Literature Review Summary and Conclusion 44

3.0 STATEMENT OF RESEARCH PROBLEM: **45**
3.1 Research Statement 45
3.2 Research Objectives 45
3.3 Methodology 45
4.0 THEORY OF DISTRIBUTED-PARAMETER SYSTEMS: **46**
4.1 Formulating the Cable Equation of Motion 46
4.2 Modes and Natural Frequencies 49
4.2.1 Applying boundary conditions: 50
4.2.2 The Out-of-Plane Motion 52
4.2.3 The In-Plane motion 53
4.2.4 Extension to Cables with Deep Profile. 60
4.2.5 The Linearized Dynamic Response of a Flat-Sag Suspended Cable. 63
4.2.6 The Nonlinear Theory of Vibration in a Taut Flat Cable 67
4.3 Analysis Example 71
4.4 Conclusion 72
5.0 SOLUTION OF TRANSCENDENTAL EIGENVALUE PROBLEM IN BUNDLED CONDUCTORS: **73**
5.1 Modeling of a bundled conductor with spacer dampers 73
5.2 Solution of the eigenvalue problem 80
5.2.1 Determinant Search Method 81
5.2.2 Alternate Approach 81
5.2.3 Continuous Spectrum Approach 82
5.3 Conclusion 84
6.0 FINITE ELEMENT MODELING: **85**
6.1 Introduction 85
6.1.1 Element Type 86
6.1.2 Updated Lagrangian Formulation 86
6.1.2.1 Truss Element derivation 86
6.1.3 Finite element model of a passive viscoelastic damper element with node connections 94
6.1.4 Solution of the non-linear FEM formulation 96
6.2 The Modeling process 99
6.3 Validation of Model 102

6.3.1 Benchmark Model 102
6.3.2 Bundled System Validation 104
6.3.2.1 Cable Properties 104
6.3.2.2 Analysis Example 105
6.3.2.3 Results and Discussions 106
6.3.3 Conclusion 111
6.4 Parametric Study 112
6.8 Conclusion 123
7.0 DISCUSSION OF RESULTS 124
7.1 Explaining the excited modes 124
7.2 Explaining the cost functions 135
7.3 Conclusion 136
8.0 MAIN CONCLUSION AND DESIGN RECOMMENDATIONS 137
9.0 RECOMMENDATIONS FOR FUTURE WORK 139
REFERENCES: 140
APPENDIX A 145

LIST OF FIGURES

Figure 1.0-1, Illustration of Stockbridge type damper with cross-sectional view of damper weight. 1
Figure 2.1-1, Illustration of the effect of vortex shedding. 4
Figure 2.1-2, Illustration of fatigue on cable strands. 4
Figure 2.1-3, Flat terrain, no obstacles to the wind: Minimum turbulence. 6
Figure 2.1-4, Cultivated country, flat terrain with few, small obstacles to the wind: Low turbulence. 6
Figure 2.1-5, Undulated terrain, forest: High turbulence 7
Figure 2.2-1, Spiral vibration damper. 11
Figure 2.2-2, Stockbridge vibration damper. 11
Figure 2.2-3, Quad-bundle spacer damper. 12
Figure 2.2-4, Torsional Damper Detuner attached to conductor. 14
Figure 2.2-5, Rigid and semi-rigid spacers 14
Figure 2.3-1, TRIVAI device showing no vibration. 15
Figure 2.3-2, Pavica device attached to conductor. 16
Figure 2.4-1, Results of galloping event. 18
Figure 2.5-1, Sagged Cable. 25
Figure 2.5-2, Beam element in the absolute nodal coordinate formulation. 29
Figure 2.5-3, Stockbridge damper with simplified model in form of damped spring mass system. 34
Figure 2.5-4, Density spectra with mean wind speed U about 16m/s: (a) laminar flow, axial load cell; (b) laminar flow, drag force cell; (c) turbulent flow, axial load cell; (d) turbulent flow, drag force cell. 40
Figure 4.1-1, A model of a vibrating cable. 47
Figure 4.2-1, Longitudinal components and associated vertical components (in-dotted) of the two antisymmetric in-plane modes, (Irvine , 1981). 55
Figure 4.2-2, General dimensionless curves for the first four natural frequencies of a flat-sag suspended cable: (a) first symmetric in-plane mode, (b) first antisymmetric in-plane mode, (c) second symmetric in-plane mode, (d) second antisymmetric in-plane mode, (Irvine, 1981). 57

Figure 4.2-3, Graphical solution for first nonzero root of equation (4.2-27), (Irvine, 1981). 58
Figure 4.2-4, Possible forms for the vertical component of the first symmetric in-plane mode, (Irvine,1981). 59
Figure 4.2-5, Ramberg and Griffin's comparison of the present theory with the experimental results of Richardson for a particular model cable, (Irvine, 1981). 60
Figure 5.1-1, Schematic diagram of quad bundle attached with N similar spacer dampers. 73
Figure 5.1-2, Forces acting at the clamp of a spacer damper. 74
Figure 5.2-1, Obtained frequencies from different methods (24.5-26.5Hz). 84
Figure 6.1-1, Truss element arrangement. *87*
Figure 6.1-2, Truss Element deformations. *87*
Figure 6.1-3, New truss position with incremental coordinates. *88*
Figure 6.1-4, Body aligned coordinate form. *88*
Figure 6.1- 5, Lumped mass presentation of a passive viscoelastic damper element *94*
Figure 6.1-6, Finite element for the viscoelastic damper element. *96*
Figure 6.2-1, A load being applied to the cables. 100
Figure 6.2-2, Cables with a mesh of 0.5m. 101
Figure 6.2-3, A dual cable arrangement with three spacers showing 101
Figure 6.3-1, First four mode shapes as obtained with Abaqus. 103
Figure 6.3-2, Definition problem of a system of two conductors. 106
Figure 6.3-3, Response Ratio vs Modes (40% UTS). 106
Figure 6.3-4, Response Ratio vs Modes (20% UTS). 107
Figure 6.3-5, Response Ratio vs Modes (15% UTS). 108
Figure 6.3-6, Response Ratio vs Modes (25% UTS). 108
Figure 6.3-7, Response Ratio vs Modes (30% UTS). 109
Figure 6.4-1, 15% UTS-Response Ratio vs Modes. 113
Figure 6.4-2, 20% UTS-Response Ratio vs Modes. 113
Figure 6.4-3, 120m Dual Line-Mode 3. 114
Figure 6.4-4, 120m Dual Line-Mode 4. 114
Figure 6.4-5, Comparison of analytical and numerical results. 119
Figure 6.4-6, Comparison of theoretical and experimental results of the cable natural frequencies (Wenji Wu, 2006). 120

Figure 7.1-1, Plot of Response Ratio vs Tension-Mode 5 (K=5kN/m-Single Spacer). 124
Figure 7.1-2, Plot of Response Ratio vs Tension-Mode 5 (K=10kN/m-Single Spacer). 125
Figure 7.1-3, Plot of Response Ratio vs Tension-Mode 5 (K=15kN/m-Single Spacer). 125
Figure 7.1-4, Plot of Response Ratio vs Tension-Mode 2 (K=5kN/m-Single Spacer). 126
Figure 7.1-5, Plot of Response Ratio vs Tension-Mode 2 (K=10kN/m-Single Spacer). 126
Figure 7.1-6, Plot of Response Ratio vs Tension-Mode 2 (K=15kN/m-Single Spacer). 127
Figure 7.1-7, Two spacers represented in the output visualization-Mode 2 (200m-span). 127
Figure 7.1-8, Plot of Response Ratio vs Tension-Mode 3 (K=5kN/m-Two Spacers). 128
Figure 7.1-9, Plot of Response Ratio vs Tension-Mode 3 (K=10kN/m-Two Spacers). 128
Figure 7.1-10, Plot of Response Ratio vs Tension-Mode 3 (K=15kN/m-Two Spacers). 129
Figure 7.1-11, Plot of Response Ratio vs Tension-Mode 4 (K=5kN/m-Three Spacers). 130
Figure 7.1-12, Plot of Response Ratio vs Tension-Mode 4 (K=10kN/m-Three Spacers). 130
Figure 7.1-13, Plot of Response Ratio vs Tension-Mode 4 (K=15kN/m-Three Spacers). 131
Figure 7.1-14, Plot of Response Ratio vs Tension-Mode 5 (K=5kN/m-Three Spacers). 131
Figure 7.1-15, Plot of Response Ratio vs Tension-Mode 5 (K=10kN/m-Three Spacers). 132
Figure 7.1-16, Plot of Response Ratio vs Tension-Mode 5 (K=15kN/m-Three Spacers). 132
Figure 7.1-17, Plot of frequency against number of dampers (K=5kN/m, C=0.2kNs/m) 133
Figure 7.1-18, Plot of frequency against number of dampers (K=10kN/m, C=0.6kNs/m) 134
Figure 7.1-19, Plot of frequency against number of dampers (K=15kN/m, C=0.8kNs/m) 134

LIST OF TABLES

Table 2.1-1, Influence of surface roughness on parameters relating to wind structure near the ground (Belloli M, et. al, 2006). 7
Table 2.5-1, First three natural frequencies of cable motion. 42
Table 4.2-1, *Natural frequencies of the first eight symmetric in-plane modes as a function of* λ^2. 57
Table 4.2-2, Frequencies of the first five in-plane modes of a deep-sag cable. 63
Table 4.2-3, Participation factors for additional tension for the first eight symmetric in-plane modes as a function of λ^2. 67
Table 4.2-4, Cable Natural Frequencies for tension of 15, 20, 25, 30 and 40% UTS. 72
Table 6.3-1, Violin string parameters. 102
Table 6.3-2, Calibration of Model, violin string problem. 103
Table 6.3-3, Cable properties (source: ASTM B 232-see Appendix A). 104
Table 6.3-4, Summary of the different cases considered. 105
Table 6.3-5, Optimisation results for different constraints on number of dampers 110
Table 6.4-1, Parameters considered in the study. 112
Table 6.4-2, 120m-Modes changing with stiffness change. 115
Table 6.4-3, 200m-Modes changing with stiffness change. 115
Table 6.4-4, 400m-Modes changing with stiffness change. 117
Table 6.4-5, Comparison of Natural frequencies at 15% UTS. 117
Table 6.4-6, Comparison of Natural frequencies at 20% UTS. 118
Table 6.4-7, Comparison of Natural frequencies at 25% UTS. 118
Table 6.4-8, Comparison of Natural frequencies at 30% UTS. 118
Table 6.4-9, Comparison of Natural frequencies at 40% UTS. 119
Table 6.4-10, Optimization results for different constraints on number of dampers-120m span. 120
Table 6.4-11, Optimization results for different constraints on number of dampers-200m span 121
Table 6.4-12, Optimization results for different constraints on number of dampers-400m span 122
Table 7.1-1, Frequencies obtained with three spacers @ 20% UTS. 133

NOMENCLETURE

f	frequency
F_r	Froude number
v	wind speed
d	conductor diameter
H	horizontal component of the static cable tension
m	cable mass per unit length
c	damping force per unit length
ε_m^i	Green-Lagrangian strain tensor
y	the vertical in-plane component of motion
v	longitudinal in-plane component of motion
τ	dynamic part of the total cable tension
E	cable Young's Modulus
I	second moment of area of cable cross section about its neutral axis
u	lateral deflection of taut cable
r	vibration mode of taut cable
ρ	cable density
A	cross-sectional area
L	cable span
l	cable length
$\mathbf{n}$	vector of discrete 0/1 design variables
s	arc length co-ordinate
u	longitudinal in-plane component of motion
w	out-of-plane component of motion
T	cable tensile load
λ^2	Irvine's parameter
M	mass matrix
K	global stiffness matrix
x	displacement

$\dot{x}$	velocity
$\ddot{x}$	acceleration
C	damping matrix
$X(t)$	cable displacement vector relative to reference configuration.
$F(t)$	external excitation force
t	time
$F_c(\omega)$	complex frequency component of the Fourier transform of the load vector
$X_c(\omega)$	complex frequency component of the response displacement vector
T^i	kinetic energy
J^i	matrix of displacement
U^i	strain energy
d	cable diameter
$A_{m_\Omega,v_\Omega}, B_{m_\Omega,v_\Omega}$	Integration constants for v_Ω^{th} subspan in m_Ω^{th} direction
$\mathbf{F}_n(t)$	Force vector for n^{th} spacer damper (a function of time)
$\mathbf{J}(s_\Omega)$	Transcendental system matrix
M_Ω	Number of arms in the spacer damper
N	Number of spacer dampers attached
P	force in truss
T_{m_Ω}	Conductor tension in m_Ω direction
$\mathbf{Z}(\mathrm{s}_\Omega)$	Complex impedance matrix of spacer damper $\in C^{4M_\Omega x 4M_\Omega}$
$\mathbf{a}$	Vector containing integration constants
b	Half spacer damper clamp width $+ l_{char}$
c_{m_Ω}	Wave velocity in m_Ω^{th} direction
l_{char}	Characteristic length of the conductor
l_n	Location of n^{th} spacer damper
m_Ω	Directional plane of the conductor vibration
s_Ω	Complex eigenvalue of the system $(= -\delta + i\omega)$
$w_{m_\Omega,v_\Omega}(x_{v_\Omega}, t)$	Transverse displacement of v_Ω^{th} subspan in m_Ω^{th} direction (a function of

	local space coordinate x_v and time t)
$\dot{\mathbf{w}}_n(t)$	Velocity vector for n^{th} spacer damper (a function of time)
Δl_{v_Ω}	Span length of v_Ω^{th} sub-span
δ	Real part of complex eigenvalue s_Ω
δ_{ij}	Kronecker delta function
λ	Wave length.
ω	Imaginary part of complex eigenvalue s_Ω
b_D	damping factor
c_D	stiffness factor
m_D	mass of damper
ρ_a	density of air
C_D	cable's drag coefficient
V	mean wind speed

1.0 INTRODUCTION:

Vibrations of electrical overhead transmission line conductors have been investigated for many decades. Special dampers, e.g., Stockbridge dampers or spacer dampers are mounted on the conductors to suppress these vibrations, which may otherwise lead to the fatigue failure of lines at the points of high strain values (see figure 1.0-1 below). Simulations are routinely carried out in order to estimate the vibration levels, to determine the need of dampers, and to optimize their locations and the impedances (J. Vecchiarelli 1998).

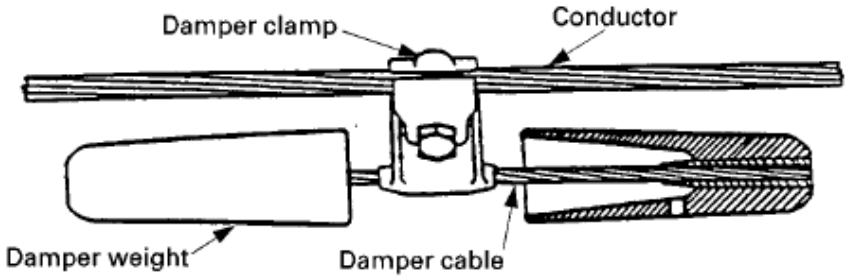

Figure 1.0-1, Illustration of Stockbridge type damper with cross-sectional view of damper weight.

Vortex-induced or aeolian vibrations (alternate formation of vortices in the downstream wake of the cable) of overhead electrical transmission lines, also referred to as conductors, are very common and can lead to fatigue damage. These vibrations are usually caused by winds ranging in velocity from 1 to 7 m/s and can occur at frequencies from 3 to 150 Hz with peak-to-peak displacement amplitudes of up to one conductor diameter (EPRI, 1979 in J. Vecchiarelli 1998). In conventional transmission line systems, one or more Stockbridge type dampers may be attached to a conductor in an effort to suppress aeolian vibrations.

Sub-conductor oscillations are caused by wake induced flutter as leeward conductors move in the non-conservative force field generated by the wakes of windward neighbours. These vibrations are usually caused by winds ranging in velocity from 6 to 20 m/s and frequencies of between 0.5 to 3 Hz. Unlike in Aeolian vibrations Stockbridge dampers are completely ineffective against sub-conductor oscillation and the only way to minimize these is by span wise positioning of the

(essentially non-dissipative) spacers (A. Simpson et. al. 1983). This study will look at the rational design and positioning of spacer-dampers by developing the analytical and computational basis of these.

Although the influence and the tendency of the particular parameters on and towards the vibration intensity are known, factors as surroundings, environmental influence etc., on the construction of new overhead lines, are decisive for the routing of line and accordingly for the line configuration. The margins for an appropriate choice of line parameters in consideration of the mechanical and dynamic characteristics is only small or even nill.

The vibration intensity is directly influenced by the conductor stress and thus by the tensile force of conductor via the self-damping of conductor. This fact has been known for a long time (Nefzger. J 1933 in Mocks, 1984). Nevertheless, it is unfeasible on the current conditions to realize a line being practically free of vibrations, only via the tensile stress. For the rest, an excess importance often is attributed to the magnitude of 'tensile stresses' and its influence on the vibration intensity. The tensile stress is only one of the above mentioned various parameters whereof the terrain factor at the current state of knowledge appears to be more important than the tensile stress.
Vibration dampers have been employed for decades in Germany and abroad to suppress conductor vibrations whereof the Stockbridge vibration dampers (Stockbridge 1925 in Mocks 1984) worldwide have been used most numerously.

This study will investigate the effect of vibrations on transmission lines and review the existing trends in design as seen later in the literature review. A brief review of vibration dampers is given; also the theoretical models of conductor behavior will be considered and validated with finite element models (FEM).

2.0 LITERATURE REVIEW:

Recent developments are now seeing the need of electrifying different parts of countries and this gives rise to transmission lines being erected in all sorts of terrains and environmental conditions in order to curb the demand for this precious and valuable resource.

It is known that accidents with transmission lines in strong winds keep happening, and in many instances it is not known why the transmission lines have failed. It has not been proved how these structures really behave in strong winds or which parameters are of major importance in their response to wind loading, and this includes the consideration of their dynamic properties. The reason for this is that both full-scale measurements during strong winds and aero elastic wind tunnel tests of meaningful sections of transmission lines are both fraught with significant problems (Davenport et. al., 1998). This chapter looks at some of the above issues and seeks to discuss them and to a greater extent offer a basis for research.

2.1 Wind Induced Vibrations

2.1.1 Types of Excitations

Aeolian vibration (*vortex shedding*): alternate formation of vortices in the downstream wake of the cable (M. Belloli et. al., 2006).

It is an unsteady flow that takes place in special flow velocities (according to the size and shape of the cylindrical body). In this flow vortices are created at the back of the body and periodically from both sides of the body. Vortex shedding is caused when air flows past the conductor, the illustration shown in figure (2.1-1) below. The airflow past the conductor creates alternating low-pressure vortexes on the downwind side of the conductor. The conductor will tend to move toward the low-pressure zone.

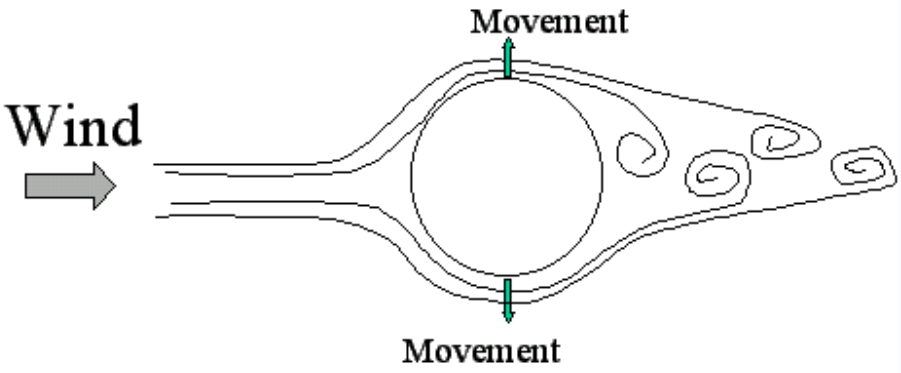

Figure 2.1-1, Illustration of the effect of vortex shedding (Wikipedia, 2006).

Eventually, if the frequency of vortex shedding matches the resonant frequency of the conductor, the conductor will begin to resonate and the conductor's movement can become self-sustaining. (Wikipedia, Dec 2006)

This has serious implications i.e. fatigue failure of the conductor strands at the suspension clamps and or collapsing of the supporting structure, figure (2.1-2) below.

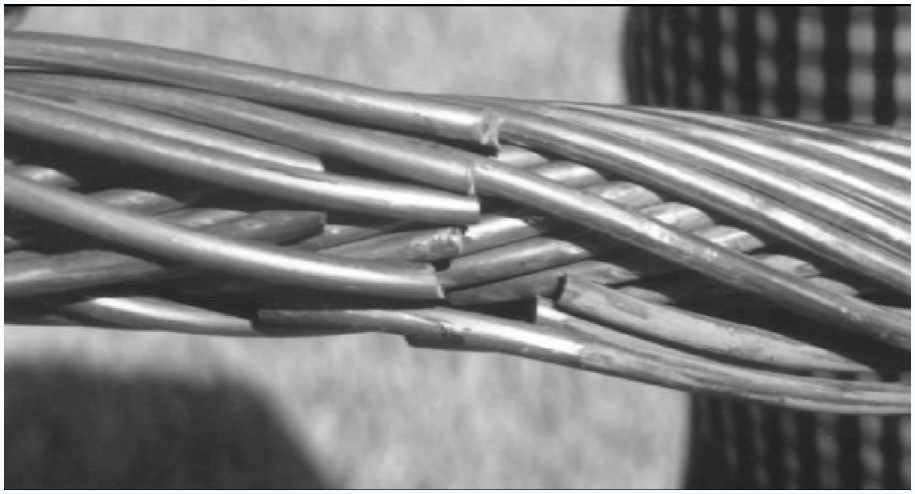

Figure 2.1-2, Illustration of fatigue on cable strands (Belloli, 2006).

Vortex shedding was one of the causes proposed for the failure of the Tacoma Narrows Bridge in 1940, but was rejected because the frequency of the vortex shedding did not match that of the bridge. (Wikipedia, Dec 2006).

Other vibrations common in electrical conductors are buffeting and galloping. Vibration due to turbulent wind (*buffeting*): mainly related to forcing effects due to variation of wind speed both

in module and direction. Aeroelastic instability (*galloping*): irregular shape, due to ice deposits *(ice galloping)*, can lead to modification of cable profile, and unstable oscillations can occur. Wake induced vibrations (*bundle galloping*): typical for cables fitted in bundles grouped in 2, 3, 4, or more formation), as occurs in electrical power transmission lines (Belloli M, et. al, 2006).

Galloping affects conductors with an unstable profile in a strong perpendicular wind. The unstable profile of a conductor is usually caused by ice build up on the conductor or non-circular conductor profiles. The main characteristic of galloping is large amplitude motion, upto the sag of the span, predominantly in the vertical plane at a frequency of around 0.5Hz. The effects of galloping on a transmission line is dependent upon the severity and duration of the galloping event but typical problems are phase to phase flashover causing outages and arcing damage to conductors, loosening of tower bolts and damage to suspension and tension clamps, spacers and vibration dampers and, in some critical cases, structural damage to towers.

2.1.2 Effects of wind on transmission structures

Wind mean speed and direction vary with the region and with the period of the year. It is important to know the mean wind speed and direction distribution typical of the region were the structure will be placed in order to evaluate the risk for the different types of wind excited vibrations and take the suitable countermeasures.
Wind can be treated as an ergodic and stationary quantity, and the related statistics (mean value, rms value, frequency distribution) can be defined on a specific site.

Wind turbulence depends on the mean wind speed, it decreases with increasing speed. It also depends on the type of surrounding, open terrain, flat surfaces, suburban area, forest, etc. The term turbulence index is the ration between speed variation and mean wind speed.

Pictures shown below give a detailed insight of the characteristics of terrains.

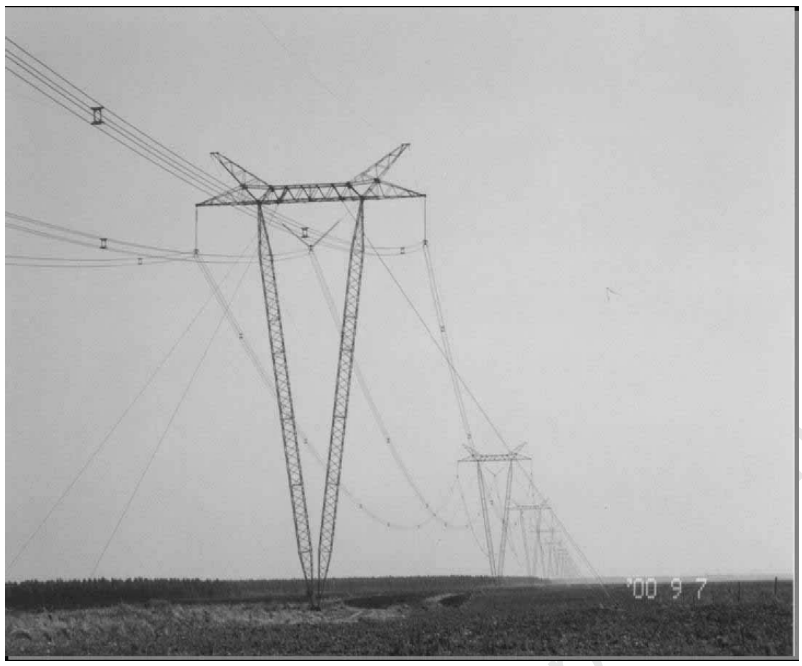

Figure 2.1-3, Flat terrain, no obstacles to the wind: Minimum turbulence (Belloli, 2006).

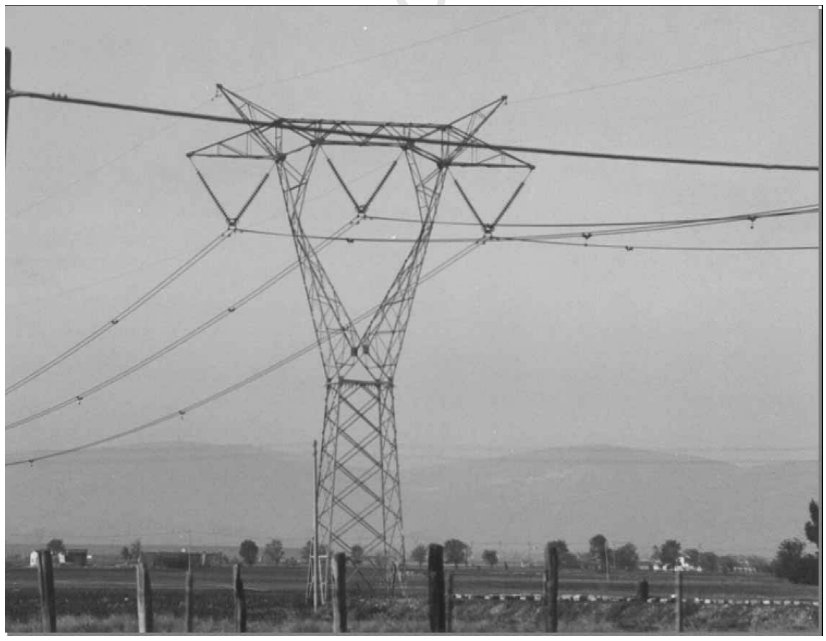

Figure 2.1-4, Cultivated country, flat terrain with few, small obstacles to the wind: Low turbulence (Belloli, 2006)

Figure 2.1-5, Undulated terrain, forest: High turbulence(Belloli, 2006)

Table (2.1-1) below, gives values of the coefficients showing the influence of surface roughness on parameters relating to wind structures near the ground.

Table 2.1-1, Influence of surface roughness on parameters relating to wind structure near the ground (Belloli M, et. al, 2006).

Type of Surface	Power law exponent	Gradient height (m)	Drag coefficient
Open terrain with very few obstacles: e.g open grass or farmland with a few trees, hedgerows and other barriers etc.; low islands of inland lakes or desert	0.16	82	0.005
Terrain uniformly covered with obstacles 1m-2m in height e.g residential surbabs; small field with bushes; trees and hedges.	0.28	118	0.015
Terrain with large and irregular objects; centers of large cities; very broken country with many windbreaks of tall trees.	0.40	156	0.050

Conductor vibration is most commonly wind-induced. Vibration damages the conductors and line hardware at clamping points (conductor fretting). Damage can occur rapidly but in general takes several years to cause failure. Lines constructed perpendicular to prevailing winds over flat

terrain or large masses of water with no wind protection from hills or mountains are highly susceptible to vibration.

As discussed earlier there are three types of wind induced vibration: aeolian vibration, subspan oscillation and conductor galloping.

Aeolian vibration affecting all types of conductors and cable suspended in the air, and with wind speeds of 1 m/s to 7 m/s. The frequency of the vibration can be calculated using the "Strouhal" relationship: (G. Stanford, 2003)

$$f = 0.85\frac{v}{d} \tag{2.1-1}$$

Where f = frequency (Hz)

v = wind speed (m/s)

d = conductor diameter (m)

Most researchers on this topic have taken the frequency of aeolian vibration as occurring between 3 to 150 Hz.

On the other hand subspan oscillation only affects lines with bundled conductors. Wind speeds of 4 m/s to 18 m/s can cause vertical, horizontal or torsional subspan vibration. Subspan vibration is complex because the conductors in the bundle are subject not only to direct wind forces but also the turbulent wake of the wind that has already passed preceding conductors in the bundle (G. Stanford, 2003). It is this type of vibration which needs the use of spacer dampers to absorb the energy from the conductor and they have to be properly deployed along the span in order to be useful as damping devices.

2.1.3 Trends in Design Practice

The continued demand of supplying electricity to different consumers has led to the idea of bundled conductors being adapted as the most efficient means, timeously and inevitably cost wise. Research by Du Plessis (1994) showed a cost benefit of R10 million per annum on his study on triple Pelican bundled conductors.

The behavior and movement of a suspended conductor is the most unpredictable variable in distribution line design. Since complex equations are used to calculate the conductor sag curve, some simplifications and approximations are used. The approximation cause small errors. The accuracy of the final calculated results decreases as the curve equation is simplified (US DoA, 2003). The need to span larger distances due to complexity in terrains complicates this curved shape of the suspended cable called the catenary.

The ruling span theory (US DoA, 2003) is used to simplify calculations in design. It assumes that the supports are at equal elevations, since the span lengths are large compared to the difference in elevation of supports, it also assumes the horizontal tension is constant throughout the stringing section since variations in span lengths will not be great enough to cause a measurable difference in the horizontal tension between any two adjacent spans and the final assumption is that the uneven spans are replaced by a series of unequal spans such that the total length of the conductor and the horizontal tension of the section is unchanged.

However some of these spans become so large and make the cable susceptible to vibrations, and the supporting towers so tall that their stiffness is reduced and they are easily excitable.

P. J. Ryle (1931) gives areas that one should seriously consider when designing transmission lines. He lists these as, conductor diameter, conductor tension and wind speeds. Evidently and as also been outline by many authors the aspect of conductor diameter is very crucial because the energy received from the wind per metre is proportional to the surface area presented and therefore the conductor diameter. Also the need to span large crossings leads to the choice of the large conductors due to stiffness considerations. Zetterholm (1960) also suggests that research conducted by an international Italian based organization CIGRE has reviewed that the influence

of the ratio of conductor weight per metre to diameter must be taken into account and that generally it is assumed that susceptibility to vibration will increase as this ratio decreases which agrees with Ryle's suggestions.

In as far as the conductor tension is concerned Ryle suggests that at high tensions the greater will be the forces required to overcome the static friction between strands and the smaller the critical radius of curvature, so that inter-strand damping will not set in until larger amplitudes are reached. Also the loop length will be greater for higher tensions and the critical radius of curvature will also be reached with large amplitudes. However Zetterholm also suggests that if the static strength of a conductor allows a certain stringing tension, the risk of vibration enforces the use of a lower tension, this also minimizes on creep failures.

Ryle suggests that the loop length is short with high winds so that the critical radius of curvature is reached before the amplitude is appreciable. Similarly he argues that at low winds, air damping and elastic hysteresis are significant in comparison with the very small energy receivable from the wind. Zetterholm in the same manor argues that the fact that overhead conductors do not, in most cases, vibrate at higher velocities of wind has been attributed to turbulence and that the self-damping characteristics of conductors at high frequencies, at the normal low stringing tensions used by many power companies, have certainly played a part, too, in suppressing vibration at these higher velocities.

To curb for the above effects special devices are deployed onto the transmission lines and serve to some extent to reduce the effects of some of these above aspects. The following section will discuss in detail the nature and behavior of these devices.

2.2 Vibration dampers

Damping devices are designed for the sole purpose of minimizing vibrations that damage conductors. The degree of protection required on a specific line depends on a number of factors. These include line design, temperature, conductor tension, conductor type, conductor joints, line fittings, exposure to wind flow in terms of direction and velocity, topography and vibration

history. It is important that these physical conditions and some general recommendations are taken into account when assessing if a line requires vibration dampers (G. Stanford, 2003). For the above reasons researchers are busy looking for the best solution to help combat the above problems. Some of the different types of dampers that research has come up with are dealt with in the following section. The word damper and spacers are used interchangeably to mean the same thing, for it is the damping effect of the spacer devices which give them the name dampers.

2.2.1 Types of dampers

There are three types of vibration dampers available for the purpose of damping conductor vibration:

spiral vibration damper – used on small phase conductors;

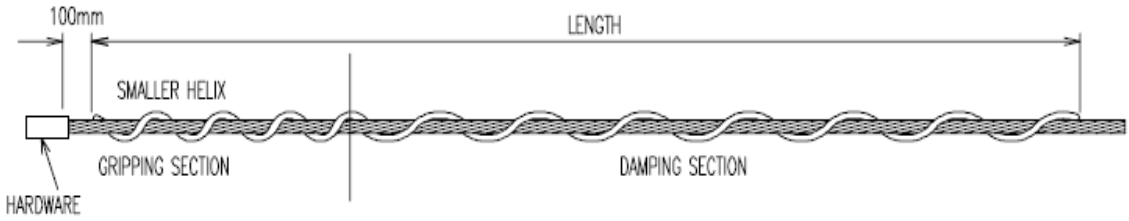

Figure 2.2-1, Spiral vibration damper.

multi-frequency Stockbridge type vibration damper – used on larger phase conductors;

Figure 2.2-2, Stockbridge vibration damper.

and

spacer dampers-used on bundle sets;

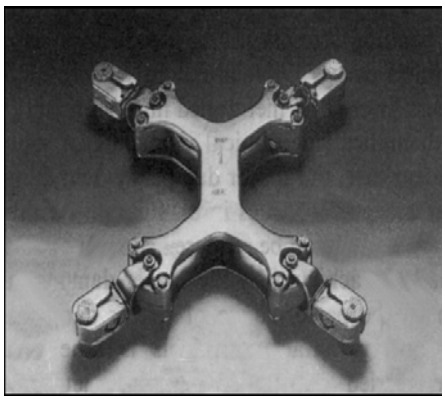

Figure 2.2-3, Quad-bundle spacer damper.

When deciding whether to use a damper and what type of damper the following information shall be determined: the average wind speed and direction for the area where the line is situated; the conductor diameter, material, rated breaking strength, stranding ratio and mass per metre; the line's voltage level, span lengths and the everyday day tension; and the sub-conductor spacing and bundle details, if the lines are constructed with bundled conductors.
The following section deals with each damper type application.

2.2.1.1 Spiral vibration dampers

This type of damper is commonly used on medium-voltage conductors with vibration problems.
Spiral vibration dampers are used on Mink and Hare conductors and on earth wires of span lengths greater than 400 m. Spiral vibration dampers are spiral shaped line fittings commonly manufactured from a PVC type material. The spiral is divided into two sections: the gripping section and the damping section.
The gripping section has a smaller helix than the damping section. This is for gripping the conductor to which the damper is to be applied. The damping section is of a larger helix section such that the vibration energy in the conductor can be degenerated. The vibration energy is degenerated by the relative movement of the larger helix to the conductor vibrations.
The ideal frequency range that spiral vibration dampers should damp is 0 Hz to 200 Hz. The damping efficiency should be 70 %.

2.2.1.2 Multi frequency Stockbridge vibration dampers

The multi frequency Stockbridge damper is a generic name to describe dampers that have an attachment clamp, messenger retaining rod and messenger weights. Multi frequency Stockbridge dampers damp out aeolian vibration on the conductor they are installed on. The attachment clamp used to connect the damper to the conductor has traditionally been a bolted type of clamp. This type of clamping is not an acceptable clamping technology for distribution lines. A good clamping technology is helically formed rods. Clamping with helically formed rods ensures consistency and effectiveness of attachment.

The messenger weights come in various shapes and sizes. The messenger weights determine the damping characteristic and the positioning of the damper. The positioning and numbers of dampers given in the annexes are a guideline. The exact positioning and number of the different types of multi frequency Stockbridge damper are different due to their different design philosophy. It is strongly recommended that the manufacturer's positioning and number requirement is used.

The ideal frequency range that multi frequency Stockbridge type dampers should damp is 0 Hz to 200 Hz. The damping efficiency should be 70 %.

Although being the most frequently used vibration damper, developed in 1926, the precise way in which it works has always been shrouded in mystery. Its success in controlling the oscillations has removed the need for better understanding (Rowbottom M.D. et. al., 1973).

2.2.1.3 Torsional Damper Detuners

Prototype Torsional Damper Detuners (TDD) were first installed on an instrumented test line in Belgium in 1992. The TDD has also been installed on a test line by STATNETT in Norway and on operating power lines by Electrabel in Belgium and Scottish Power in the UK. The galloping has been substantially reduced on all lines where the TDD has been installed and recent field records from Belgium, see diagram, show that the system is very efficient in the control of galloping and also free of any side-effects. (T.D.D.E Online).

Figure 2.2-4, Torsional Damper Detuner attached to conductor (TDEE, 2008)

2.2.1.4 Spacer dampers and rigid spacers

Spacer dampers and rigid spacers are used to secure the bundle of conductors and to prevent the conductors in the bundle from clashing when subjected to conductor motion. Vibrations in the conductors are caused by the turbulent wake of the first conductor hit by the wind. By ensuring the conductors are spaced adequately, vibrations can be minimized.

The spacer damper is used as a spacer and as a damper of vibration on bundled conductors. Spacer dampers should be able to damp low frequencies from 0 Hz to 100 Hz. The rigid spacer only spaces the conductors in a bundle to ensure the constant distance between conductors in the bundle. The rigid spacer can be used in conjunction with multi frequency Stockbridge dampers to give good damping and spacing results.

Figure 2.2-5, Rigid and semi-rigid spacers

The rigid spacer and multi frequency Stockbridge damper combination is the preferred practice. Rigid spacers with helically formed attachment devices are the preferred rigid spacers.

2.3 Use of vibration indicators and analysers

In special cases where vibration of a conductor is of particular concern on a line, a vibration indicator or vibrator analyser shall be used to determine the damping requirements of the line. There are two different types of instruments that can be used for this purpose:

2.3.1 Technology Research and Investigation Vibration Activity Indicator (TRIVAI)

The TRIVAI is used to determine the presence or absence of aeolian vibration on distribution line conductors. It is not intended to measure the exact vibration levels, but rather to indicate if high levels of vibration are exceeding the conductors rated safe bending amplitudes. This device is simple to operate. When there is no vibration the sphere is seen under the particles as shown in figure (2.3-1) and due to the extent of the vibration the sphere moves up through the particles.

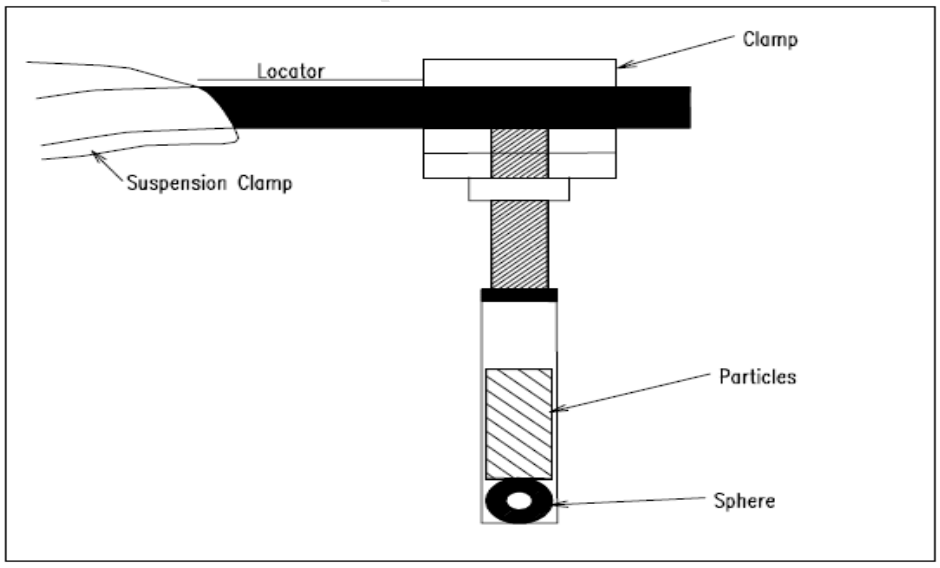

Figure 2.3-1, TRIVAI device showing no vibration (Cigre, 1999)

2.3.2 Pavica device

The Pavica device was designed for installation on line conductors to measure the amplitude and the frequency of aeolian vibrations. The device is capable of analyzing the effects of vibration and amplitude on the conductor. It can also determine the life expectancy of the conductor, in years, by comparing the given data with benchmarks or merit figures. This device is based on internationally accepted IEEE and CIGRE methods.

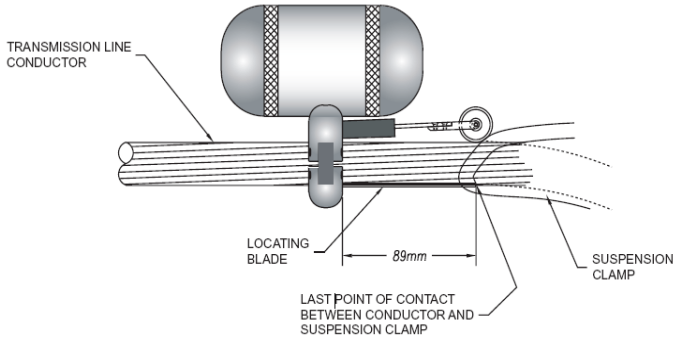

Figure 2.3-2, Pavica device attached to conductor (Cigre, 1999).

2.3.3 Fibre optic Bragg grating Sensors

This is the most recent method on measuring Aeolian vibrations based on fibre-optic Bragg grating sensors. The method offers various advantages such as no need for power supply at the sensors locations, small size and mass and no influence of the high voltage environment (L. Bjerkan, 2004).

In general vibration data obtained with this method can be used to optimize vibration damper arrangements or verify existing damper performance. Accumulated vibration data can furthermore provide information of the mechanical condition of the conductor and its remaining lifetime. In addition the method can also be used to detect other environmental loads like galloping and ice accretion in remote areas.

L. Bjerkan however concludes that the high sensitivity of the sensors results in measurements with a great deal of high frequency contents, and this complicates the analysis of the measurements.

2.4 Current Practices in damper usage

By far the stockbridge damper continues to be the most preferred damper worldwide in as far as aeolian vibration damping is concerned, however the following damper types continue to be acceptable in the field:

spiral vibration damper – used on small phase conductors;

multi-frequency Stockbridge type vibration damper – used on larger phase conductors;

and

spacer dampers-used on bundle sets.

Besides the above mentioned dampers various vibration indicators are being installed on the transmission lines to monitor the conductor vibrations and determine the damping requirements of the line. These are:

Technology Research and Investigation Vibration Activity Indicator (TRIVAI)-used to determine the presence or absence of aeolian vibration on distribution line conductors. This device is simple to operate.

The Wake-Induced Vibration Indicator (WIVI) was also developed for the main purpose of detecting and measuring the extent of wake-induced vibration. This device continuously scans the vibrations and if present, detect and present the vibration in terms of maximum displacement Peak to Peak.

Pavica device was designed for installation on line conductors to measure the amplitude and the frequency of aeolian vibrations.

Torsional Damper Detuners were first installed on an instrumented test line in Belgium in 1992. The TDD has also been installed on a test line by STATNETT in Norway and on operating power lines by Electrabel in Belgium and Scottish Power in the UK. The galloping has been substantially reduced on all lines where the TDD has been installed and recent field records from Belgium, see fig (2.4-1), show that the system is very efficient in the control of galloping and also free of any side-effects.

Figure 2.4-1 shows results obtained with TDD during a galloping event that occurred at the experimental station of Villeroux (included in the 400 kV network), in Belgium.

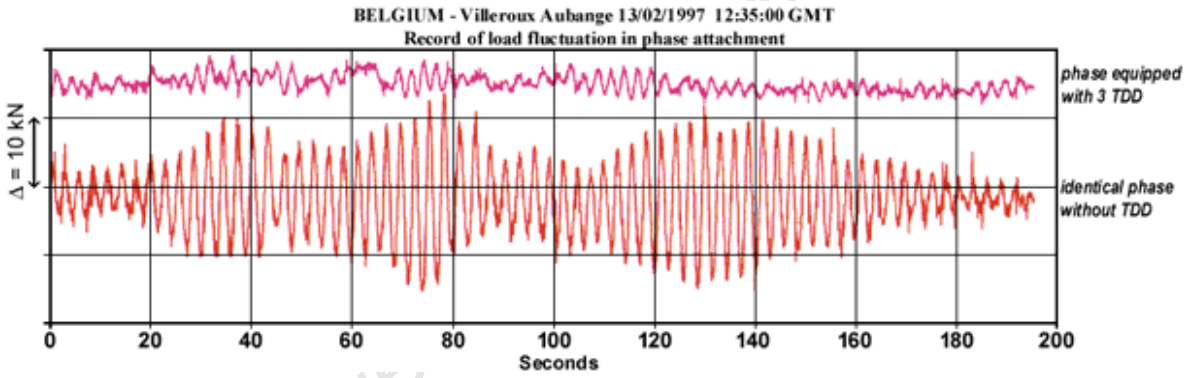

Figure 2.4-1, Results of galloping event, (TDEE, 2008).

The graph shows the tension fluctuation at anchoring levels for different phase arrangements (triple conductor, twin reference conductor, twin with pendulums and twin with TDD). Only relative change is of importance and is given in kN. A reference galloping of about 6 meters peak to peak (giving a tension variation of about 30 kN per insulator string - which means 60 kN peak to peak variation) is reduced to about 15 kN by pendulums (wind speed was about 8 to 10 m/s) and to 5 kN by the TDD. It is clearly visible that such a device subsequently limits galloping amplitudes (T.D.E.E 2008).

The use of the above types of dampers has proved very effective but choice of dampers still varies very much from country to country, due to aspects of cost and local availability. The following section will deal with a brief historical review of the dynamics of cables.

2.5 Cable Dynamics-A Historical Review

In the review by U. Starossek (1994) the history of the theory of cable vibrations is considered, as early as the 18th century. The basic equation of linear dynamics of an extensible sagging cable is given below, equation (2.5-1). A discussion of dynamic excitation mechanisms and of dynamic interacting between cables and other structural elements conclude this contribution.

$$H\frac{\partial^2 v}{\partial x^2}+h_\tau\frac{d^2 y}{dx^2}=m\frac{\partial^2 v}{\partial t^2}+c\frac{\partial v}{\partial t} \tag{2.5-1}$$

The auxiliary quantity h_τ is defined as

$$h_\tau=\tau\frac{dx}{ds}. \tag{2.5-2}$$

where τ is the dynamic part of the total cable tension that is supposed to be invariable along the cable.

In his review Starossek notes that the vibrating string was one of the first physical systems to which the new analytical tools of modern mechanics and mathematics were applied. Treatises on this problem were presented by Brook Taylor, d'Alembert, Euler, Johann and Daniel Benoulli during the first half of the eighteenth century (Szabo 1979). Starossek notes that by 1788 Lagrange and others before had reached solutions of varying degrees of completeness for the vibrations of an extensible, mass less string, fixed at each end, from which numerous weights were hung. This corresponds to a discretization of the cable continuum. The general partial differential equations of the motion of a cable element under the action of a general force system were given by Poisson in 1820 (Clough et. al., 1975). The reviewer argues that by this time no

solutions of sagged cables were known, apart from Lagrange's work on the equivalent discrete system.

Starossek highlights that in 1968, after preliminary work by Stokes and Rohrs, Routh gave exact solutions for an inextensible sagging cable which hung in a cycloid (Routh 1955). Cable elasticity was considered for the first time by Kloppel and Lie in 1942. Pugsley (1949), proposed a semi-empirical theory for the natural frequencies of cables with great sag ($1{:}10 \leq$ ratio of sag to span $\leq 1{:}4$). In 1953, by assuming again that the cable was inextensible, Saxon and Cahn (Saxon et. al., 1953) gave theoretical solutions for cables with great sag.

The reviewer outlines that until the 1970s there had neither theoretical nor experimental work been done which dealt with a remarkable discrepancy between the theories known by then; when reducing the sag to zero, the frequencies of the symmetric in-plane modes of an inextensible cable do equal the corresponding natural frequencies of a taut string. Irvine et al, 1974 later showed that description of that transition range requires consistent inclusion of cable elasticity. Their work (Irvine et. al., 1974) revealed an extensible comprehension of the linear theory of free vibrations of a rigidly supported horizontal cable with a ratio of sag to span from approximately 1:8 to zero (horizontal meaning same level supports). Their basic and straightforward assumption was that dynamic cable tension is a function of time alone, (i.e. the elastic deformation is assumed to be quasi-static). They pointed out that the dynamic behavior of a cable essentially depends on only one geometric-elastic system parameter, the so-called 'cross-over' points, the natural frequencies of symmetric in-plane modes coincide.

Starossek notes that later on Irvine extended the theory to inclined cables (Irvine 1978). For this, the weight component parallel to the cable chord was neglected. The same author jointly with Griffin, also made valuable contributions to the analysis of cable response to dynamic loading as it occurs in the case of support acceleration due to earthquake (Irvine et. al., 1976). Triantallou in 1984 gave a more precise solution for the free vibration of an inclined extensible and sagging cable. For this spatial variability of dynamic tension and weight component parallel to chord were taken into consideration. For the frequency curves of inclined cables it follows that each 'cross-over' is replaced by an 'avoided crossing' (i.e., nearly a 'cross-over'). Nevertheless, validity of Irvine's theory was confirmed for a wide range of parameters.

In his conclusion the reviewer notes that the linear theory of vibrating cables can now be considered a simple but powerful tool to examine small vibrations of single cables, and composed systems containing cables, for a large range of system parameters. He says in the last couple of years, nonlinear cable dynamics also has made considerable progress. While nonlinear theory is inherently much more involved, and less applicable to everyday engineering analysis, the theories developed to date seem capable of reproducing the very unique phenomena that appear when large cable vibrations are considered.

The section that follows will deal with a number of selected papers that deal with modeling of overhead cables. Some of them are also a part of this historical review presented herein.

2.5.1 Modeling of overhead cables

The vibration of cable structures has been investigated by many researchers and in this chapter the main objective is to give a brief of the research findings. The chapter will divide these findings into analytical, numerical and experimental modeling approaches taking into consideration both undamped and damped systems.

2.5.1.1 Analytical modeling of overhead cables

Claren et al, 1969

In their research they assess the laws governing the cable response to the exciting forces. Assuming a constant flexural rigidity and ignoring damping, they give the equation of motion for the undamped system as:

$$EI\frac{\partial^4 u}{\partial x^4} - T\frac{\partial^2 u}{\partial x^2} = -m\frac{\partial^2 u}{\partial t^2} \tag{2.5-3}$$

and if assuming

$$u(x,t) = \varphi(x)\psi(t) \tag{2.5-4}$$

The motion equation changes to

$$\frac{1}{m\varphi(x)}\left[EI\frac{d^4\varphi(x)}{dx^4} - T\frac{d^2\varphi(x)}{dx^2}\right] = -\frac{1}{\psi(t)}\frac{d^2\varphi(t)}{dt^2} \tag{2.5-5}$$

As seen from the above equation we have one term as a function of x and the other as a function of t. The authors equate both these terms to a constant say ω^2 which then yields

$$EI\frac{d^4\varphi(x)}{dx^4} - T\frac{d^2\varphi(x)}{dx^2} = \omega^2 m\varphi(x) \tag{2.5-6}$$

and

$$\frac{d^2\psi(t)}{dt^2} = -\omega^2\psi(t) \tag{2.5-7}$$

A solution is also given for equation 2.5-3 and is,

$$\psi(t) = \psi_0 \sin(\omega t + \beta) \tag{2.5-8}$$

The authors assume for equation 2.5-5 a solution $\varphi(x) = \phi e^{x\alpha}$ and the end condition of pivoted extremities of $\varphi(x) = 0$ and $\left[d^2\varphi(x)\right]/dx^2 = 0$ for $x = 0$ and $x = l$, then equation 2.5-3 yields:

$$\omega_r^{\,2} = \left(\frac{r\pi}{l}\right)^2 \frac{T}{m}\left[1 + \left(\frac{r\pi}{l}\right)^2 \frac{E\,I}{T}\right] \tag{2.5-9}$$

Where ω_r are the resonance frequencies of the system; that is, the frequencies corresponding to the principal modes of vibration of the cable. The symbols used are explained as:

E	cable Young's Modulus
I	second moment of area of cable cross section about its neutral axis
m	mass of cable per unit length
T	tensile load applied to cable
u	lateral deflection of taut cable
r	vibration mode of taut cable

A brief analysis of the cable problem shows that calculations of flexural rigidity $E\,I$ of a cable are unreliable, because in the bent part of the cable individual strands may move on the tension side while strands under pressure may glide or buckle.

Simpsons et al, 1984

Simpson presents a mathematical model of a multi-conductor overhead power line with spacer-dampers. He suggests that the Stockbridge type of damper is completely ineffective against sub-conductor oscillation and the only means of minimizing the effect of this is careful span wise positioning of the spacers.

He highlights that field observations indicate that the aeolian vibration problem is less severe for multi-conductor bundles than it is for single conductors, with an extent which increases with number of conductors within the bundle, as expected since the stiffness of the bundle increases with the number of conductors in the bundle. The researcher found out that on a 'quad' conductor line with only six sub spans (between spacer dampers), more than 2500 natural frequencies occur over the aeolian frequency range (7-80Hz) when the line is typically tensioned and therefore applying continuum methods of analysis is not possible i.e. sensible. He gives the description of the transverse dynamics of taut catenary segments accurately by the stiff-stretched string partial differential equation.

$$E_j \frac{\partial^4 u}{\partial x^4} + T \frac{\partial^2 u}{\partial x^2} dx = \rho A \frac{\partial^2 u}{\partial t^2}. \qquad (2.5\text{-}10)$$

He points out that when using the stiff stretched string equation above, the equation of which value of conductor flexural rigidity to employ must be answered. The EI value lying between $EI_{\min}$ (based on strands acting individually) and $EI_{\max}$ (based on the assumption of no inter-strand slippage). At zero tension, EI is close to $EI_{\min}$ although (Claren and Diana, 1967) suggest that about 10-40% of field results show that EI is close to $EI_{\max}$. Typically $EI_{\max} \approx 50\text{-}100 * EI_{\min}$, it is sensible in a design analysis to assume that all sub conductor segments carry zero bending moment at their extremities and that their flexural rigidity, EI is $EI_{\max}$, thus a sub conductor segment may be viewed as being universally hinged at both extremities. He gives appropriate dynamic stiffness relation for motion in any transverse plane of a typical sub conductor segment as:

$$\begin{bmatrix} f_0 \\ f_1 \end{bmatrix} = \frac{H\lambda^2}{l\beta(1+\beta^2/\alpha^2)} \begin{bmatrix} \cot\beta - (\beta/\alpha)^3 \coth\alpha & -\cos ec\beta + (\beta/\alpha)^3 \cos ech\alpha \\ -\cos ec\beta + (\beta/\alpha)^3 \cos ech\alpha & \cot\beta - (\beta/\alpha)^3 \coth\alpha \end{bmatrix} \begin{bmatrix} w_0 \\ w_1 \end{bmatrix} \qquad (2.5\text{-}11)$$

The authors outline that in practice, the effectiveness of the spacer distribution at high frequency may be checked by using a short computer program wherein the objective functions

$$Q_{r_0} = \sum_{i=1}^{N} \sin^2(\pi \xi_i r_0), \qquad r_0 = p+2,..., N, \qquad (2.5\text{-}12)$$

where $\xi_i L$ is the location of the ith spacer relative to the L.H. support, are formed. If $Q_{r_0} = 0$ for any value of the integer r_0, all spacers must be at whole-span nodes and are thus totally ineffective. L representing the span and N the number of spacers.

In conclusion it is noted that it is possible to control much of the aeolian vibrations provided that line tensions are not excessive.

Irvine et al, 2004

Of the many models that have been established for modeling the behaviour of sagged cables, this researcher has come up with the most accurate and highly used formulation (Starossek 1994).

The researcher assumes for cables with sag to span ratio of 1:8 or less to behave more like taut cables with high tensions induced in them and so the modeling tends to incline more towards the linear theory of sagged cables. The most common approach to the modeling problem has been dealt with by many researchers and is argued quite clearly by Irvine and Caughey (2004) in the following motion equations,

$$\left.\begin{aligned}
&\frac{\partial}{\partial s}\left\{(T+\tau)\left(\frac{dx}{ds}+\frac{\partial u}{\partial s}\right)\right\}=m\frac{\partial^2 u}{\partial t^2},\\
&\frac{\partial}{\partial s}\left\{(T+\tau)\left(\frac{dy}{ds}+\frac{\partial v}{\partial s}\right)\right\}=m\frac{\partial^2 v}{\partial t^2}-mg,\\
&\frac{\partial}{\partial s}\left\{(T+\tau)\frac{\partial w}{\partial s}\right\}=m\frac{\partial^2 w}{\partial t^2},
\end{aligned}\right\} \tag{2.5-13}$$

where s is the arc length co-ordinate; u is the longitudinal in-plane component of motion; v is the vertical in-plane component of motion; w is the out-of-plane component of motion; m is the mass per unit length of the cable; T is cable tension; and τ is the additional cable tension due to the vibration.

Sugiyama et. al., (2003) gives a clear definition diagram of cable vibrations as shown in figure (2.5-1) below, which is similar to the one assumed by Irvine (2004).

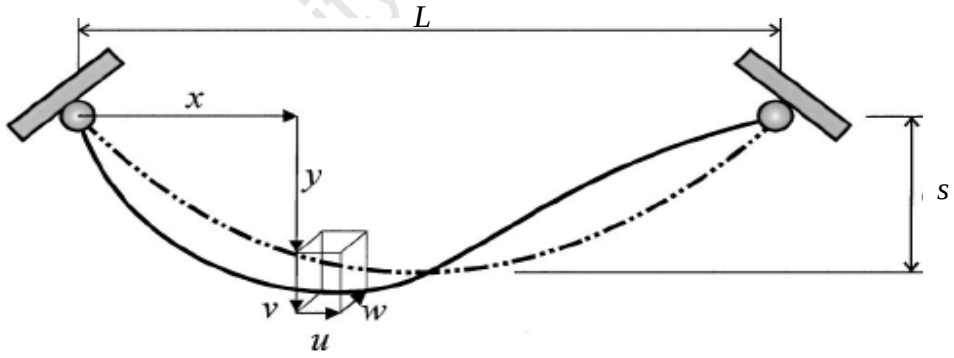

Figure 2.5-1, Sagged Cable.

Sugiyama uses the same approximation used by Irvine as well as numerous researchers and since the approximation is interested with sag to span ratio of 1:8 and less. Equation (2.5-13) finally approximates to:

$$\left.\begin{aligned} H\frac{\partial^2 v}{\partial x^2}+h\frac{d^2 y}{dx^2}&=m\frac{\partial^2 v}{\partial t^2}\\ H\frac{\partial^2 w}{\partial x^2}&=m\frac{\partial^2 w}{\partial t^2}\end{aligned}\right\} \tag{2.5-14}$$

Where H and h are the horizontal components of the initial cable tension at the static equilibrium configuration and the additional cable tension due to the dynamic motion, respectively. From above it is seen that the change in tension does not influence the out-of-plane motion, while the in-plane transverse motion depends on the cable tension. However in first order the cable equation is

$$\frac{h(ds/dx)^3}{EA}=\frac{\partial u}{\partial x}+\frac{dz}{dx}\frac{\partial w}{\partial x}, \tag{2.5-15}$$

which can be integrated to the form

$$\frac{hL}{EA}=\frac{mg}{H}\int_0^L w dx\ . \tag{2.5-16}$$

It is concluded that in the in-plane transverse motion, there exist both symmetric and antisymmetric modes. These are classified according to nature of the change in tension. The authors also note that symmetric in-plane motion consists of symmetric transverse components and antisymmetric longitudinal components and vice-versa were for antisymmetric modes, the assumption made is that there is no change in tension due to motion.

Thus from the above Sugiyama gives the dynamic response of a cable under arbitrary vertical excitation f_v can be assumed by the following nondimensional modal form:

$$\bar{v}(\bar{x},\bar{t})=\sum_n \phi_n(\bar{x})\xi_n(\bar{t}) \tag{2.5-17}$$

where

$\bar{t}=t(H/m)^{1/2}/L$ and the modal functions are given by $\tilde{v}_n=A_n\sin\left(\frac{2n\pi x}{L}\right)$, n=1, 2, 3….

Using this assumed modal solution leads to the equation of motion for forced vibration in terms of the modal coordinate ξ_n associated with the n-th mode as

$$\frac{d^2\xi_n}{d\bar{t}^2} + \bar{\omega}_n^2 \xi_n = -\frac{\int_0^1 \bar{f}_v(\bar{x},\bar{t})\phi_n(\bar{x})d\bar{x}}{\int_0^1 \phi_n(\bar{x})\phi_n(\bar{x})d\bar{x}} \tag{2.5-18}$$

where $\bar{f}_v = f_v/(\rho A g)$.

The authors conclude by noting that use of the linearized equations in the perturbation form gives the natural frequencies and the associated mode shapes of a cable at an arbitrary configuration. The generalization of the nonlinear method to three-dimensional cable problems as well as the implementation in general multibody algorithms can be incorporated by using the above approach.

2.5.1.2 Finite Element modeling of overhead cables

Numerical methods based on finite element analysis have the advantage of being applicable to specific line sections with variable degrees of details. The influence of different line parameters can also be studied without having to erect costly scale models. However, the results obtained with an analytical method depend on the numerical parameters selected and therefore necessitate a thorough understanding of the concepts of dynamics and of the physical problem at hand. It is emphasized that careful validation of analytical models with full scale test results is still lacking. (McClure 2003)

This section will dwell briefly on the different modeling approaches employed by different authors in as far of the aspect of finite element modeling is concerned.

Sugiyama et. al., 2003

In their research, the finite element absolute nodal coordinate formulation is used to obtain a fully nonlinear solution of the cable problem. In the formulation, the nodal coordinates are defined as a set of global nodal displacements and slopes, thereby making it possible to represent the exact rigid body dynamics and obtain a constant mass matrix. The authors assume a two dimensional beam problem (Omah et. al., 2001), the interpolation function is defined as cubic function of x and linear in y, where x and y are the element spatial coordinates. By adopting an absolute nodal coordinate formulation, a position vector r^i on a beam element i defined in a global coordinate system XY as shown in figure (2.5-2) is given by

$$r^i = S^i(x^i, y^i)e^i \tag{2.5-19}$$

where $S^i(x^i, y^i)$ is the element shape function matrix and e^i is the nodal coordinate vector defined for a finite element i at $(y_i = 0)$ as

$$e^i = \begin{bmatrix} e_1^i & e_2^i & e_3^i & e_4^i & e_5^i & e_6^i & e_7^i & e_8^i & e_9^i & e_{10}^i & e_{11}^i & e_{12}^i \end{bmatrix}^T$$

$$= \left[\mathbf{r}^{iT}\Big|_{x^i=0} \left(\frac{\partial \mathbf{r}^i}{\partial x^i}\right)^T\Big|_{x^i=0} \left(\frac{\partial \mathbf{r}^i}{\partial y^i}\right)^T\Big|_{x^i=0} \mathbf{r}^{iT}\Big|_{x^i=l^i} \left(\frac{\partial \mathbf{r}^i}{\partial x^i}\right)\Big|_{x^i=l^i} \left(\frac{\partial \mathbf{r}^i}{\partial y^i}\right)^T\Big|_{x^i=l^i} \right]$$

The shape function matrix S^i used in this investigation is

$$\mathbf{S}^i = \begin{bmatrix} \mathbf{s}_1^i\mathbf{I} & \mathbf{s}_2^i\mathbf{I} & \mathbf{s}_3^i\mathbf{I} & \mathbf{s}_4^i\mathbf{I} & \mathbf{s}_5^i\mathbf{I} & \mathbf{s}_6^i\mathbf{I} \end{bmatrix} \tag{2.5-20}$$

where I is a 2 by 2 identity matrix and

$$s_1^i = 1 - 3\xi^{i^2} + 2\xi^{i^3}, \quad s_2^i = l^i(\xi^i - 2\xi^{i^2} + \xi^{i^3}), \quad s_3^i = l^i(\eta^i - \xi^i\eta^i)$$

$$s_4^i = 3\xi^{i^2} - 2\xi^{i^3}, \quad s_5^i = l^i(-\xi^{i^2} + \xi^{i^3}), \quad s_6^i = l^i\xi^i\eta^i,$$

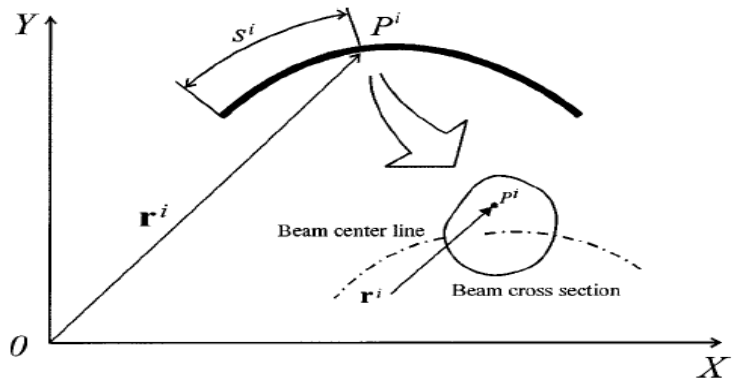

Figure 2.5-2, Beam element in the absolute nodal coordinate formulation.

The author defines the nondimensional quantities ξ^i and η^i as

$$\xi^i = x^i / l^i, \qquad \eta^i = y^i / l^i$$

and l^i is the length of the beam element in the undeformed configuration. Generalized inertia forces can be obtained by evaluating the kinetic energy T^i as

$$T^i = \frac{1}{2}\int_{V^i} \rho^i \dot{\mathbf{r}}^{iT} \dot{\mathbf{r}}^i dV^i = \frac{1}{2}\dot{\mathbf{e}}^{iT}\mathbf{M}^i\dot{\mathbf{e}}^i \tag{2.5-21}$$

where the mass matrix M^i is constant, and as a consequence, the centrifugal and Coriolis inertia force vectors are identically zero. The Green-Lagrangian strain tensor ε_m^i can be written as

$$\boldsymbol{\varepsilon}_m^i = \frac{1}{2}(\mathbf{J}^{\mathrm{iT}}\mathbf{J} - \mathbf{I}) \tag{2.5-22}$$

where I is a 2 by 2 matrix and J^i is the matrix of displacement (Omah et. al., 2001). The strain energy can be written as

$$U^i = \frac{1}{2}\int_{V^i} \boldsymbol{\varepsilon}^{iT}\mathbf{E}^i\boldsymbol{\varepsilon}^i dV^i \tag{2.5-23}$$

where E_i is the matrix of elastic coefficients defined for plane stress problems as

$$\mathbf{E}^i = \begin{bmatrix} \lambda^i + 2\mu^i & \lambda^i & 0 \\ \lambda^i & \lambda^i + 2\mu^i & 0 \\ 0 & 0 & \mu^i \end{bmatrix} \tag{2.5-24}$$

where $\lambda^i = E^i v^i / \left[(1+v^i)(1-2v^i)\right]$, $\mu^i = E^i / \left[2(1+v^i)\right]$, E^i is Young's modulus, v^i is Poisson's ratio and ε^i is the strain vector obtained by the strain tensor ε_m^i.

$$\varepsilon^i = \begin{bmatrix} \varepsilon_1^i & \varepsilon_2^i & \varepsilon_3^i \end{bmatrix}^T \tag{2.5-25}$$

where $\gamma_{12}^i = 2\varepsilon_{12}^i$.

Using the strain energy, one obtains the generalized elastic force vector Q_k^i as

$$\mathbf{Q}_k^i = \left(\frac{\partial U^i}{\partial \mathbf{e}^i}\right)^T = \mathbf{K}^i\mathbf{e}^i \tag{2.5-26}$$

where K_i is the nonlinear stiffness matrix that depends on the nodal coordinates. The authors then give the equation of motion as:

$$\mathbf{M}^i\ddot{\mathbf{e}}^i + \mathbf{Q}_k^i = \mathbf{Q}_a^i \tag{2.5-27}$$

where Q_a^i is the vector of generalized applied forces. It should be noted that the preceding equation accounts for all geometric non-linearities since nonlinear strain-displacement relations are used.

In conclusion it is noted that the comparison with the analytical solution obtained using the classical cable theory demonstrates the good performance of the absolute nodal coordinate formulation when the model is linearized.

Hagedorn et al, 2004

The authors use the energy balance principle (EBP) for estimating the vibration amplitudes, and hence, the strain levels in the transmission line conductors. Besides the parameters of the conductor and of the dampers, the aerodynamic forces acting on the vibrating conductor are the main input data required for the energy balance. For the wind power input, the authors note that researchers still depend on the experimental data of drag and lift forces of a vibrating cylinder obtained from wind tunnel testing. In case of the bundled conductors, many combinations regarding the number of conductors, spacing of the conductors as well as their orientations are possible, which make wind tunnel tests very expensive and formidable. The authors argue very much that it is useful to replace the wind tunnel tests by numerical simulations, as far as possible.

In the latest research, the authors outline the first step towards obtaining the wind power inputs for different configurations of bundled conductors. In the current work, the flow around a vibrating conductor is simulated with the finite-volume method, by considering it as a circular cylinder. The two-dimensional Navier–Stokes equations are solved first. The drag and the lift forces are then calculated by integrating the pressure and the shear values on the boundary of the cylinder, which ultimately cause the impartation of wind power. The numerically obtained wind power input is then compared with that obtained by different researchers in wind tunnel tests.
In the present paper some approaches towards the transcendental eigenvalue problem (EVP) for the bundled conductors with spacer dampers are discussed. It is formulated as an algebraic transcendental EVP, which however presents several numerical difficulties. In conclusion the authors state that they found a very good match between the experimental and the numerical values of wind power input.

Liu et al, 1996

The authors introduce a linear frequency-domain dynamic method to calculate large motions of slender structures. In their study the work done by the motion of the cable in the time domain is equated with that done in the frequency domain (Berggren, 1992) taking into account the influences of excitation frequency and excitation amplitude.

For the time-domain simulations, the set of nonlinear partial differential equations are transformed into ordinary differential equations by means of the principle of virtual work as used in finite element analysis. The cable is thereby decomposed into a number of straight finite elements (bars) with linear shape functions except for the distributed mass and added mass which are lumped to the end points (nodes) of the elements in order to obtain an easily invertible mass-matrix. The author states that the time-domain is made by explicit numerical integration and that the explicit method is conditionally stable, this implies that the time increments may not be too large.

The authors argue that the case of less severe non-linearity, frequency-domain analysis can be a useful tool to solve the dynamic problems. The following equations are used by the authors in their formulation.

The linearized equation of motion in the time domain is given as:

$$(M + A)\ddot{X}(t) + C\dot{X}(t) + KX(t) = F(t) \tag{2.5-28}$$

where

M, A	mass and added mass matrix, respectively.
K	global stiffness matrix
C	equivalent damping matrix
$X(t)$	cable displacement vector relative to reference configuration.
$\dot{X}(t), \ddot{X}(t)$	velocity and acceleration vectors relative to reference configuration
$F(t)$	external excitation force

t time

The matrices A, K and C are all established for the static equilibrium, reference configuration. Equation (2.5-28) can be changed to complex for use in the frequency domain as:

$$\left[K - (M + A)\omega^2 + i\omega C\right]X_c(\omega) = F_c(\omega) \tag{2.5-29}$$

where: $F_c(\omega)$ is the complex frequency component of the Fourier transform of the load vector $F(t)$; $X_c(\omega)$ is the complex frequency component of the response displacement vector; and $i = \sqrt{-1}$.

The authors then establish that the complex response is then:

$$X_c(w) = \left[K - (M + A)\omega^2 + i\omega C\right]^{-1} F_c(\omega). \tag{2.5-30}$$

It can be seen that the frequency components of the response to the load spectrum make up the response spectrum. The characteristic responses like standard deviation, significant value or most probable maximum cable tension, displacement e.t.c. along the cable can subsequently be calculated. Alternatively, time series of the cable tension or displacement can be created by inverse Fourier transformation.

In conclusion it is seen that the frequency-domain calculations give basically similar results to those of the time-domain and also for a freely hanging cable, the frequency-domain calculation compares well with the time-domain simulation. Due to numerical integration problems, the time-domain solution needs some kind of smoothing or filtering of numerically excited high-frequency components.

2.5.1.3 An Experimental modeling of overhead cables

Lotar Mocks, 1984

In his work on damping of high voltage overhead line conductor vibrations looks only at short-wave vibrations, also designated as Karman vibrations. Much emphasis is spent on the Stockbridge damper as a means of reducing these short-wave vibrations mainly its principle of performance.

The vibration damper (figure 2.5-3a) composed of a damper clamp which incorporates a flexural steel messenger cable and two masses (weights) attached to the cable ends forms a damped vibration system. A damped spring-mass system with sinusoidal support excitation $u(t)$ is chosen as a physical model of the damper for the first approximation (figure 2.5-3b). If the support (damper clamp) is subject to forced motion and energy is dissipated.

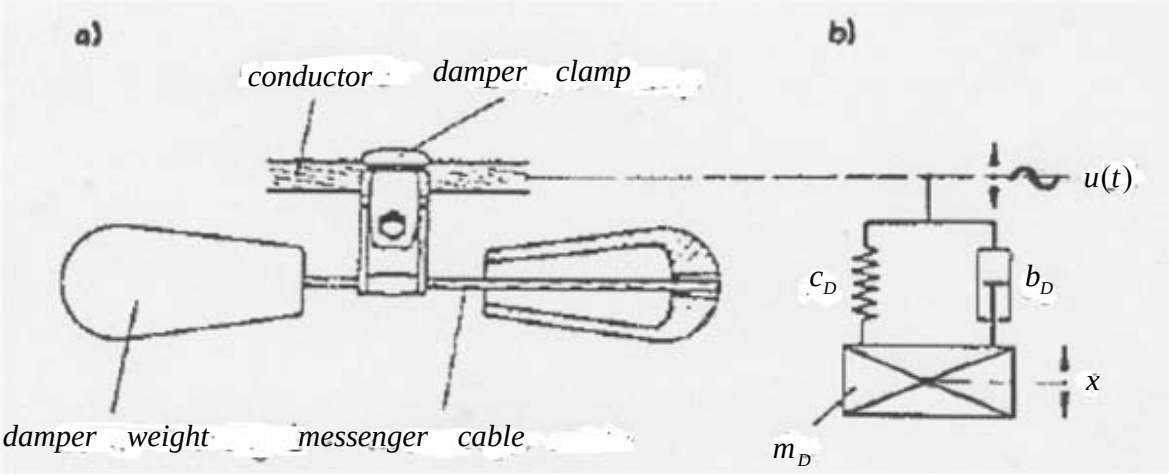

Figure 2.5-3, Stockbridge damper with simplified model in form of damped spring mass system.

were b_D is the damping factor, c_D is the stiffness factor, m_D the mass of the damper and x the displacement. In general, the Stockbridge damper (in case of symmetric shape) involves two degrees of freedom and accordingly, two vibration modes and two resonant frequencies. He points out that according to existing experience, failures of Stockbridge dampers are mainly related to wire breaks of the messenger cable.

Mocks points out that a reliable method to consider the influence of turbulences on the wind power input is not available; and wind tunnels give the closest approximation. He highlights that it has not been possible to calculate the conductor self-damping with a satisfactory degree of accuracy.

Mocks also points out that field measurements which have been conducted for decades, mainly in the US and in Canada have revealed that vibration damages at the suspension point do not occur in case that the alternative bending strain of conductor strands measured in the immediate vicinity of the mouth of clamp does not exceed a value of $E_{admissible} = 150\ \mu m/m$.

Mocks in this study concludes that his method in determining of the wind power input is conservative, i.e. the results throughout are in the conservative range and that values measured on the line for comparison with the wind tunnel measurements are not yet available up to now.

Vecchiarelli et al, 1998

The uniform flow of air or water across a stationary, rigid cylinder whose axis is normal to the streamwise direction has been studied by many investigators; (Strouhal 1878 and von Karman 1912) were among the first to do so. Various flow regimes can evolve, depending on the Reynolds number, Re.

The author notes that this periodic vortex shedding is continuous from Re of 40 to 300 000 (Lienhard 1966). This range of Re includes that which corresponds to light to moderate winds blowing across overhead conductors, for Re based on conductor diameter.

The nature of uniform flow across a rigid cylinder which is mounted on flexible supports is quite different from that of a stationary cylinder. This topic has been explored by numerous investigators, such as Parkinson et. al., (1968); in-depth reviews are provided by Blevins (1977)

and Sarpkaya (1979). Motion of the cylinder in the transverse direction may be initiated when the velocity of the flow is such that the vortex-shedding frequency is close to the natural vibration frequency of the cylinder. The author states that the cylinder motion can subsequently (i) increase the strength of the shed vortices, (ii) enhance the spanwise correlation of vortex shedding, and (iii) change the vortex-shedding frequency to equal or almost equal the natural frequency. The first effect amplifies the magnitudes of the vortex-induced lift forces along the cylinder. The second effect causes these forces to act in phase; that is, they become synchronized (the net lift force which acts on an oscillating cylinder is much greater than that which would exist if the cylinder were stationary). The third effect results in resonance and is referred to as the lock-in phenomenon. As a consequence of these effects, the cylinder may experience a significant level of vibration.

Diana & Falco (1971), measured the lift force that acts during the aeolian vibration of a rigid cylinder in a uniform flow. It was found that, like the displacement of the cylinder, the lift force is virtually harmonic in time at steady state.

Wind-tunnel experiments, in which the wind power input was measured during the aeolian vibration of a circular cylinder, have been performed by many investigators, including: Bate & Callow (1934), Farquharson & McHugh (1956), Diana & Falco (1971), Macdonald et. al., (1989) and Brika & Laneville (1993). The wind power input is defined as the wind energy transferred to the cylinder over one cycle of vibration divided by the period of vibration.

Differences in the wind power input data from various investigators vary by factors up to 2. Regarding the aeolian vibration of a flexible cable in a uniform flow, an important conclusion was drawn by Griffin & Ramberg (1974). Based on their wind-tunnel investigation, it was determined that the near wake at a given location along a vibrating cable can be represented reasonably well by the near wake of a rigid cylinder (a) whose diameter is equal to that of the cable and (b) which oscillates at the same frequency and amplitude of the cable at that location. In conclusion the author highlights, it may be inferred that the local wind power input along a conductor depends on the local displacement amplitude and frequency of vibration in the same manner that the wind power input for a rigid cylinder depends on the cylinder displacement amplitude and frequency of oscillation. Also the authors add that the impact of cable stranding on wind power input is minor (Macdonald et. al., 1989).

Loredo-Souza et al, 2001

In this study the behavior of transmission line cables in severe boundary layer winds is presented. Transverse and oblique wind incidences are tested and much emphasis is placed on making a correction in the variance of the response measured in the distorted model. Again the authors highlight the major difficulties in verifying the theoretical models of the aerodynamic behavior of transmission lines.

The authors present the aeroelastic modeling of the cables but state that in order that this is simulated in the models, the mass, drag forces, reduced frequency and aerodynamic damping should be simulated, together with the properties of the natural wind. To follow are some of the conditions the authors say should be met, the symbols used are explained as; L is the span, l the cable length, s the cable sag, m the mass per unit length, ρ_a the air density, C_D and d the cable's drag coefficient and diameter, f the cable's natural frequency, V the mean wind velocity and E the modulus of elasticity of the material. In the formulation the authors use these two subscripts (m) and (p) representing the model and the prototype respectively. The conventional modeling approach is as follows:

(a) geometrical similarity (λ_L =length scale)

The ratio between model and prototype dimensions should be preserved

$$\frac{L_m}{L_p} = \frac{s_m}{s_p} = \lambda_L \tag{2.5-31}$$

(b) mass modeling $(\lambda_m = \lambda_L^2)$

The authors argue that the mass ratio should be maintained the same for the model and prototype (Tanaka 1988). This being acceptable for consistence between forces of structure and the flow.

$$\left(\frac{m}{\rho_a L^2}\right)_m = \left(\frac{m}{\rho_a L^2}\right)_p \tag{2.5-32}$$

(c) drag force scaling

The drag force, F is in both model and prototype is given by

$$F = \tfrac{1}{2}\rho_a V^2 C_D dl \tag{2.5-33}$$

The ratio $\lambda_F = F_m / F_p$ can be written

$$(C_D d)_m = (C_D d)_p \lambda_L$$

The authors state that C_D and d are scaled jointly due to the difficulty in scaling down the cable diameter due to the dependence of C_D on the Reynolds number.

(d) reduced frequency

The relationship between length, time and velocity for a particular mode of vibration is based on the equality of the reduced frequency in the model and full scale. For the cable the frequency depends a great deal on its sag, which is the important characteristic dimension.

$$\left(\frac{fs}{V}\right)_m = \left(\frac{fs}{V}\right)_p . \tag{2.5-34}$$

(e) aerodynamic damping

The authors argue that the cable motion is dominated by aerodynamic damping, the structural damping, $\zeta_S \cong 0.0005$ (Bachmann et. al., 1995), being not so important, especially in strong winds. Aerodynamic damping being the retarding force which is derived from the relative motion between structure and air. This is given by the expression below (Vickery 1995 and Davenport 1988)

$$\zeta_{aj} = \left(\frac{C_D}{4\pi}\right)\left(\frac{\rho_a d^2}{m}\right)\left(\frac{V}{f_i d}\right). \tag{2.5-35}$$

So $(\zeta_a)_m = (\zeta_a)_p$, then

$$\lambda_L \frac{(C_D)_m}{(C_D)_p} = \frac{m_m}{m_p}.$$

(f) wind/gravity forces

this important to maintain and is given by

$$\lambda_V^2 \frac{(C_D d)_m}{(C_D d)_p} = \frac{m_m}{m_p}. \tag{2.5-36}$$

(g) velocity scaling (Froude number)

The authors state that for structures where resistance to deformation is influenced by the action of gravity, it is necessary to maintain Froude number, F_r, similarity, which requires that

$$\lambda_V^2 = \lambda_L. \tag{2.5-37}$$

(h) axial force scaling (Cauchy number)

To simulate the action of axial forces through the use of equivalent models, the Cauchy number, C_a, must be maintained constant in model and prototype

$$(Ed^2)_m = (Ed^2)_p \lambda_L^3 \tag{2.5-38}$$

They note that the force scaling should be given by $\lambda_F = \lambda_L^3$ and that the axial tension is not very important for this purpose (Armitt et. al., 1975) and therefore not simulated.

In conclusion the authors note that mean values measured from normal and distorted models agree well among themselves and with those predicted from theory. Also they conclude that the results obtained demonstrate the effect of turbulence in the dynamic response. Theory says that the variance of the response is directly proportional to the ratio between turbulence length scale

and the structure's span, and that is exactly what is demonstrated in their experiments by modifying the structure and leaving the wind characteristics unchanged.

Bartoli et al, 2006

The authors present an analysis of the main characteristics of the dynamic behavior of cable under wind loading in both laminar and turbulent flow. The experimental model of the cable was built using 48 cylinders, each one with a diameter of 40mm and a length of 40mm.

The authors give an elaborated logged data to obtain the spectral density function. In Figs (2.5-4,a-d) we have the spectra obtained for the axial load cells and the overall drag force cells, both in the laminar and in turbulent flow, for a wind speed of about 16m/s.

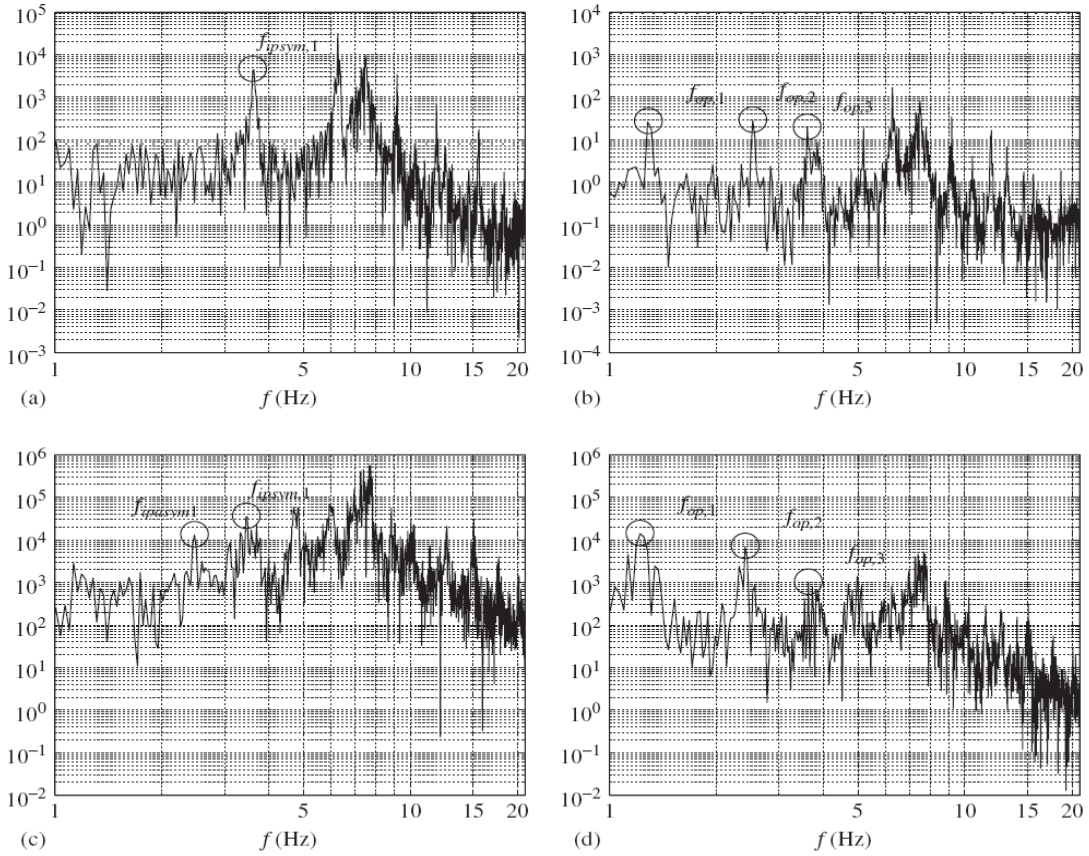

Figure 2.5-4, Density spectra with mean wind speed U about 16m/s: (a) laminar flow, axial load cell; (b) laminar flow, drag force cell; (c) turbulent flow, axial load cell; (d) turbulent flow, drag force cell, Bartoli, 2006.

It is seen that the figure shows several peaks which are in agreement with the frequencies of the natural modes of the cable that can be found by analytical analysis, as in Irvine M (1981). In particular, for out-of-plane motion, frequencies are given by

$$f_{op,n} = \frac{n}{2l}\sqrt{\frac{H}{m}}, \qquad n=1, 2, 3, \ldots \tag{2.5-39}$$

For asymmetric in-plane motion (where no overall additional tension is induced) by

$$f_{ipasym,n} = \frac{n}{l}\sqrt{\frac{H}{m}}, \qquad n=1, 2, 3, \ldots \tag{2.5-40}$$

and for symmetric in-plane modes, the frequencies are found by solving:

$$\tan\left(\frac{f_{ipasym,n}l}{4\pi(H/m)^2}\right) = \frac{f_{ipasym,n}l}{4\pi(H/m)^2} - \frac{4}{\lambda^2}.\left(\frac{f_{ipasym,n}l}{4\pi(H/m)^2}\right)^3, \tag{2.5-41}$$

where m is the mass per unit length of the cable, H is the horizontal component of cable tension, l is the distance between the supports and λ^2 is the Irvine's parameter, which account for geometric and elastic effect, defined as

$$\lambda^2 = \left(\frac{mgl}{H}\right)^2 l \Big/ \left(\frac{HL_e}{EA_0}\right), \tag{2.5-42}$$

where $L_e \cong l(1+8(f/l)^2$, f/l is the sag to span ratio, A_0 is the uniform cross-sectional area, E is the Young's modulus. The authors found out that for the case in study $\lambda^2 = 256\pi^2$ and give the first three analytical frequencies for each kind of motion of the cable as reported in table (2.5-1) below:

Table 2.5-1, First three natural frequencies of cable motion.

Motion	f_1 (Hz)	f_2 (Hz)	f_3 (Hz)
Out-of-plane	1.22	2.43	3.65
In-plane: antisymmetric	2.43	4.86	7.30
In-plane: symmetric	3.48	5.97	8.45

In conclusion the authors see that their data permits to estimate the drag coefficient of the cable as a whole and to evaluate the natural frequencies which were compared with analytical ones. They also formulated a numerical model of the cable, assuming a non linear geometrical behavior. They reason that a good agreement in terms of mean values was seen between the experimental data and the numerical ones, and that further experimental tests should be done to check the influence of the sag to span ratio with regards to the stochastic characteristics of the response.

2.6 Existing Problems

The theory of bundled conductors is not well understood and many assumptions continue to be the order of the day. As shown in his review paper, Starossek (1994) outlines great need to make the gained findings more easily accessible to the design engineer since there is no great understanding especially in the area of damping and this has resulted in many assumptions being made.

The aeolian vibrations due to laminar wind on conductors cause small vibration amplitudes which from records of natural vibrations show that the phenomenon is far from having a nice sinusoidal form. However this motion of the conductor has no detrimental effect along the span but if the motion is constraint, e.g., at the suspension clamp, a singular point is created.

It is at such a location that conductor curvatures are much larger than in the free span. Interstrand microslip amplitude increases, small cracks are generated and some propagate upto complete strand failures caused by fatigue. Similarly at damper, marker or spacer clamps a similar phenomenon is experienced thus we aim to tackle this problem at hand.

Spacer dampers prove to be useless if placed at places which result in the occurrence of a node and careful attention should be taken when selecting the deployment configurations.

Solving the eigenvalue problem for the bundled conductors with spacer dampers gives rise to formulating an algebraic transcendental EVP, which however presents several numerical difficulties.

2.7 Literature Review Summary and Conclusion

The literature review has shown different modeling approaches that can be used to design safe transmission line structures but as that is not enough it is also quite clear that there is a lack of published information in as far as conductor damping and usage is concerned. Many electricity supply bodies assume the distances of separation for the spacers and just hope that it works with no proper literature available to assist them in coming up with the most efficient damper deployment (Stanford G et. al, 2003).

It is seen (A. Simpson et. al., 1984) that in the process of spacer damper design there is no substitute for a very complete modal analysis in which all natural frequencies, modes and logarithmic decrements are computed across the frequency range of interest. It then becomes quite clear that with conventional subspan lengths and properly designed semi-rigid spacer dampers, Aeolian vibration may be controlled successfully, provided that the conductors are not unduly highly tensioned.

With work done by Hagedorn et. al., (2004), one can say that the new approach established in the solution of transcendental EVP gives a very good engineering solution for transmission line bundled conductors. The solution of the EVP gives the necessary input data for applying the energy balance.

It was also seen that the frequency-domain calculations give basically similar results to those of the time-domain and also for a freely hanging cable, the frequency-domain calculation compares well with the time-domain simulation. Due to numerical integration problems, the time-domain solution needs some kind of smoothing or filtering of numerically excited high-frequency components.

3.0 STATEMENT OF RESEARCH PROBLEM:

3.1 Research Statement

The detailed literature survey has revealed that different authors have proposed various methods of conductor modeling, some with the shortcomings stated in the literature review summary and conclusions. Following these findings, the statement of the research problem is stated as:

The dynamic response of the system of bundled conductors and damper deployment is not well understood in the design of overhead transmission lines.

3.2 Research Objectives

The first objective is to establish a suitable form of analytical equations to describe the motion of a bundled system of conductors induced to vibrations.

The second objective is to come up with the relevant solutions that give a description of frequencies and mode shapes of the bundled onductor vibration problem.

Finally, numerical parametric studies will be conducted and these are validated with the analytical solutions thus achieved from the above objectives, together with other published results.

3.3 Methodology

Firstly the theoretical formulations are solved and this is done by the use of available algebra systems, such as Matlab and excel. Also a numerical study based on Finite Element Modeling (FEM) is set up to tackle the bundled conductor vibration problem. The numerical analysis will be performed using the finite element analysis package, Abaqus. Results from the above analysis are compared with available published results, as a means of validating them.

4.0 THEORY OF DISTRIBUTED-PARAMETER SYSTEMS:

In order to understand the theory behind the vibrating cable and thus be able to integrate this into systems of different bundled cable arrangements, this chapter spends much time in developing the analytical equations of motion used in the study. Most of the work is derived from previous efforts by Timoshenko (1921) and some contributions by Palm III (2006).

Flexibility of structural components arises when the mass and stiffness properties are modeled as being distributed throughout the spatial definition of the component. The particular system of study having an infinite number of degrees of freedom, and hence an infinite number of natural frequencies which increases concern about resonance in design. Since we are looking at a distributed or continuous system it is impossible to identify discrete masses or dampers therefore we consider the continuous distribution of the mass, damping, and elasticity and assume that each of the infinite number of points of the system can vibrate. Discrete system modeling gives rise to ordinary differential equations as the main governing equations, of which these are quite easy to solve. Contrary to this continuous system models give rise to governing equations having partial differential equations which are more difficult to solve (a nightmare to many engineers). This chapter aims to come up with the governing equations (equation of motion) for the vibration system. Chapter 4.1 will deal with the formulation of the equation of motion and chapter 4.2 will look at the solution of the equations in term of modes and natural frequencies. Chapter 4.3 will investigate an analysis example that will help in validating the numerical results obtained. A brief conclusion sums up the findings of the chapter.

4.1 Formulating the Cable Equation of Motion

Considering the cable if figure (4.1-1), the following assumptions are made: the cable is stretched along the x-axis to a length L and that its ends are fixed at $x = 0$ and at $x = L$. We want to obtain an equation that can be solved for the deflection y at any point x, as a function of time t. It is seen that y is a function of both x and t that describes the shape of the cable at any time and thus we must use the partial derivative of y with respect to x and t.

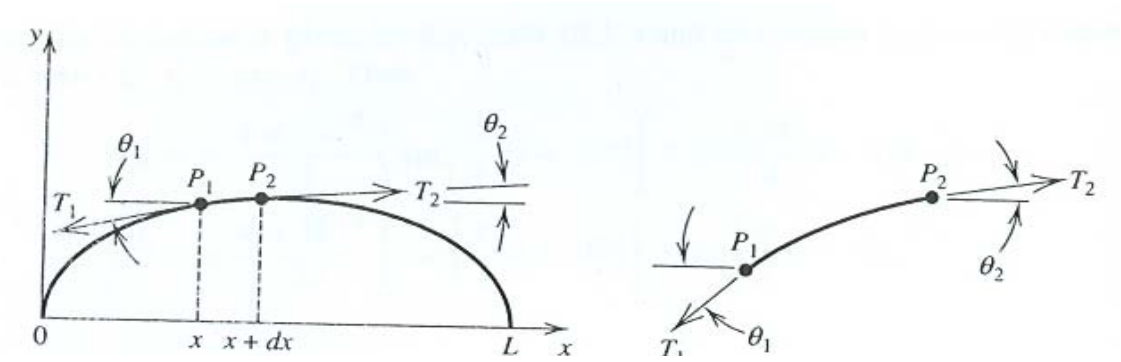

Figure 4.1-1, A model of a vibrating cable.

Assumptions:

mass per unit length, v of the cable is constant.

cable is perfectly elastic, it does not offer any existence to bending.

tension produced by stretching the cable is so large that the extent of gravity is ignored.

motions of the cable are only vertical , and they are small. Slope is small.

Considering the infinitesimal cable element of length dx shown in figure (4.1-1), the tension forces T_1 and T_2 at points P_1 and P_2 result from the cable being stretched between its two end points. We might or might not know the values of T_1 and T_2. The cable has a mass per unit length m, so the mass of an infinitesimal element of length dx is mdx. Because the cable does not move horizontally the sum of forces in the x-direction must be zero. This gives:

$$T_1 \cos\theta_1 - T_1 \cos\theta_1 = 0$$

If we define $T = T_1 \cos\theta_1$, then we see that $T = T_2 \cos\theta_2$ also.

Summing forces in the y direction, we obtain

$$mdx\frac{\partial^2 y}{\partial t^2} = T_2 \sin\theta_2 - T_1 \sin\theta_1$$

where the acceleration $\partial^2 y/\partial t^2$ is taken to be evaluated at some point between x and $x + dx$. Dividing both sides by T gives

$$\frac{m}{T}dx\frac{\partial^2 y}{\partial t^2} = \frac{T_2 \sin\theta_2}{T} - \frac{T_1 \sin\theta_1}{T}$$

Since $T = T_1 \cos\theta_1 = T_2 \cos\theta_2$, this becomes

$$\frac{m}{T}dx\frac{\partial^2 y}{\partial t^2} = \frac{T_2 \sin\theta_2}{T_2 \cos\theta_2} - \frac{T_1 \sin\theta_1}{T_1 \cos\theta_1} = \tan\theta_2 - \tan\theta_1 \qquad (4.1\text{-}1)$$

But $\tan\theta_1$ and $\tan\theta_2$ are the slopes of the cable at x and $x + dx$:

$$\tan\theta_1 = \left(\frac{\partial y}{\partial x}\right)\Big|_x \qquad \tan\theta_2 = \left(\frac{\partial y}{\partial x}\right)\Big|_{x+dx}$$

Substituting these expressions into Equation (4.1-1) and dividing by dx, we obtain

$$\frac{m}{T}\frac{\partial^2 y}{\partial t^2} = \frac{1}{dx}\left[\left(\frac{\partial y}{\partial x}\right)\Big|_{x+dx} - \left(\frac{\partial y}{\partial x}\right)\Big|_x\right] \qquad (4.1\text{-}2)$$

The expression on the right-hand side becomes $\partial^2 y/\partial x^2$ if we let $dx \to 0$. Thus the model becomes

$$\frac{m}{T}\frac{\partial^2 y}{\partial t^2} = \frac{\partial^2 y}{\partial x^2} \qquad (4.1\text{-}3)$$

Defining the constant c such that $c^2 = T/m$, the model becomes

$$\frac{\partial^2 y}{\partial t^2} = c^2\frac{\partial^2 y}{\partial x^2} \qquad (4.1\text{-}4)$$

Equation 4.1-3 above is similar to the second part of equation 2.5-13 given earlier in the literature review and also known as the wave equation.

4.2 Modes and Natural Frequencies

In this section the technique of separation of variables is used to solve the cable equation of motion. There are vast approaches to the cable equation solution but this was chosen because of its vast merits as discussed in the section to follow. The solution leads to a natural way to modal analysis and the concepts of mode shapes and natural frequencies for distributed-parameter systems (Inman, 2001). The solution procedures reviewed here are detailed also in Boyce and DiPrima (1997). The following presentation contains work done by Palm III (2006) and Irvine (1974).

The displacement $w(x,t)$ is assumed that it can be written as a product of two functions, one depending only on x and the other depending only on t. Thus

$$w(x,t) = X(x)T(t) \tag{4.2-1}$$

Substitution of this separated form into the string equation yields

$$c^2 X''(x)T(t) = X(x)\ddot{T}(t) \tag{4.2-2}$$

where

$X''(x)$ denotes total differentiation with respect to x and $\ddot{T}(t)$ denotes total differentiation with respect to time, t.

Eq (4.2.2) can be arranged further and becomes,

$$\frac{X''(x)}{X(x)} = \frac{\ddot{T}(t)}{c^2 T(t)} \tag{4.2-3}$$

Because the left-hand side is a function only of t and the right-hand side is a function only of x, the only way this equation can be true is if each side is equal to the same constant, which is denoted by α. Therefore

$$\frac{X''(x)}{X(x)} = \frac{\ddot{T}(t)}{c^2 T(t)} = \alpha \tag{4.2-4}$$

Leading us to two ordinary differential equations:

$$\ddot{T} - c^2 \alpha T = 0 \tag{4.2-5}$$

$$X'' - \alpha X = 0 \tag{4.2-6}$$

4.2.1 Applying boundary conditions:

Assuming the end points to be fixed, which is mainly the case on dead spans, we have these specific boundary conditions, thus take $u(x,t) = u(L,t)$, where L is the length of the cable. Referring to the assumed solution (Equation 4.1.3) this implies that

$$u(0,t) = X(0)T(t) = 0 \qquad \text{for all } t \tag{4.2-7}$$

and

$$u(0,t) = X(L)T(t) = 0 \qquad \text{for all } t \tag{4.2-8}$$

A possible solution to the above equation is $X(t) = 0$ for all t, but this also implies that $u(x,t) = 0$ for all t which is trivial. So Equations (4.2-7) and (4.2-8) yield:

$$X(0) = 0 \qquad \text{and} \qquad X(L) = 0$$

To obtain α, three cases are considered:

1. $\alpha = 0$

   For this case the solution of Equation (4.2-6) is $X(x) = ax + b$ where a and b are constants. Equation (4.2-9) then gives $a = b = 0$, which is a trivial solution $X(x) = 0$, for all x and implies that $u(x,t) = 0$ for all x.

2. $\alpha > 0$

   Taking $r^2 = \alpha$, Equation (4.2-6) becomes $X'' - r^2 X = 0$, which has the solution

   $X(x) = Ae^{rx} + Be^{-rx}$

   Now applying Equation (4.2-9), this gives $A = B = 0$, and thus again $X(x) = 0$ for all x.

3. $\alpha < 0$

   Taking $r^2 = -\alpha$, Equation (4.2-6), becomes $X'' + p^2 X = 0$ which has the solution $X(x) = A\cos px + B\sin px$ which implies the solution to the wave equation is of the form:

$$u(x,t) = (A\cos px + B\sin px)T(t) \tag{4.2-9}$$

Now applying the specific boundary conditions given by Equation (4.2-9), we obtain $X(x) = A = 0$ and $X(L) = B\sin pL = 0$. If $B = 0$, the solution is again trivial, $F(x) = 0$. So the only possibility left is $\sin pL = 0$ implies that

$$p = \frac{n\pi}{L} \qquad n \text{ integer} \tag{4.2-10}$$

It is seen here that there are an infinite number of solutions for $X(x)$, all of the form

$$X_n = B_n \sin\left(\frac{n\pi}{L}x\right) \qquad n \text{ integer} \tag{4.2-11}$$

which can easily be expressed as

$$X_n(x) = \sin\left(\frac{n\pi}{L}\right) \qquad n=1, 2, 3\ldots \tag{4.2-12}$$

The values $p = \frac{n\pi}{L}$ are called the spatial frequencies because they describe the wave shape of the cable. Thus the wave shape is sinusoidal, $\sin n\pi x/L$ and the spatial wavelength is $2L/n$.

If the left-hand end of the cable is free to move, so that $u(0,t) \neq 0$ the boundary conditions of Equation (4.2-9) do not apply and so the constant $A = 0$, therefore Equation (4.2-10) gives the general solution. One can expand the above findings and consider the motion of the cable in all planes thus we consider the out-of-plane and the in-plane motions of which some of the assumptions made earlier do not apply.

4.2.2 The Out-of-Plane Motion

The swinging modes being the easiest to analyze will be considered first. By writing $y(x,t) = \tilde{y}(x)e^{i\omega t}$, where ω is the natural circular frequency of vibration (equation 4.1.3) is reduced to

$$T\frac{d^2\tilde{y}}{dx^2} + m\omega^2\tilde{y} = 0 \tag{4.2-13}$$

Now the boundary conditions being $\tilde{y}(0) = \tilde{y}(L) = 0$, we have the natural frequencies and associated modes as

$$\omega_n = \frac{n\pi}{L}\left(\frac{T}{v}\right)^{1/2}, \qquad n=1,2,3\ldots \tag{4.2-14}$$

$$\tilde{y}_n = A_n \sin\frac{n\pi x}{L}, \qquad n=1,2,3\ldots \tag{4.2-15}$$

n signifying the first, second, third modes, respectively, and so on. The frequency of the first out-of-plane mode is the lowest of any given flat-sag suspended cable.

4.2.3 The In-Plane motion

This is obtained in a similar manor as above. The first part of the equation of motion given by equation 2.5-12 is evaluated. Similarly we use the substitution $w(x,t) = \tilde{w}(x)e^{i\omega t}$ and the equation reduces to

$$T\frac{d^2\tilde{w}}{dx^2} + m\omega^2\tilde{w} = 0 \tag{4.2-16}$$

The cable equation is reduced to a statement of geometric compatibility after substituting $u(x,t) = \tilde{u}(x)e^{i\omega t}$ and yields

$$\frac{d\tilde{u}}{dx} + \frac{dz}{dx}\frac{d\tilde{w}}{dx} = 0 \tag{4.2-17}$$

Now we input the boundary conditions $\tilde{w}(0) = \tilde{w}(L/2) = 0$ to equations (4.2-16) and (4.2-17) and we obtain the natural frequencies and modal components of the antisymmetric in-plane modes. It follows that

$$\omega_n = \frac{2n\pi}{L}\left(\frac{T}{m}\right)^{1/2} \tag{4.2-18}$$

where n = 1, 2, 3, … signify natural frequencies of the first, second, third antisymmetric modes and so on. The vertical modal components are given by

$$\tilde{w} = A_n \sin\left(\frac{2n\pi x}{L}\right), \quad n = 1, 2, 3, ... \tag{4.2-19}$$

Equation (4.2-17) gives the longitudinal components which are symmetric since dz/dx is zero at midspan and the product $dz/dx.d\tilde{w}/dx$ changes sign at midspan. The value of $\tilde{u}_n$ is given after substitution, integration, and rearrangement by

$$\tilde{u}_n = -\frac{1}{2}\left(\frac{mgl}{T}\right)A_n\left\{\left(1-\frac{2x}{L}\right)\sin\left(\frac{2n\pi x}{L}\right)+\frac{1-\cos(2n\pi x/L)}{n\pi}\right\}, \qquad (4.2\text{-}20)$$

and as seen earlier A_n is the amplitude of the vertical component of the nth antisymmetric in-plane mode.

As the cable becomes flatter (as $mgL/T \to 0$) the amplitude of the longitudinal components become very small. Figure (4.2-1) shows some of peculiar properties displayed by these components because the maximum displacement occurs at the quarter-span points and not at midspan in the case of the first modal component (the displacement is a local minimum at midspan). For the second component the slope and displacement are also both zero at midspan. Irvine (1974) argues that this pattern repeats itself for the higher modes. Thus

$$\tilde{u}_{n,\max}/A_n = (mgL/T)\{1-(1/2-1/\pi)/n\}/2, \qquad (4.2\text{-}21)$$

from the above equation the peak longitudinal displacement is no more than half the vertical component as the limit applicability is reached in the flat-sag assumption.

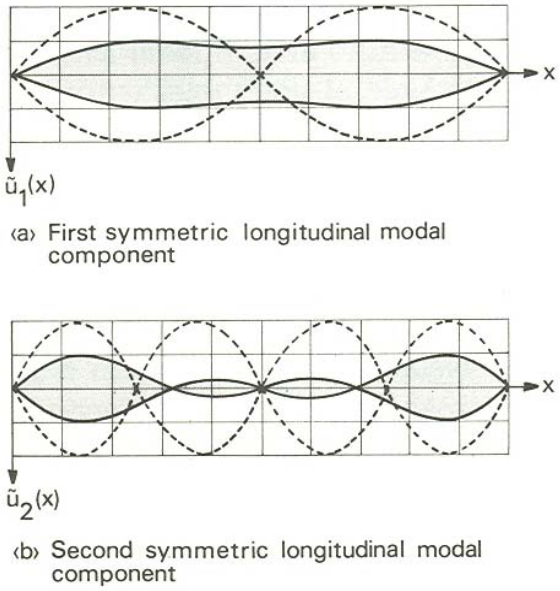

Figure 4.2-1, Longitudinal components and associated vertical components (in-dotted) of the two antisymmetric in-plane modes, (Irvine , 1981).

Luongo and Rega (1978) give a comparative numerical study that suggests that the essential features of the antisymmetric in-plane modes have been preserved with one exception. Thus even though the overall, or mean, additional tension is zero, at the scale of the cable element it is nonzero. Luongo and Rega indicate that an antisymmetric distribution of additional tension $\tilde{\tau}(x)$ is possible, so that $\int_0^L \tilde{\tau}(x)dx = 0$. The task to demonstrate this involves the use of the longitudinal equation of motion below,

$$\frac{d\tilde{\tau}}{dx} = -\left(T\frac{d^2\tilde{u}}{dx^2} + m\omega^2\tilde{u} \right), \tag{4.2-22}$$

Removing time from the above equation, substituting, integrating and meeting of the requirement of antisymmetry in $\tilde{h}(x)$ yields

$$\frac{\tilde{\tau}_n(x)}{T} = -\frac{mgL}{T}\frac{A_n}{L}\left\{ n\pi\left(1-\frac{2x}{L}\right) + \sin\left(\frac{2n\pi x}{L}\right)\right\}. \tag{4.2-23}$$

This latter case is misleading, for if we use results for the symmetric in-plane modes and compare peak additional tensions on the basis of the same amplitude of vibration in both the

antisymmetric and symmetric in-plane modes, the result is a ratio of magnitude $(mgL/T)^2 n\pi\{1-\sec(\omega/2)\}/\omega^2$. Now comparing the first antisymmetric and symmetric mode for a cable of deep profile, the ratio of additional tensions is about 0.22, which indicates that this source of additional tension is not profound importance.

Considering the symmetric in-plane modes, additional tension is induced, so that the first part of equation (2.5-12) can be written as

$$T\frac{d^2\widetilde{w}}{dx^2}+m\omega^2\widetilde{w}=\frac{mg}{T}\widetilde{\tau} \tag{4.2-24}$$

Now taking a solution that satisfies zero boundary conditions is

$$\widetilde{w}=\frac{\widetilde{h}}{\omega^2}(1-\tan\frac{\omega}{2}\sin\omega x-\cos\omega x), \tag{4.2-25}$$

where

$\widetilde{\mathbf{w}}=w/(mgL^2/T)$, $\mathbf{x}=x/L$, $\widetilde{\mathbf{h}}=\widetilde{h}/T$, and $\boldsymbol{\omega}=\omega L/(T/m)^{1/2}$, and its value specifies the particular (symmetrical) vertical modal component. Now using the first order of cable equation $\widetilde{\mathbf{h}}$ can be eliminated and what remains is the following transcendental equation from which the natural frequencies of the symmetric in-plane modes can be found:

$$\tan\frac{\boldsymbol{\omega}}{2}=\frac{\boldsymbol{\omega}}{2}-\frac{4}{\lambda^2}\left(\frac{\boldsymbol{\omega}}{2}\right)^3, \tag{4.2-26}$$

where, $\lambda^2=(mgL/T)^2 L/(TL_e/EA)$.

The above equation is of fundamental importance in the theory of cables. The first eight symmetric in-plane modes are tabulated in table (4.2-1) below, for a wide range of values of the parameter involving cable elasticity and geometry.

Table 4.2-1, *Natural frequencies of the first eight symmetric in-plane modes as a function of* λ^2 *,(Irvine, 1981).*

λ^2	ω_1/π	ω_2/π	ω_3/π	ω_4/π	ω_5/π	ω_6/π	ω_7/π	ω_8/π
∞	2.86	4.92	6.94	8.95	10.96	12.97	14.97	16.98
$256\pi^2$	2.86	4.91	6.93	8.93	10.93	12.91	14.81	$16.0\dot{0}$
$196\pi^2$	2.85	4.91	6.92	8.92	10.91	12.81	$14.0\dot{0}$	15.15
$144\pi^2$	2.85	4.90	6.91	8.90	10.81	$12.0\dot{0}$	13.15	15.05
$100\pi^2$	2.85	4.89	6.89	8.80	$10.0\dot{0}$	11.15	13.04	15.02
$64\pi^2$	2.84	4.87	6.79	$8.0\dot{0}$	9.14	11.04	13.02	15.01
$36\pi^2$	2.82	4.78	$6.0\dot{0}$	7.14	9.04	11.02	13.01	15.01
$16\pi^2$	2.74	$4.0\dot{0}$	5.12	7.03	9.01	11.01	13.00	15.00
100	2.60	3.48	5.05	7.01	9.01	—	—	—
80	2.48	3.31	5.04	7.01	9.01	—	—	—
60	2.29	3.18	5.03	7.01	—	—	—	—
$4\pi^2$	$2.0\dot{0}$	3.09	5.02	7.01	—	—	—	—
20	1.61	3.04	5.01	7.00	—	—	—	—
10	1.35	3.02	5.00	—	—	—	—	—
8	1.28	3.01	—	—	—	—	—	—
6	1.22	—	—	—	—	—	—	—
4	1.15	—	—	—	—	—	—	—
2	1.08	—	—	—	—	—	—	—
1	1.04	—	—	—	—	—	—	—
0	$1.0\dot{0}$	$3.0\dot{0}$	$5.0\dot{0}$	$7.0\dot{0}$	$9.0\dot{0}$	$11.0\dot{0}$	$13.0\dot{0}$	$15.0\dot{0}$

The following figures 4.2-2 and 4.2-3 will assist in the following discussion.

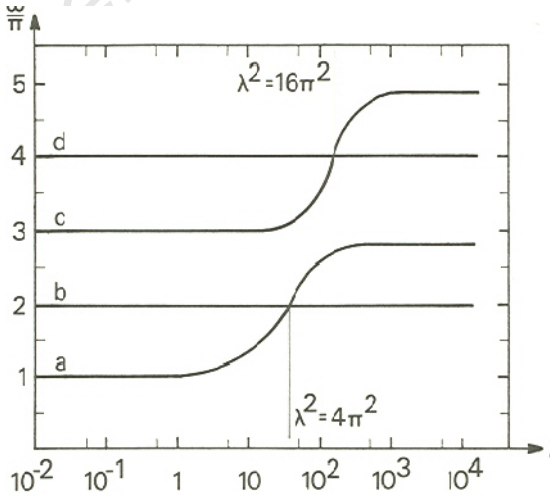

Figure 4.2-2, General dimensionless curves for the first four natural frequencies of a flat-sag suspended cable: (a) first symmetric in-plane mode, (b) first antisymmetric in-plane mode, (c) second symmetric in-plane mode, (d) second antisymmetric in-plane mode, (Irvine, 1981).

When λ^2 is very large the cable may be assumed inextensible, and (4.2-26) becomes

$$\tan\frac{\boldsymbol{\omega}}{2}=\frac{\boldsymbol{\omega}}{2}. \tag{4.2-27}$$

The above equation was first given by Rohrs in 1851. The roots are given quite accurately by $\boldsymbol{\omega}_n=(2n+1)\pi\left\{1-4/((2n+1)^2\pi^2)\right\}$, $n=1, 2, 3, \ldots$

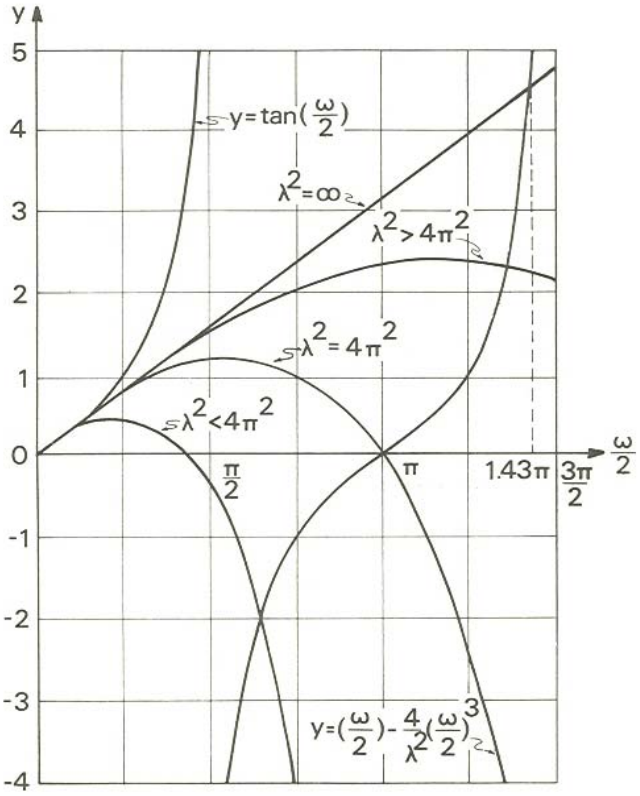

Figure 4.2-3, Graphical solution for first nonzero root of equation (4.2-27), (Irvine, 1981).

As the cable profile approaches that of a taut string, a limiting value of λ^2 occurs. The roots corresponding to the frequencies of the symmetric modes of the taut string, namely, $\boldsymbol{\omega}_n=(2n-1)\pi$, $n=1, 2, 3, \ldots$

Thus the condition of inextensibility causes a shift of almost 2π in the roots obtained from the frequency equation governing the symmetric modes of the taut string, since the first non-zero

root of equation (4.2-26) lies between $\pi/2$ and 1.43π, the second root lies between $3\pi/2$ and 2.46π, and so on: the actual values depend on λ^2.

In the case of the first modes three important ranges may be established:

1. If $\lambda^2 < 4\pi^2$, the frequency of the first symmetric mode is less than the frequency of the first antisymmetric mode. The vertical component of the symmetric mode has no internal nodes figure (4.2-4).
2. If $\lambda^2 = 4\pi^2$, the frequencies of these modes are equal. The vertical modal component is tangential to the profile at the supports. This value of λ^2 gives the first modal crossover.
3. If $\lambda^2 > 4\pi^2$, the frequency of the symmetric mode is now greater, and two internal nodes to appear.

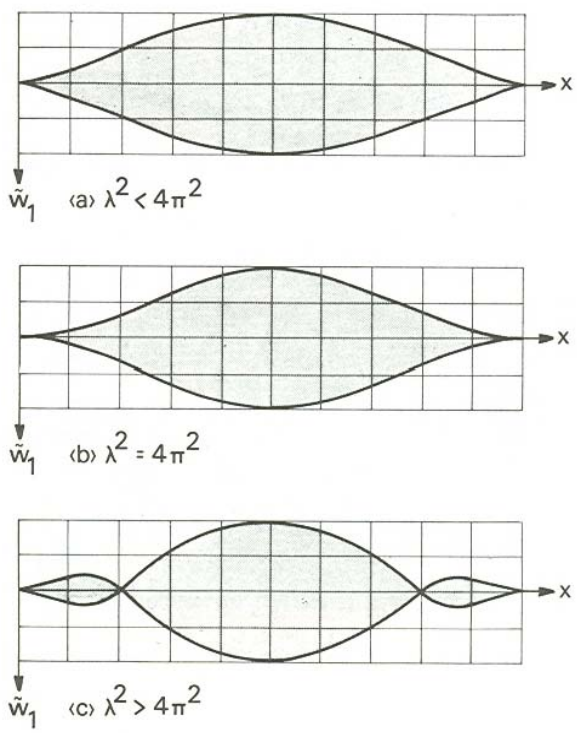

Figure 4.2-4, Possible forms for the vertical component of the first symmetric in-plane mode, (Irvine,1981).

Now figure (4.2-5) shows results by Ramberg and Griffin (1977) giving a brief comparison of the theories employed for some similar study they conducted.

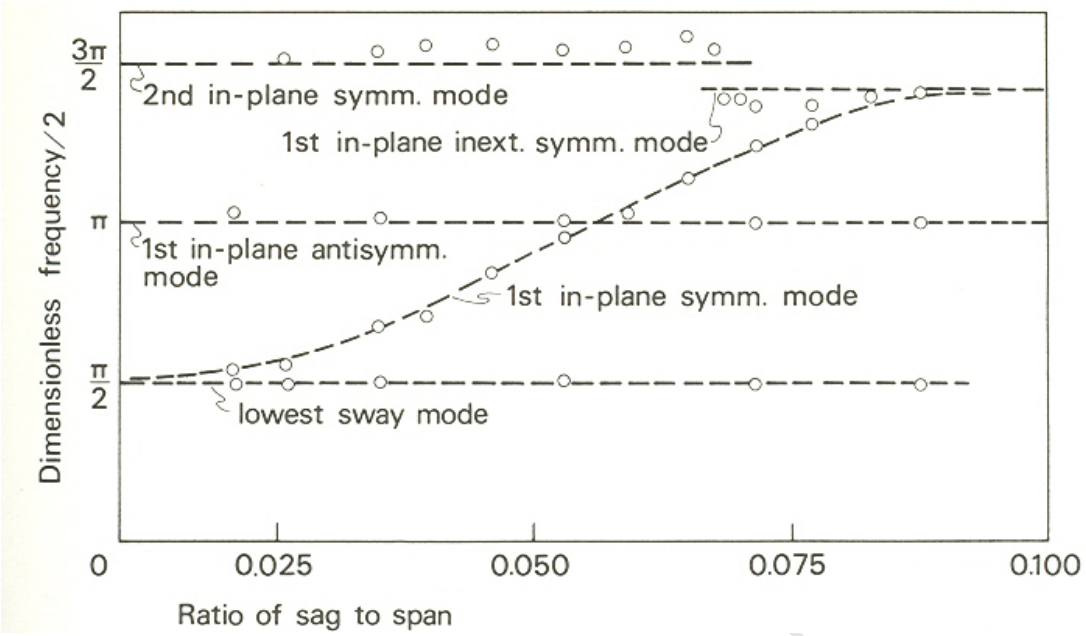

Figure 4.2-5, Ramberg and Griffin's comparison of the present theory with the experimental results of Richardson for a particular model cable, (Irvine, 1981).

4.2.4 Extension to Cables with Deep Profile.

Saxon and Cahn (1953) analyzed the in-plane modes of vibration of deep-sag cables by using an ingenious approximate method. The analysis is very involving and so this chapter seeks to list the asymptotic solutions for natural frequencies and compare them with known limits and existing experimental results.

Now for a catenary of length l hanging between two level supports the angle of inclination to the horizontal at the supports is given by

$$\tan\psi_0 = \frac{4d/l}{\left\{1-(2d/l)^2\right\}}, \tag{4.2-28}$$

where s is the sag. The span is

$$L = \frac{l \sinh^{-1}(\tan\psi_0)}{\tan\psi_0}. \tag{4.2-29}$$

Now defining a new dimensionless frequency according to the equation

$$\boldsymbol{\omega}_*^2 = \frac{\omega^2 l}{(2g \tan\psi_0)} \tag{4.2-30}$$

we can then write the following frequency equations to be written:

1. for the antisymmetric in-plane modes, where by definition the modal component perpendicular to the cable is odd about midspan and the tangential component is even,

$$\tan\left(\boldsymbol{\omega}_* A + \frac{B}{\boldsymbol{\omega}_*}\right) = -\frac{C}{\boldsymbol{\omega}_*}, \tag{4.2-31}$$

2. for the symmetric in-plane modes, in which the perpendicular modal component is even and the tangential component is odd,

$$\tan\left(\boldsymbol{\omega}_* A + \frac{B}{\boldsymbol{\omega}_*}\right) = \frac{\boldsymbol{\omega}_*}{\mathbf{D}}, \tag{4.2-32}$$

where $A(\psi_0) = \int_0^{\psi_0} \sec^{3/2}\psi d\psi$, $B(\psi_0) = 11/8 \int_0^{\psi_0} (1 + (1/44)\tan^2\psi)\cos^{3/2}\psi d\psi$,

$C(\psi_0) = \psi_0 \cos^{5/2}\psi_0 / (\cos\psi_0 + \psi_0 \sin\psi_0)$, and $D(\psi_0) = \cos^{5/2}\psi_0 / \sin\psi_0$.

The equations in the above form are similar to the previous results. Thus when ψ_0 is small, (4.2-31) and (4.2-32) become $\tan\boldsymbol{\omega}/2 \approx 0$ and $\tan\boldsymbol{\omega}/2 \approx \boldsymbol{\omega}/2$ because $\boldsymbol{\omega}_*\psi_0 \to \boldsymbol{\omega}/2$.

Each of these equations is transcendental in $\boldsymbol{\omega}_*$, and, if $\boldsymbol{\omega}_*$ is sufficiently large for terms of order $1/\boldsymbol{\omega}_*^2$ to be ignored, then we have

$$\boldsymbol{\omega}_{*n} \approx \frac{n\pi}{A}\left\{1-\frac{A(B+C)}{(n\pi)^2}\right\}, \qquad n=1, 2, 3, ..., \tag{4.2-33}$$

as the frequencies of the antisymmetric modes, and

$$\boldsymbol{\omega}_{*n} \approx \frac{(n+1/2)\pi}{A}\left\{1-\frac{A(B+D)}{(n+1/2)^2\pi^2}\right\}, \qquad n=1, 2, 3, ..., \tag{4.2-34}$$

for the symmetric modes.

Table (4.2-2) below shows the first three antisymmetric modes and first two symmetric modes. Upper row values are evaluated from flat-sag theory (equations (4.2-18) and (4.2-27)). It is quite clearly seen that agreement is excellent when ψ_0 is small and up to a sag of 1:4, it is still good. It is seen that the upper two rows for the symmetric modes are suspect on account of the neglect of elasticity.

Table 4.2-2, Frequencies of the first five in-plane modes of a deep-sag cable, (Irvine, 1981).

ψ_0	d/L	Antisymmetric			Symmetric	
		ω_{*1}/π	ω_{*2}/π	ω_{*3}/π	ω_{*1}/π	ω_{*2}/π
5°	0.022	11.42 (11.36)	22.86 (22.73)	34.31 (34.09)	16.38 (16.25)	28.13 (28.0)
10°	0.044	5.64 (5.68)	11.35 (11.36)	17.04 (17.04)	8.14 (8.12)	13.98 (13.97)
20°	0.088	2.70 (2.76)	5.52 (5.54)	8.30 (8.31)	3.96 (4.00)	6.82 (6.85)
30°	0.13	1.68 (1.78)	3.50 (3.56)	5.29 (5.34)	2.52 (2.55)	4.36 (4.39)
40°	0.18	1.13 (1.26)	2.44 (2.52)	3.71 (3.79)	1.76 (1.81)	3.06 (3.11)
50°	0.23	0.79 (0.95)	1.76 (1.88)	2.70 (2.82)	1.27 (1.35)	2.23 (2.32)
60°	0.29	0.54	1.27	1.95	0.91	1.61
70°	0.35	0.34	0.87	1.35	0.61	1.11
75°	0.38	0.25	0.68	1.07	0.47	0.88
80°	0.42	0.15	0.50	0.80	0.34	0.65
82°	0.44	0.12	0.42	0.68	0.28	0.55
84°	0.45	0.075	0.34	0.56	0.22	0.45
86°	0.47	0.031	0.25	0.43	0.15	0.34
88°	0.48	0.021	0.15	0.27	0.074	0.21

Note: Values in brackets were obtained with the flat-sag theory.

As the sag becomes particularly pronounced, the theoretical results are likely to be in error, because we are at this point severely stressing the assumption of $\boldsymbol{\omega}_*$ made in the solution formulation.

4.2.5 The Linearized Dynamic Response of a Flat-Sag Suspended Cable.

We take as the equation of motion

$$\frac{\partial^2 \mathbf{w}}{\partial \mathbf{x}^2} - \frac{\partial^2 \mathbf{w}}{\partial \mathbf{t}^2} = \boldsymbol{\tau}(\mathbf{t}) + \mathbf{p}(\mathbf{x},\mathbf{t}), \tag{4.2-35}$$

where

$$\mathbf{h(t)} = \lambda^2 \int_0^1 \mathbf{w(x,t)dx} \tag{4.2-36}$$

the objective now is to construct a general solution for $\mathbf{w}$ and $\boldsymbol{\tau}$ by superposing modal responses. The new dimensionless terms introduced are $t = t(T/m)^{1/2}/L$ and $\mathbf{p} = p/mg$. Boundary conditions being the zero additional displacements at each end of the cable, and initial conditions may if necessary be prescribed.

Now rather than applying a distributed dynamic load, the forcing is considered to be provided by displacements or accelerations imposed at the cable ends. Damping is included later.

The main interest is with the in-plane dynamic response and in particular with the additional tension generated. Cases with $\mathbf{p(x,t)}$ even about the midspan will be confined to.

The solution to (4.2-35) may be written as (Irvine H.M. et. al., 1976)

$$\mathbf{w(x,t)} = \sum_n \xi_n(\mathbf{x})\phi_n(\mathbf{t}), \tag{4.2-37}$$

where $\xi_n(\mathbf{x})$ is the vertical component of the nth symmetric in-plane mode of vibration and $\phi(\mathbf{t})$ is the associated normal coordinate. For convenience we reiterate that ξ_n is the solution of

$$\frac{d^2\xi_n}{d\mathbf{x}^2} + \boldsymbol{\omega}_{\mathrm{n}}^2\xi_n = \boldsymbol{\tau}_n, \tag{4.2-38}$$

where

$$\boldsymbol{\tau}_n = \lambda^2 \int_0^1 \xi_n d\mathbf{x}, \tag{4.2-39}$$

with $\xi_n(0) = \xi_n(1) = 0$. The solutions are given by (4.2-25) and (4.2-26).

Now making substitution of (4.2-37), (4.2-38), and (4.2-39) into (4.2-35) and (4.2-36) and using orthogonality leads to the normal coordinate equations

$$\frac{d^2\phi_n}{d\mathbf{t}^2} + 2\boldsymbol{\omega}_n\xi_n\frac{d\phi_n}{d\mathbf{t}} + \omega_n^2\phi_n = -\frac{\int_0^1 \mathbf{p(x,t)}\xi_n(\mathbf{x})d\mathbf{x}}{\int_0^1 \xi_n^2(\mathbf{x})d\mathbf{x}}, \tag{4.2-40}$$

and the additional tension is

$$\boldsymbol{\tau}(\mathbf{t}) = \sum_n \left\{\lambda^2 \int_0^1 \xi_n(\mathbf{x})d\mathbf{x}\right\}\phi_n(\mathbf{t}) = \sum_n \boldsymbol{\tau}_n\phi_n(\mathbf{t}), \tag{4.2-41}$$

where ξ_n is the fraction of critical damping in the nth mode.

Here provision for viscous damping has been made at this step. Damping due to structural causes is usually small in cables, although it is affected by such factors as the lay of the strands. In this situation rubbing between individual helices can supply a reasonable amount of energy absorption. For example, tests by Yu on power transmission lines suggest values of $\xi = 2\%$ or more.

Also results from tests by Ramberg and Griffin (1977) on the damping characteristics of suspended cables have some interesting ramifications. They found that an order of magnitude increase in structural damping could be expected (say from $\xi \approx 0.4\%$ to $\xi = 4\%$) if the cable was rather slack rather than taut.

Taking into consideration a case were the loading is uniform along the span, the general solution to (4.2-40) is

$$\phi_n(\mathbf{t}) = \frac{\alpha_n\boldsymbol{\omega}_n^2}{\boldsymbol{\tau}_n}D_n(\mathbf{t}), \tag{4.2-42}$$

where

$$D_n(\mathbf{t}) = \exp(-\xi_n \boldsymbol{\omega}_n \mathbf{t})\left\{\phi_{n0}\cos\left[(1-\xi_n^2)^{1/2}\boldsymbol{\omega}_n \mathbf{t}\right] + \frac{\dot{\phi}_{n0} + \xi_n \boldsymbol{\omega}_n \phi_{n0}}{(1-\xi_n^2)^{1/2}\boldsymbol{\omega}_n}\sin\left[(1-\xi_n^2)^{1/2}\boldsymbol{\omega}_n \mathbf{t}\right]\right\}$$

$$-\int_0^t \frac{1}{(1-\xi_n^2)^{1/2}\boldsymbol{\omega}_n}\exp\left\{-\xi_n \boldsymbol{\omega}_n(\mathbf{t}-\breve{\mathbf{t}})\right\}\sin\left[(1-\xi_n^2)^{1/2}\boldsymbol{\omega}_n(\mathbf{t}-\breve{\mathbf{t}})\right]\mathbf{p}(\breve{t})d\breve{t},$$

in which $\phi_{n0} = \phi_n(0)$ and $\dot{\phi}_{n0} = d\phi(0)/d\mathbf{t}$. The integral is Duhamel's integral, and usually it must be evaluated numerically. By employing the continuum approach to start with, and by supposing that only a few modes are important, the size of the problem remains manageable, and modal analysis techniques are efficient.

Defining the parameter α_n as the participation factor for additional tension; it is given by

$$\alpha_n = \frac{\int_0^{\omega_n/2}(1-\sec\boldsymbol{\omega}_n/2\cos\mathbf{z})d\mathbf{z}}{\int_0^{\omega_n/2}(1-\sec\boldsymbol{\omega}_n/2\cos\mathbf{z})^2 d\mathbf{z}}, \tag{4.2-43}$$

which, on carrying out the integration and using (4.2-26), leads to

$$\alpha_n = \frac{2/3}{\left[1+\lambda^2\{\tan(\boldsymbol{\omega}_n/2)/(\boldsymbol{\omega}_n/2)\}^2/2\right]}. \tag{4.2-44}$$

Table (4.2-7) lists values of α_n for the eight modes from wide range of values of λ^2. Two identities are established

$$\sum \alpha_n \omega_n^2 = \lambda^2 \text{ and } \sum_n \frac{1}{(1+12/\lambda^2)}. \tag{4.2-45}$$

It is seen that the participation factors reach maximum values when $\tan(\boldsymbol{\omega}_n/2) = 0$, which occurs when $\lambda^2 = 4\pi^2, 16\pi^2, 32\pi^2, \ldots$

When λ^2 is very large, $\sum \alpha_n \to 1$, and the cable is behaving essentially as a rigid body. Alternatively, when λ^2 is small, $\alpha_n \to \lambda^2 / (2(\boldsymbol{\omega}_n / 2)^4)$, and, as expected, the additional tension becomes vanishingly small.

Table 4.2-3, Participation factors for additional tension for the first eight symmetric in-plane modes as a function of λ^2, (Irvine, 1981).

λ^2	α_1	α_2	α_3	α_4	α_5	α_6	α_7	α_8
$256\pi^2$	0.003	0.004	0.005	0.007	0.011	0.025	0.126	0.666
$196\pi^2$	0.004	0.005	0.007	0.012	0.026	0.127	0.666	0.116
$144\pi^2$	0.006	0.008	0.012	0.027	0.118	0.666	0.115	0.017
$100\pi^2$	0.010	0.014	0.028	0.129	0.666	0.114	0.016	0.005
$64\pi^2$	0.016	0.031	0.131	0.666	0.112	0.015	0.005	0.002
$36\pi^2$	0.035	0.135	0.666	0.110	0.014	0.004	0.002	0.001
$16\pi^2$	0.141	0.666	0.104	0.011	0.003	0.001	0.000	0.000
100	0.345	0.506	0.033	0.005	0.001	0.001	—	—
80	0.480	0.362	0.021	0.004	0.001	0.001	—	—
60	0.610	0.206	0.013	0.003	0.001	0.000	—	—
$4\pi^2$	0.666	0.090	0.007	0.002	0.001	—	—	—
20	0.590	0.302	0.003	0.001	0.000	—	—	—
10	0.440	0.012	0.001	0.000	—	—	—	—
8	0.389	0.009	0.001	0.000	—	—	—	—
6	0.325	0.07	0.001	—	—	—	—	—
4	0.245	0.004	0.001	—	—	—	—	—
2	0.140	0.002	0.000	—	—	—	—	—
1	0.076	0.001	—	—	—	—	—	—
0.1	0.008	0.000	—	—	—	—	—	—

From the table above, it appears that, when λ^2 is moderate to large, the higher modes are likely to participate most strongly in the generation of additional tension.

4.2.6 The Nonlinear Theory of Vibration in a Taut Flat Cable

Herein the vibration of a taut flat cable is presented. In this case nonlinearity is geometric; the equivalent spring is of hardening variety, and the additional tension generated is non-negative.

Now if the amplitude of the vibration is such that its square is no longer negligible, appreciable levels of additional tension may be generated, and the equation of motion of free planar vibrations takes the form

$$(1+\boldsymbol{\tau}(\mathbf{t}))\frac{\partial^2 \mathbf{w}}{\partial \mathbf{x}^2}-\frac{\partial^2 \mathbf{w}}{\partial \mathbf{t}^2}=0, \tag{4.2-46}$$

with

$$\boldsymbol{\tau}(\mathbf{t})=\frac{\lambda^2}{2}\int_0^1\left(\frac{\partial \mathbf{w}}{\partial \mathbf{x}}\right)^2 d\mathbf{x}, \tag{4.2-47}$$

where $\mathbf{w}(0,\mathbf{t})=\mathbf{w}(1,\mathbf{t})=0$ and $\mathbf{w}(\mathbf{x},0)=\mathbf{w}_0(\mathbf{x}),\ \partial\mathbf{w}(\mathbf{x},0)/\partial\mathbf{t}=\dot{\mathbf{w}}_0(\mathbf{x})$. This problem being first studied by Carrier (1949).

Here two points are noted. First, the frequencies of the system will be to some extent amplitude-dependent, in fact dependant on the second power of the amplitude. This amplitude dependence is usual in non-linear vibrations. Second, the modes of vibration are identical to those of the classical linear system; therefore the governing partial differential equation may be reduced to a system of ordinary differential equations.
The ease with which the variables may be separated in this instance is rather uncommon, but unfortunately it does not work when sag is introduced.

To illustrate these points, let an initial displacement $\mathbf{w}_0(\mathbf{x})$ be prescribed, and for convenience let the initial velocity $\mathbf{w}_0(\mathbf{x})$ be zero. Suppose the solution of the ensuing vibration is of the form

$$\mathbf{w}(\mathbf{x},\mathbf{t})=\sum_{n=1}^{\infty}\mathbf{A}_n \sin n\pi\mathbf{x}\,\xi_n(\mathbf{t}), \tag{4.2-48}$$

where $\mathbf{A}_n = A_n/(mgL^2/T)$.

On account of the orthogonality of the trigonometric functions, there are no cross terms in the expression for the additional tension. It is simply a sum of squares:

$$\boldsymbol{\tau}(\mathbf{t}) = \frac{\lambda^2}{4}\sum_{n=1}^{\infty}\mathbf{A}_n^2 n^2\pi^2\xi_n(\mathbf{t}). \tag{4.2-49}$$

Substituting (4.2-48) and (4.2-49) into (4.2-46), leads to a series of equations in time alone of the form

$$\frac{d^2\xi_n}{d\mathbf{t}^2} + n^2\pi^2\mathbf{A}_n^2\left\{1+\frac{\lambda^2}{4}\sum_{n=1}^{\infty}\mathbf{A}_i^2 i^2\pi^2\xi_i^2\right\}\xi_n = 0, \tag{4.2-50}$$

where the coefficients are $\mathbf{A}_n = 2\int_0^1 \mathbf{w}_0(\mathbf{x})\sin n\pi\mathbf{x}d\mathbf{x}$, and the initial conditions are $\xi_n(0) = 1, \dot{\xi}(0) = 0$, n= 1, 2, 3, ... and thus as predicted the modes of vibration of the nonlinear system are identical to those of the linear system.

There is no exact solution to these coupled equations. Therefore perturbation techniques are required: Chikwedu and Kevorkian (1972) give a two variable procedure that can be adapted. Expressions for time history of displacement and additional tension may be shown to be

$$\mathbf{w}(\mathbf{x},\mathbf{t}) \approx \sum_{n=1}^{\infty}\mathbf{A}_n \sin n\pi\mathbf{x}\cos n\pi\left[1+\frac{\lambda^2}{32}\left\{n^2\pi^2\mathbf{A}_n^2 + 2\sum_{n=1}^{\infty} i^2\pi^2\mathbf{A}_i^2\right\}\right]\mathbf{t}, \tag{4.2-51}$$

$$\boldsymbol{\tau}(\mathbf{t}) \approx \frac{\lambda^2}{4}\sum_{n=1}^{\infty} n^2\pi^2\mathbf{A}_n^2\cos^2 n\pi\left[1+\frac{\lambda^2}{32}\left\{n^2\pi^2\mathbf{A}_n^2 + 2\sum_{n=1}^{\infty} i^2\pi^2\mathbf{A}_i^2\right\}\right]\mathbf{t}, \tag{4.2-52}$$

the only condition being that $\lambda^2 n^2\pi^2 A_n^2$ should not become too large. This interferes with the geometric approximations made in setting up the equation of motion and will also lead to tensions that do not lie within the confines of linear elasticity. The results appear to be periodic as expected.

Taking a particular case when the initial displacement is a mode such as

$$\mathbf{w_0(x)} = \mathbf{A}_z \sin z\pi\mathbf{x}, \tag{4.2-53}$$

the exact solution of (4.2-50) may be found in terms of the elliptical integral of the first kind. The solution then is best extracted from (4.2-51) and (4.2-52). It reads

$$\mathbf{w(x,t)} \approx \mathbf{A}_z \sin z\pi\mathbf{x} \cos z\pi\left(1 + \frac{3\lambda^2 z^2 \pi^2 \mathbf{A}_z^2}{32}\right)\mathbf{t}, \tag{4.2-54}$$

$$\boldsymbol{\tau}\mathbf{(t)} \approx \frac{\lambda^2 z^2 \pi^2 \mathbf{A}_z^2}{4} \cos^2 z\pi\left(1 + \frac{3\lambda^2 z^2 \pi^2 \mathbf{A}_z^2}{32}\right)\mathbf{t}. \tag{4.2-55}$$

This gives an amplitude-dependant natural frequency of the z th mode given by

$$\omega_z = z\pi\left(1 + \frac{3\lambda^2 z^2 \pi^2 A_z^2}{32}\right). \tag{4.2-56}$$

In the case of forced response the problem is rather more complicated.
Assuming a sinusoidal forcing of the form

$$\mathbf{p}\sin(1+k)^{1/2} n\pi\mathbf{t}, \qquad n = 1, 2, 3, ...,$$

is applied, where $\mathbf{p} = p/mg$ and k is a small parameter, either positive or negative (which indicates how close the forcing frequency is to the n th natural frequency of the linear system). It may be shown that just one mode is excited in the steady state response. (Now since the loading is uniform across the span, only symmetric modes may be excited, and consequently n is odd.) If the cable is constrained to vibrate in a single plane, that response is

$$\mathbf{w(x,t)} = -\mathbf{A}_n \sin n\pi x \sin(1+k)^{1/2} n\pi\mathbf{t}, \tag{4.2-57}$$

with

$$\boldsymbol{\tau(t)} = \frac{\lambda^2 n^2 \pi^2 \mathbf{A}_n^2}{4} \sin^2 (1+k)^{1/2} n\pi \mathbf{t}, \tag{4.2-58}$$

where the level of the response is found from the cubic

$$q^3 - rq - 2 = 0, \tag{4.2-59}$$

in which $q = \mathbf{A}_n / \left\{32\mathbf{p}/\left(3\lambda^2 n^5 \pi^5\right)\right\}^{1/3}$ and $r = \left\{4k^3 n^4 \pi^4 / 3\lambda^2 \mathbf{p}^2\right\}^{1/3}$. Written in this form, the roots depend on just one independent parameter that may be positive or negative, depending on whether k is positive or negative. Consequently there is always one positive real root.

4.3 Analysis Example

The example below is the benchmark used to calibrate the model in the study and the results obtained are compared with those from the numerical analysis. The chosen length is 85m and this was chosen in order to compare these results with experimental ones because the experiment rig is 85m long. It was not possible to carry out the experiments but nonetheless the analytical values were validated against the numerical ones.

It was seen earlier in solving the cable equation that the final solution describing the motion of the cable is given by equation 2.4-39. The table below shows the results obtained from the analytical analysis.

Table 4.2-4, Cable Natural Frequencies for tension of 15, 20, 25, 30 and 40% UTS.

Modes	Frequency (Hz)				
	15%	20%	25%	30%	40%
1	0.66	0.76	0.85	0.93	1.07
2	1.32	1.52	1.70	1.86	2.15
3	1.97	2.28	2.55	2.79	3.22
4	2.63	3.04	3.40	3.72	4.30
5	3.69	3.80	4.25	4.65	5.37

4.4 Conclusion

Clearly the undamped nonlinear steady-state response of a taut flat cable constrained to vibrate in a plane reduces to the solution of Duffing's equation for an undamped mass-hardening spring system (Meirovitch, L. 1975). It is difficult to say what importance should be attached to nonlinear vibrations in cable structures in practice. The temptation to use linearized theories is hard to resist because, when nonlinear response is likely to be important, the nature of the loading and damping is likely to be equally important and considerably more uncertain.

More work is definitely needed in this area of study and most progress can be made using the increasingly powerful numerical techniques being implemented worldwide. However the chosen approach has given us a solution and thus we obtain the cable natural frequencies and their corresponding mode shapes.

Finally the solutions obtained in this chapter are used in an analysis example in chapter 6 to come. These natural frequencies are compared with the results obtained also by using the finite element method. The plots showing the different variations and their comparisons are also presented in chapter 6.

5.0 SOLUTION OF TRANSCENDENTAL EIGENVALUE PROBLEM IN BUNDLED CONDUCTORS:

This chapter presents the formulation of the equations describing the behavior of bundled conductors. The solution to these equations, thus the transcendental eigenvalue problem which arises when solving the system of bundled conductors is also presented. The solution as reported in this chapter is derived from work done by Verma et. al., (2004).

Mathematical models are necessary for the computation of the conductor vibrations for studying the efficiency of damping measures. As seen in the literature review different models can be used but it all boils down to computer time and ease of computation of the equations set up. Taking a typical example for a 400m span with seven spacers, this results in a spacer dynamic stiffness matrix of the order 42x42 for arbitrary end supports and 30x30 for fixed supports (A. Simpson 1971). The so called energy balance method gives good results for estimating the vortex excited vibrations of overhead electrical transmission lines. In its standard form it requires the knowledge of the eigenfunctions, which are routinely calculated for the single conductor lines. However, the problem becomes more involved in the case of bundled conductors with spacer dampers due to very dense spectrum of the natural frequencies.

5.1 Modeling of a bundled conductor with spacer dampers

This chapter will look at the behavior of conductors with spacer dampers attached and will give the equations describing the motion. The following figures are used to formulate the equations.

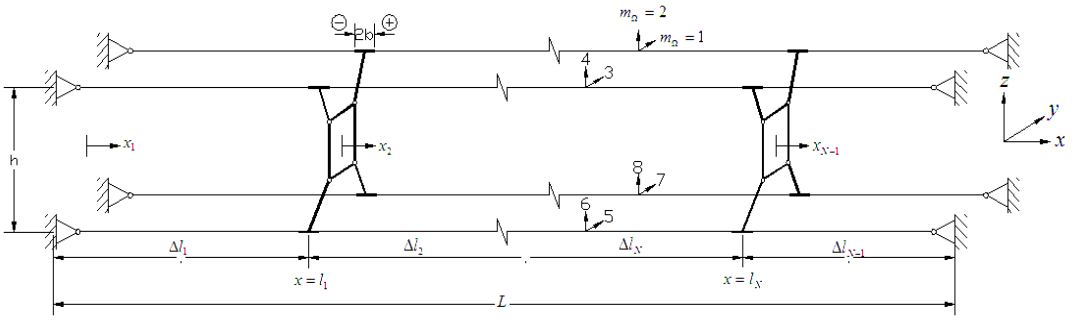

Figure 5.1-1, Schematic diagram of quad bundle attached with N similar spacer dampers.

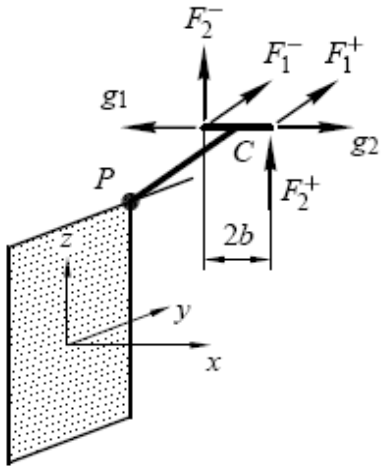

Figure 5.1-2, Forces acting at the clamp of a spacer damper.

Before proceeding with the derivations, the following nomenclature is adapted.

$A_{m_\Omega,v_\Omega}, B_{m_\Omega,v_\Omega}$	Integration constants for v_Ω^{th} subspan in m_Ω^{th} direction
$\mathbf{F}_n(t)$	Force vector for n^{th} spacer damper (a function of time)
$\mathbf{J}(s_\Omega)$	Transcendental system matrix
M_Ω	Number of arms in the spacer damper
N	Number of spacer dampers attached
T_{m_Ω}	Conductor tension in m_Ω direction
$\mathbf{Z}(\mathrm{s}_\Omega)$	Complex impedance matrix of spacer damper $\in C^{4M_\Omega x 4M_\Omega}$
a	Vector containing integration constants
b	Half spacer damper clamp width $+ l_{char}$
c_{m_Ω}	Wave velocity in m_Ω^{th} direction
l_{char}	Characteristic length of the conductor
l_n	Location of n^{th} spacer damper
m_Ω	Directional plane of the conductor vibration
s_Ω	Complex eigenvalue of the system $(= -\delta + i\omega)$
$w_{m_\Omega,v_\Omega}(x_{v_\Omega},t)$	Transverse displacement of v_Ω^{th} subspan in m_Ω^{th} direction (a function of local space coordinate x_v and time t)

$\dot{\mathbf{w}}_n(t)$	Velocity vector for n^{th} spacer damper (a function of time)
Δl_{v_Ω}	Span length of v_Ω^{th} sub-span
δ	Real part of complex eigenvalue s_Ω
δ_{ij}	Kronecker delta function
λ	Wave length.
ω	Imaginary part of complex eigenvalue s_Ω

Now considering a conductor bundle consisting of M_Ω subconductors with N similar spacer dampers attached as shown in figure (5.1-1). Each spacer damper has M number of arms. The spacer dampers are placed at $x = l_n$ where $n = 1, 2, 3, ..., N$, from the left hand. The spacers divide the total span of length L, into $N+1$ subspans of corresponding lengths, $\Delta l_1, \Delta l_2, ..., \Delta l_{N+1}$. The following assumptions have been made for simplifying the formulation:

1. The sag to span ratio is small so that the sag can be neglected.
2. The bending stiffness EI of the conductor is disregarded because of $\sqrt{\frac{EI}{T}} << \frac{\lambda}{2\pi}$. The conductor is considered as a string.
3. The conductors are assumed to be clamped at the span ends.
4. The bundle vibrates in one of its eigenmodes and exhibits synchronous motion.

Aeolian vibration excitation is prominently in the vertical direction, but due to the presence of dampers the motion is distorted and so transverse displacements of conductors in both vertical and horizontal directions have to be considered. The transverse motion of the conductor in the v_Ω^{th} subspan $(v_\Omega = 1,2,3,..., N+1)$ is expressed by the wave equation

$$\rho A \ddot{w}_{m_\Omega v_\Omega}(x,t) - T_{m_\Omega} w''_{m_\Omega, v_\Omega}(x,t) = 0, \quad m_\Omega = 1,2,3,...,2M_\Omega \tag{5.1-1}$$

where m_Ω represents the plane of motion of the conductor. Odd values of m_Ω corresponding to the vertical displacements (see fig 5.1-1). Now since the conductors are clamped at both ends, the displacements are zero at the supports, i.e.

$$w_{m_\Omega,1}(0,t) = 0, \tag{5.1-2}$$

$$w_{m_\Omega,N+1}(L,t) = 0. \tag{5.1-3}$$

The above equations (5.1-1) through to (5.1-3) define a boundary value problem. For convenience, we consider new subspan coordinates x_v, defined as

$$x_{v_\Omega} = x - l_{v_\Omega - 1}, \qquad 0 < x_{v_\Omega} < \Delta l_{v_\Omega} \tag{5.1-4}$$

with $l_0 = 0$. By separating the space and time variables as

$$w_{m_\Omega,v_\Omega}(x_{v_\Omega},t) = W_{m_\Omega,v_\Omega}(x_{v_\Omega})e^{st} \tag{5.1-5}$$

and substituting in Equation (5.1-1), we get the solution in the form

$$W_{m_\Omega,v_\Omega}(x_{v_\Omega}) = A_{m_\Omega,v_\Omega}e^{\left(\frac{s_\Omega x_{v_\Omega}}{c_{m_\Omega}}\right)} + B_{m_\Omega,v_\Omega}e^{\left(\frac{-s_\Omega x_{v_\Omega}}{c_{m_\Omega}}\right)} \tag{5.1-6}$$

where c_{m_Ω} is he wave velocity in m_Ω^{th} direction defined as $c_{m_\Omega} = \sqrt{T_{m_\Omega}/\rho A}$. Substituting this solution in the boundary conditions (5.1-2) and (5.1-3) gives

$$A_{m_\Omega,1} + B_{m_\Omega,1} = 0, \tag{5.1-7}$$

$$A_{m,N+1}e^{\left(\frac{s_\Omega \Delta l_{N+1}}{c_{m_\Omega}}\right)} + B_{m_\Omega,N+1}e^{\left(\frac{-s_\Omega \Delta l_{N+1}}{c_{m_\Omega}}\right)} = 0. \tag{5.1-8}$$

The force and velocity vector at the n^{th} spacer, as shown in figure (5.1-2), are

$$\mathbf{F}_n(t)=\begin{bmatrix} F^-_{1,n} \\ F^-_{2,n} \\ F^+_{1,n+1} \\ F^+_{2,n+1} \\ F^-_{3,n} \\ F^-_{4,n} \\ . \\ . \\ . \\ F^+_{2M_\Omega-1,n+1} \\ F^+_{2M_\Omega,n+1} \end{bmatrix}, \qquad \dot{\mathbf{w}}_n(t)=\begin{bmatrix} \dot{w}^-_{1,n}(\Delta l_n-b,t) \\ \dot{w}^-_{2,n}(\Delta l_n-b,t) \\ \dot{w}^+_{1,n+1}(b,t) \\ \dot{w}^+_{2,n+1}(b,t) \\ \dot{w}^-_{3,n}(\Delta l_n-b,t) \\ \dot{w}^-_{4,n}(\Delta l_n-b,t) \\ . \\ . \\ . \\ \dot{w}^+_{2M_\Omega,n+1}(b,t) \\ \dot{w}^+_{2M_\Omega,n+1}(b,t) \end{bmatrix} \tag{5.1-9}$$

they can be expressed as

$$\mathbf{F}_n(t)=\Re\left[\hat{\mathbf{F}}_n e^{st}\right], \qquad \dot{\mathbf{w}}_n(t)=\Re\left[\dot{\mathbf{w}}_n e^{st}\right]. \tag{5.1-10}$$

Here b is sum of half the clamp width and characteristics length of the conductor due to bending ($l_{char}=\sqrt{EI/T}$). In modeling of bundled conductors, the effect of spacer dampers is incorporated by mean of their impedance matrices, which are obtained by considering the mass, geometric and damping properties of the spacer dampers. In doing so, it is treated as a multibody system with linear elastic joints (e.g. four arms and the central frame of a quad spacer are treated as five interconnected rigid bodies). The formulation results in a square matrix, elements of which are functions of the frequency of conductor vibration. The impedance matrix $\mathbf{Z}(\mathrm{s}_\Omega)$ is of size $4M_\Omega X 4M_\Omega$. The impedance matrix relates the $4M_\Omega$ velocities at the clamps to the $4M_\Omega$ transverse forces acting at the clamps. Four transverse forces acting at each clamp can be seen in Fig. 5.1-2. The amplitudes $\hat{\mathbf{F}}_n$ and $\dot{\mathbf{w}}_n$ are related to each other through the relation

$$\hat{\mathbf{F}}_\mathrm{n}=\mathbf{Z}(\mathrm{s}_\Omega)\hat{\dot{\mathbf{w}}}_\mathrm{n}, \qquad n=1,2,3,...,N. \tag{5.1-11}$$

The impedance matrix $\mathbf{Z}(s_\Omega)$ for the spacer damper is assumed to be known beforehand. The forces at the clamp ends of any spacer damper will be in equilibrium with the transverse components of tensions on respective sides of the clamp

$$F^{-}_{m_\Omega,n}(t) = -T_{m_\Omega} w'_{m_\Omega,n}(\Delta l_n - b, t), \tag{5.1-12}$$

$$F^{+}_{m_\Omega,n+1}(t) = T_{m_\Omega} w'_{m_\Omega,n+1}(b, t). \tag{5.1-13}$$

Substituting for $w_{m_\Omega,n}$ from equations (5.1-5) and (5.1-6) gives

$$\hat{F}^{-}_{m_\Omega,n} = -\frac{T_{m_\Omega}}{c_{m_\Omega}}\left(A_{m_\Omega,n} e^{\left(\frac{s_\Omega \Delta l_n}{c_{m_\Omega}}\right)} e^{\left(\frac{-s_\Omega b}{c_{m_\Omega}}\right)} - B_{m_\Omega,n} e^{\left(\frac{-s_\Omega b}{c_{m_\Omega}}\right)} e^{\left(\frac{s_\Omega b}{c_{m_\Omega}}\right)} \right), \tag{5.1-14}$$

$$\hat{F}^{+}_{m_\Omega,n+1} = \frac{T_{m_\Omega} s_\Omega}{c_{m_\Omega}}\left(A_{m_\Omega,n} e^{\left(\frac{s_\Omega b}{c_{m_\Omega}}\right)} - B_{m_\Omega,n} e^{\left(\frac{-s_\Omega b}{c_{m_\Omega}}\right)} \right). \tag{5.1-15}$$

Taking $\xi^{\pm}_{m_\Omega}(s_\Omega) = e^{\left(\pm\frac{s_\Omega b}{c_{m_\Omega}}\right)}$, $\chi^{\pm}_{m_\Omega,n} = e^{\left(\pm\frac{s_\Omega \Delta l_n}{c_{m_\Omega}}\right)}$, the expressions for forces and velocities at the clamps can be written as

$$\hat{F}^{-}_{m_\Omega,n} = -\frac{T_{m_\Omega} s_\Omega}{c_{m_\Omega}}\left(A_{m_\Omega,n} \chi^{+}_{m_\Omega,n} \xi^{-}_{m_\Omega} - B_{m_\Omega,n} \chi^{-}_{m_\Omega,n} \xi^{+}_{m_\Omega} \right), \tag{5.1-16}$$

$$\hat{F}^{+}_{m_\Omega,n+1} = \frac{T_{m_\Omega}}{c_{m_\Omega}}\left(A_{m_\Omega,n+1} \xi^{+}_{m_\Omega} - B_{m_\Omega,n+1} \xi^{-}_{m_\Omega} \right). \tag{5.1-17}$$

and

$$\hat{\dot{w}}_{m_\Omega,n}\Big|_{x_n = \Delta l_n - b} = s_\Omega\left(A_{m_\Omega,n} \chi^{+}_{m_\Omega,n} \xi^{-}_{m_\Omega} + B_{m_\Omega,n} \chi^{-}_{m_\Omega,n} \xi^{+}_{m_\Omega} \right), \tag{5.1-18}$$

$$\hat{\dot{w}}_{m_\Omega,n+1}\Big|_{x_{n+1} = b} = s_b\left(A_{m_\Omega,n+1} \xi^{+}_{m_\Omega} + B_{m_\Omega,n+1} \xi^{-}_{m_\Omega} \right). \tag{5.1-19}$$

Equations (5.1-16) and (5.1-17) express the forces as a product of tension and slope and Equation (5.1-11) expresses them as a product of velocity and impedance. Equating these two set of equations gives us $4M_\Omega N$ equations as explained below. Consider the first element of the force vector from Eqn (5.1-11)

$$\hat{F}_{1,n}^{-} = \begin{Bmatrix} Z_{1,1} & Z_{1,2} & \dots & Z_{1,4M_\Omega} \end{Bmatrix} \hat{w} \tag{5.1-20}$$

and from Eqn. (5.1-16)

$$\hat{F}_{1,n}^{-} = -\frac{T_1 s}{c_1}\left(A_{1,n}\chi_{1,n}^{+}\xi_1^{-} - B_{1,n}\chi_{1,n}^{-}\xi_1^{+}\right) \tag{5.1-21}$$

Now equating the right hand sides of Equation (5.1-20) and (5.1-21) and rearranging gives

$$\begin{aligned} 0 = {} & A_{1,n}\chi_{1,n}^{+}\xi_1^{-}\left(Z_{1,1} + \frac{T_1}{c_1}\right) + B_{1,n}\chi_{1,n}^{-}\xi_1^{+}\left(Z_{1,1} + \frac{T_1}{c_1}\right) \\ & + \left(A_{2,n}\chi_{2,n}^{+}\xi_2^{-} + B_{2,n}\chi_{2,n}^{-}\xi_1^{+}\right)Z_{1,2} \\ & + \left(A_{1,n+1}\chi_{1,n+1}^{+}\xi_1^{-} + B_{1,n+1}\chi_{1,n+1}^{-}\xi_1^{+}\right)Z_{1,3} \\ & + \left(A_{2,n+1}\chi_{2,n+1}^{+}\xi_2^{-} + B_{2,n+1}\chi_{2,n+1}^{-}\xi_1^{+}\right)Z_{1,4} \\ & . \\ & . \\ & + \left(A_{2M_\Omega,n+1}\chi_{2M_\Omega,n+1}^{+}\xi_{2M_\Omega}^{-} + B_{2M_\Omega,n+1}\chi_{2M_\Omega,n+1}^{-}\xi_{2M_\Omega}^{+}\right)Z_{1,4M_\Omega}. \end{aligned}$$

Corresponding to each spacer we will have $4M_\Omega$ such equations. These $4M_\Omega N$ equations for N spacers and the $4M_\Omega$ equations from boundary conditions at the span ends in (5.1-7, 5.1-8) which results in a transcendental EVP:

$$\mathbf{J}(s_\Omega)\mathbf{a} = \mathbf{0}, \tag{5.1-23}$$

where

$$\mathbf{a} =< A_{1,1}, B_{1,1}, A_{2,1} B_{2,1}, ..., A_{2M_\Omega,1}, B_{2M_\Omega,1}, ...,$$
$$A_{1,v_\Omega}, B_{1,v_\Omega}, A_{2,v_\Omega}, B_{2,v_\Omega}, ..., A_{2M_\Omega,v_\Omega}, B_{2M_\Omega,v_\Omega}, ...,$$
$$A_{1,N+1}, B_{1,N+1}, A_{2,N+1}, B_{2,N+1}, ..., A_{2M_\Omega,n+1}, B_{2M_\Omega,N+1} >^T \quad (5.1\text{-}24)$$

and $\mathbf{J}(s_\Omega)$ has the following form

$$J(s_\Omega) = \begin{bmatrix} L \longleftarrow \text{Due to left boundary } (2M_\Omega x 4M_\Omega) & & & \\ & S_1 & & \\ & & S_2 & \\ & & & \ddots \\ & & & S_n \\ \text{Due to } n^{th} \text{ spacer } (4M_\Omega x 8M_\Omega) & & & \\ & & & S_{N+1} \\ & & & R \\ & \text{Due to right boundary } (2M_\Omega x 4M_\Omega) & & \end{bmatrix}$$

where $\mathbf{S}_1, \mathbf{S}_2, ..., \mathbf{S}_n$ are matrices of size $4M_\Omega * 8M_\Omega$ The elements of matrices $\mathbf{L}, \mathbf{R}$ and $\mathbf{S}_n$ are described in the Appendix.

5.2 Solution of the eigenvalue problem

The matrix equation in Equation (5.1-23) constitutes an EVP having infinitely many eigenvalues. Since the matrix $\mathbf{J}(s_\Omega)$ contains system parameters it is referred to as the system matrix. It can be seen that the elements of the system matrix are transcendental functions of the parameter s_Ω, which is a complex number $(s_\Omega = -\delta + i\omega)$. The imaginary part of s_Ω represents a decay coefficient. From its constitution, it can be observed that the elements of system matrix have a large variation in the order of magnitudes, which makes it to behave numerically poor. The following sections discuss the different approaches for solving this numerically poor transcendental eigenvalue problem.

5.2.1 Determinant Search Method

Now this method is one by which the transcendental EVP is solved. Here one searches the values of s_Ω for which

$$\det(\mathbf{J}(s_\Omega)) = 0. \tag{5.2-25}$$

The search domain is two dimensional due to the fact that the parameter s_Ω is a complex number. The system matrix $\mathbf{J}(s_\Omega)$, charactrised by its poor numerical behavior makes it easy to miss many values of s_Ω for which actually the determinant of $\mathbf{J}(s_\Omega)$ is zero. Though normalization of the basic variables leads to a better conditioned system matrix, difficulties are faced when trying to find the eigenvalues for big system matrices with the determinant search method.

The major difficulty one faces is that, for a big system matrix the optimizer does not converge to zero, rather it sticks to a minimum. The prime reason for this being the large variation in the order of numerical values of the elements of the system matrix. These elements, together with the large number of algebraic operations involved in calculating the determinant, lead to such numerical problems. Additional checks are required to confirm whether the obtained values are eigenvalues of the system or not.

5.2.2 Alternate Approach

Now in overcoming the difficulties faced in the determinant search method, an alternate approach is used. The homogeneous set of $4M_\Omega(N+1)$ simultaneous equations, given by Equation (5.1-23), is first transformed into a non-homogeneous system by using any $\{4M_\Omega(N+1)-1\}$ equations. A simple and better optimization criterion is then defined for the remaining equations. Following is a description of the steps followed:

1. Let $A_{1,1} = 1$.
2. Substitute the value of $A_{1,1}$ into any $\{4M_\Omega(N+1)-1\}$ homogeneous equations of Equation (5.1-23), so as to transform them into a set of non-homogeneous equations. Determine

other system variables, i.e. $B_{1,1}, A_{2,1}, B_{2,1}, ..., A_{2M_\Omega,N+1}, B_{2M_\Omega,N+1}$ (see Equation 5.1-24), by solving these $\{4M_\Omega(N+1)-1\}$ non-homogeneous equations with the help of Gauss elimination technique.

3. Substitute the values of $B_{1,1}, A_{2,1}, B_{2,1}, ..., A_{2M_\Omega,N+1}, B_{2M_\Omega,N+1}$ back into remaining one [say l^{th}] equation. Since the previously assumed $A_{1,1}$ was not the correct one, these values will not satisfy the l^{th} equation and will result in an error ε, given by

$$J_{l,1} + B_{1,1}J_{l,2} + A_{2,1}J_{l,3} + B_{2,2}J_{l,4} + ... + A_{2M_\Omega,N+1}J_{l,\{4M_\Omega(N+1)-1\}} + B_{2M_\Omega,N+1}J_{l,4M_\Omega(N+1)} = \varepsilon. \quad (5.2\text{-}26)$$

Now the optimization criterion, now, is to search such values of s_Ω, in the complex domain, for which $|\varepsilon|$ equals (or tends to) zero. The result from this approach is a numerically well-behaving optimization criterion, which converges faster than the determinant search method. This gives most, if not all, of the eigenvalues provided we give a good initial guess. One can always be sure that the value of s_Ω found after minimizing ε, is an eigenvalue of the system in Equation (5-1-23). This approach however requires good initial guesses, otherwise it fails to find very closely spaced eigenvalues, because of the two dimensional search method.

5.2.3 Continuous Spectrum Approach

Verma et. al., observes that in the case of very big system matrices (e.g. bundled conductors attached with many spacer dampers), the previously mentioned approaches fail to find some of the eigenvalues, even if the given initial guesses are good enough. A possible reason for missing eigenvalues being the two dimensional search domain. Also in bundled conductors the system frequencies are very closely spaced (@0.001Hz). If two parameters (i.e. δ and ω) are simultaneously searched, it is very likely that the optimizer will stick to one combination of these parameters for many consecutive guess values. It poses a major difficulty of missing the eigenvalues even with good initial guesses.

The continuous spectrum approach utilizes the dense frequency spectrum of the bundled conductors to reduce the search domain from two dimensional to one dimensional. Since for a bundled conductor the spacing of the eigenfrequenies is very close, it can be assumed to have a continuous frequency spectrum (Hagedorn, 1982). It would then be reasonable to assume that every frequency, in the range of consideration, is a natural frequency of the system. This means that, we know the complex parts ω of eigenvalues s_Ω, beforehand. Now corresponding to each ω value there exist one δ value which satisfies

$$\mathbf{J}(\delta)\mathbf{a} = \mathbf{0}. \tag{5.2-27}$$

Now the criterion becomes finding the corresponding δ value for closely spaced ω values, using any of the above approaches. This simplification converts our two dimensional optimization problem (in complex domain). After finding the eigenvalues s_Ω of the system matrix, the corresponding eigenvectors were found by solving an equivalent algebraic matrix EVP of the form

$$\left[\mathbf{J}(s_\Omega) - \lambda I\right]\mathbf{a} = \mathbf{0}. \tag{5.2-28}$$

The eigenvector corresponding to any eigenvalue s_Ω of the transcendental EVP of Equation (5.1-23) is obtained by finding the eigenvector associated to $\lambda = 0$ in the equivalent algebraic EVP of Equation (5.2-28).

In an analysis example carried out by the authors the transcendental EVP was solved with the above described approaches and the eigenvalues were searched in the frequency range of 20 to 30 Hz. Figure 5.2-1 shows the comparison from the three approaches.

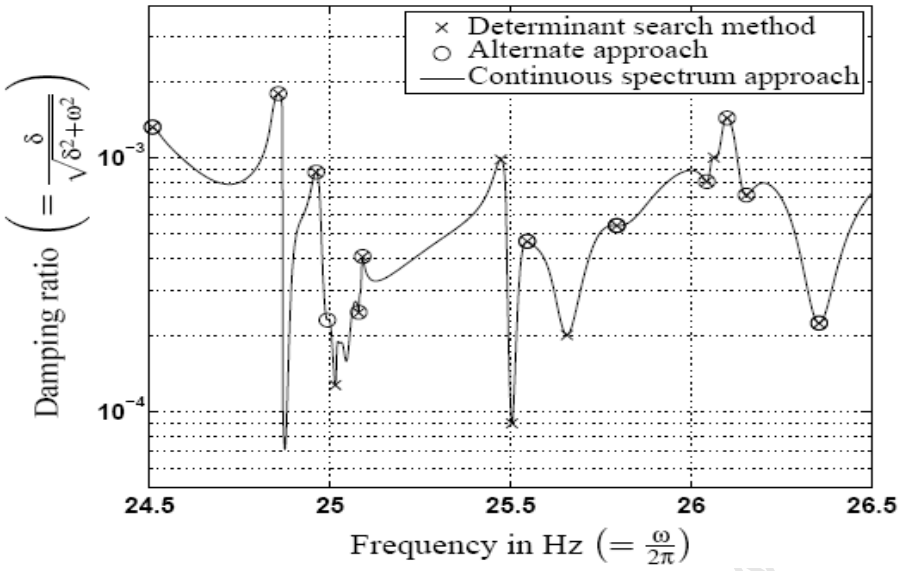

Figure 5.2-1, Obtained frequencies from different methods (24.5-26.5Hz).

5.3 Conclusion

The classical determinant search method and one alternate approach were discussed for solving the transcendental EVP. Verma shows the new approach, named as continuous spectrum approach, and presents the solution of EVP in the case of bundled conductors. The new approach provides a good engineering solution for the transcendental EVP.

The continuous spectrum approach provides us with a continuous curve of damping ratios corresponding to all the frequencies in the range of interest. For the transmission line engineer the major interest is in knowing the maximum strain levels in transmission line, corresponding to each eigenvalue. Strains can now be computed after knowing the mode shapes and the actual vibration amplitudes, which are obtained by energy balance principle.

The following chapter looks at the finite element modeling of the same system of bundled transmission lines with spacers placed at midpoint, third points and quarter points of the selected span of interest.

6.0 FINITE ELEMENT MODELING:

6.1 Introduction

The finite element analysis program ABAQUS was chosen because of its ability to offer an efficient solution to the problem at hand. The cable element was modeled as a 2-node linear 3D truss element (T3D2), this was chosen because of the ability of truss elements to carry tensile load and having no resistance to bending and allowing for translational degrees of freedom at the nodes, which closes resembles the cable behavior (ABAQUS 2000). Also an updated Langrangian Formulation is presented to validate this element. The dampers were modeled as BAR elements with node connections.

The boundary conditions created pinned the cable to one end and at the other translation was allowed were at this point a prestressing force was applied. The prestressing force was applied initially to the cables to give the required sag, thus representing the initial field cable arrangement. The job was run in two steps, the first step basically was for preloading the cable and this was done in the ABAQUS general static step, which included the non-linear effects of large deformations and displacements (NLGEOM). The second step was for extracting the modes and frequencies of the cable. The eigenfrequency extraction procedure used is a dynamic implicit-linear perturbation procedure and here also the non-linear effects NLGEOM parameter was left on since for both steps initial stress effects are associated with the geometrically nonlinear formulation. Since we are interested in the first few modes, thus the use of the subspace iteration eigensolver for the small number of eigenvalues and eigenfrequencies.

In the bundled sets of conductors springs were allowed for, these were assigned a stiffness value equivalent to to the effect of the actual spacer. These were applied at the different specified locations and the corresponding stiffness value applied. These springs were placed using the connectivity type; connect two points. The cable element was then meshed with the mesh type element, 2 node 3 dimensional trusses (T3D2) for the reasons discussed above. The job was then run and the results obtained are presented in the section that follows. As seen in the literature review it is the damping effect of the spacer devices that give them the name dampers and so in

this whole presentation the words spacers and dampers are used interchangeably to mean the same thing.

6.1.1 Element Type

As stated in the introduction the element chosen is a 2-node linear 3D truss element, the updated Lagrangian formulation of this element is presented in detail below. The formulation is taken from work presented by Prof J.K. Bathe (1986) in his lecture videos (MIT Video Course, 1986).

6.1.2 Updated Lagrangian Formulation

The general continual mechanics equations are analytically used to derive directly the finite element equations, thus obtaining the finite element matrices corresponding to the truss elements. These are derived in closed form and are able to give us what exactly the individual terms in the continual mechanics mean. The formulation proceeds with some assumptions:

6.1.2.1 Truss Element derivation

The following assumptions are considered,

1. stresses are transmitted only in the direction normal to the cross-section,
2. the stress is constant over the cross-section
3. the cross-sectional area remains constant during deformations

The first two assumptions are the typical ones used in the linear analysis problems. Now we consider the large rotation-small strain finite element formulation for a straight truss element with constant cross-sectional area. To avoid clutter the 2D formulation is chosen but similarly for 3D the same procedure is still valid. The following figure shows the element arrangement.

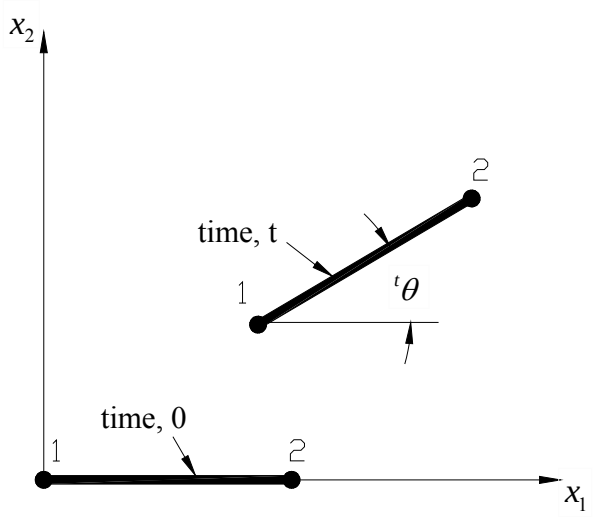

-Elastic material with Young Modulus, E.

-Cross-section Area, A.

-Element lies in x1-x2 plane and is initially aligned to the x-axis.

Figure 6.1-1, Truss element arrangement.

Now the deformations of the truss element are specified by the displacements of its nodes. The above arrangement is given in nodal coordinates as shown below. The deformations of the nodes from time 0 to time t are ${}^t u_1^1$, ${}^t u_2^1$, ${}^t u_1^2$ and ${}^t u_2^2$.

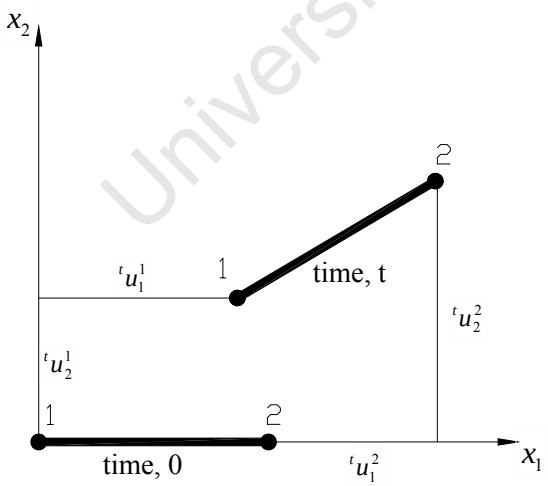

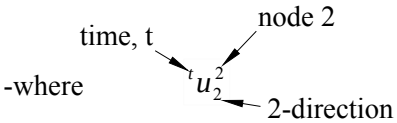

Figure 6.1-2, Truss Element deformations.

Now since the configuration at time t is know, we want to calculate the configuration at time, $t + \Delta t$. Figure 6.1-2 changes and we have the following incremental coordinates, u_1^1, u_2^1, u_1^2 and u_2^2. Figure 6.1-3 below shows the view graph of this transformation.

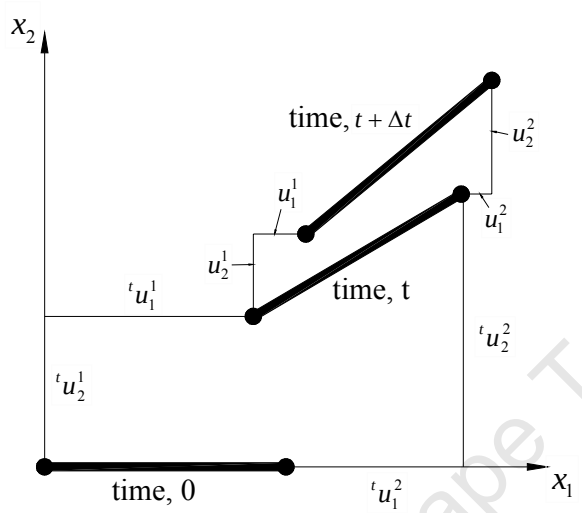

Figure 6.1-3, New truss position with incremental coordinates.

To obtain the configuration at time, $t + \Delta t$ we apply the formulation thus; we introduce an auxiliary coordinate frame, which is aligned with one of its axis along the element. We have $\tilde{x}_1$ and $\tilde{x}_2$ coordinates representing the body aligned coordinate frame, see figure 6.1-4.

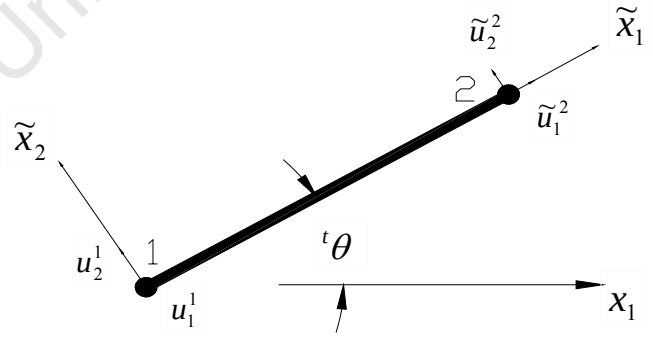

Figure 6.1-4, Body aligned coordinate form.

As shown in figure (6.1-4) above ${}^{t}\theta$ is the rotation which the element has undergone, we need the stiffness matrix in the x_1 and x_2 stationary coordinate frame. If we have calculated the matrix in the $\tilde{x}_1$ and $\tilde{x}_2$ body attached coordinate frame we can easily transform to the stationary coordinate frame.

Now we wish to obtain the K-matrix and F-vector corresponding to this body attached coordinate frame. To do this we visit the standard continual mechanics equations. Now written in the rotated coordinate system, the equation of the principle of virtual work is:

$$\int_{{}^{t}V} {}_{t}^{t+\Delta t}\tilde{S}_{ij}\,\delta\,{}^{t+\Delta t}\varepsilon_{ij}\,{}^{t}dV = {}^{t+\Delta t}\tilde{\Re} \qquad (6.1\text{-}1)$$

which linearizes to

$$\int_{{}^{t}V} {}_{t}\tilde{C}_{ijrs}\,{}_{t}\tilde{e}_{rs}\,\delta\,{}_{t}\tilde{e}_{ij}\,{}^{t}dV + \int_{{}^{t}V} {}^{t}\tilde{\tau}_{ij}\,\delta\,{}_{t}\tilde{\eta}_{ij}\,{}^{t}dV = {}^{t+\Delta t}\Re - \int_{{}^{t}V} {}^{t}\tilde{\tau}_{ij}\,\delta\,{}_{t}\tilde{e}_{ij}\,{}^{t}dV \qquad (6.1\text{-}2)$$

Now for the truss element the only non-zero stress is the stress along the length acting normal to the cross-section of the truss, thus ${}^{t}\tilde{\tau}_{11}$. Equation (6.1-2) above becomes

$$\int_{{}^{t}V} {}_{t}\tilde{C}_{1111}\,{}_{t}\tilde{e}_{11}\,\delta\,{}_{t}\tilde{e}_{11}\,{}^{t}dV + \int_{{}^{t}V} {}^{t}\tilde{\tau}_{11}\,\delta\,{}_{t}\tilde{\eta}_{11}\,{}^{t}dV = {}^{t+\Delta t}\Re - \int_{{}^{t}V} {}^{t}\tilde{\tau}_{11}\,\delta\,{}_{t}\tilde{e}_{11}\,{}^{t}dV \qquad (6.1\text{-}3)$$

Considering one component of the strain tensor, we notice that the terms of the equation above are identified to be:

tensor term, ${}_{t}\tilde{C}_{1111} = E$ stress term, ${}^{t}\tilde{\tau}_{11} = \dfrac{{}^{t}P}{A}$ P-force in the truss,

volume of truss, ${}^{t}V = AL$ L-length of truss (constant)

Now with the above, equation (6.1-3) becomes

$$(EA)_t \tilde{e}_{11} \delta_t \tilde{e}_{11} L + {}^t P \delta_t \tilde{\eta}_{11} L = {}^{t+\Delta t}\Re - {}^t P \delta_t \tilde{e}_{11} L \qquad (6.1\text{-}4)$$

To proceed, we must express the strain increments in terms of the (rotated) displacement increments.

$${}_t\tilde{e}_{11} = {}^t_t \underline{B}_L \hat{\underline{\tilde{u}}},$$

$$\delta_t \tilde{\eta}_{11} = (\delta \hat{\underline{\tilde{u}}}^T {}_t \underline{\tilde{B}}^T{}_{NL})({}^t_t \underline{\tilde{B}}_{NL} \hat{\underline{\tilde{u}}})$$

where $\hat{\underline{\tilde{u}}} = \begin{bmatrix} \tilde{u}_1^1 \\ \tilde{u}_2^1 \\ \tilde{u}_1^2 \\ \tilde{u}_2^2 \end{bmatrix}$ for 2D and $\hat{\underline{\tilde{u}}} = \begin{bmatrix} \tilde{u}_1^1 \\ \tilde{u}_2^1 \\ \tilde{u}_3^1 \\ \tilde{u}_1^2 \\ \tilde{u}_2^2 \\ \tilde{u}_3^2 \end{bmatrix}$ for 3D truss formulations.

To evaluate the above terms the total strain is given from general continual mechanics equations and is shown below:

$${}_t\tilde{\varepsilon}_{11} = {}_t\tilde{u}_{1,1} + \frac{1}{2}(({}_t\tilde{u}_{1,1})^2 + ({}_t\tilde{u}_{2,1})^2) \qquad (6.1\text{-}5)$$

we recognize from Equation 6.1-5 that the linear strain is

$${}_t\tilde{e}_{11} = {}_t\tilde{u}_{1,1}$$

$${}_t\tilde{\eta}_{11} = \frac{1}{2}(({}_t\tilde{u}_{1,1})^2 + ({}_t\tilde{u}_{2,1})^2)$$

and

$$\delta_t \tilde{\eta}_{11} = \delta_t \tilde{u}_{1,1}\, {}_t\tilde{u}_{1,1} + \delta_t \tilde{u}_{2,1}\, {}_t\tilde{u}_{2,1}$$

$$= \underbrace{\begin{bmatrix} \delta\, {}_t\widetilde{u}_{1,1} & \delta\, {}_t\widetilde{u}_{2,1} \end{bmatrix} \begin{bmatrix} {}_t\widetilde{u}_{1,1} \\ {}_t\widetilde{u}_{2,1} \end{bmatrix}}_{MATRIX-FORM}$$

We can now unite the displacement derivatives in terms of the displacements (this is simple because all quantities are constant along the truss). Thus for example:

$${}_t\widetilde{u}_{1,1} = \frac{\partial \widetilde{u}_1}{\partial {}^t\widetilde{x}_1} = \frac{\Delta \widetilde{u}_1}{\Delta {}^t x_1} = \frac{\widetilde{u}_1^2 - \widetilde{u}_1^1}{L}$$

hence we obtain

$$\begin{bmatrix} {}_t\widetilde{u}_{1,1} \\ {}_t\widetilde{u}_{2,1} \end{bmatrix} = \frac{1}{L} \begin{bmatrix} -1 & 0 & 1 & 0 \\ 0 & -1 & 0 & 1 \end{bmatrix} \begin{bmatrix} \widetilde{u}_1^1 \\ \widetilde{u}_2^1 \\ \widetilde{u}_1^2 \\ \widetilde{u}_2^2 \end{bmatrix}$$

and

$${}_t e_{11} = \underbrace{\frac{1}{L}\begin{pmatrix} -1 & 0 & 1 & 0 \end{pmatrix}}_{{}_t^t\underline{B}_L} \underline{\hat{\tilde{u}}}$$

$$\delta\, {}_t\widetilde{\eta}_{11} = \underbrace{\delta\underline{\hat{\tilde{u}}}^T \overbrace{\begin{pmatrix} \frac{1}{L}\begin{bmatrix} -1 & 0 \\ 0 & -1 \\ 1 & 0 \\ 0 & 1 \end{bmatrix} \end{pmatrix}}^{{}_T^T\underline{B}_{NL}^T}}_{\begin{bmatrix} \delta {}_t\widetilde{u}_{1,1} & \delta {}_t\widetilde{u}_{2,1} \end{bmatrix}} \underbrace{\overbrace{\begin{pmatrix} \frac{1}{L}\begin{bmatrix} -1 & 0 & 1 & 0 \\ 0 & -1 & 0 & 1 \end{bmatrix} \end{pmatrix}}^{{}_t^t\underline{B}_{NL}^T} \underline{\hat{\tilde{u}}}}_{\begin{bmatrix} {}_t\widetilde{u}_{1,1} \\ {}_t\widetilde{u}_{2,1} \end{bmatrix}}$$

With the above information we can directly develop the K-matrices. The linear strain stiffness matrix is obtained from the expression:

$$EA_{\,t}\tilde{e}_{11}\delta_{\,t}\tilde{e}_{11}L \Rightarrow \delta\hat{\underline{\tilde{u}}}^{T}\overbrace{\left(\frac{{}^{t}P}{L}\begin{bmatrix}1 & 0 & -1 & 0\\ 0 & 1 & 0 & -1\\ -1 & 0 & 1 & 0\\ 0 & -1 & 0 & 1\end{bmatrix}\right)}^{{}^{t}_{t}\tilde{K}_{L}}\hat{\underline{\tilde{u}}}$$

The nonlinear strain stiffness matrix is obtained from:

$${}^{t}P\delta_{\,t}\tilde{\eta}_{11}L \Rightarrow \delta\hat{\underline{\tilde{u}}}^{T}\overbrace{\left(\frac{{}^{t}P}{L}\begin{bmatrix}1 & 0 & -1 & 0\\ 0 & 1 & 0 & -1\\ -1 & 0 & 1 & 0\\ 0 & -1 & 0 & 1\end{bmatrix}\right)}^{{}^{t}_{t}\tilde{K}_{NL}}\hat{\underline{\tilde{u}}}$$

and finally the force vector is given by:

$${}^{t}P\delta_{\,t}e_{11}L \Rightarrow \delta\hat{\underline{\tilde{u}}}^{T}\overbrace{\left({}^{t}P\begin{bmatrix}-1\\ 0\\ 1\\ 0\end{bmatrix}\right)}^{{}^{t}_{t}F}$$

Having now obtained the required element matrices, expressed in the coordinate system aligned with the truss at time t, we need to determine the element matrices in the stationary global coordinate system.

We express the rotated displacement increments $\hat{\underline{\tilde{u}}}$ in terms of the unrotated displacement increments $\underline{\tilde{u}}$. We can show that:

$$\begin{bmatrix}\tilde{u}_1\\ \tilde{u}_2\end{bmatrix} = \begin{bmatrix}\cos^{t}\theta & \sin^{t}\theta\\ -\sin^{t}\theta & \cos^{t}\theta\end{bmatrix}\begin{bmatrix}u_1\\ u_2\end{bmatrix}$$

Applying this at the nodes we directly obtain the following transformation.

$$\underbrace{\begin{bmatrix} \tilde{u}_1^1 \\ \tilde{u}_2^1 \\ \tilde{u}_2^1 \\ \tilde{u}_2^2 \end{bmatrix}}_{\underline{\hat{\tilde{u}}}} = \underbrace{\begin{bmatrix} \cos^t\theta & \sin^t\theta & 0 & 0 \\ -\sin^t\theta & \cos^t\theta & 0 & 0 \\ 0 & 0 & \cos^t\theta & \sin^t\theta \\ 0 & 0 & -\sin^t\theta & \cos^t\theta \end{bmatrix}}_{T} \underbrace{\begin{bmatrix} u_1 \\ u_2^1 \\ u_1^2 \\ u_2^2 \end{bmatrix}}_{\underline{\hat{u}}}$$

Using this transformation in the equation of motion gives the following, from the basic equations:

the linear strain stiffness matrix,

$$\delta\underline{\hat{\tilde{u}}}^T \underline{{}_t^t\tilde{K}}_L \underline{\hat{\tilde{u}}} \rightarrow \delta\underline{\hat{u}}^T \underbrace{\underline{T}^T \underline{\tilde{K}}_L \underline{T}}_{\underline{{}_t^tK}_L} \underline{\hat{u}}$$

where $\underline{{}_t^tK}_L$ is the linear stiffness matrix of the element corresponding to the stationary global coordinates.

the non-linear strain stiffness matrix,

$$\delta\underline{\hat{\tilde{u}}}^T \underline{{}_t^t\tilde{K}}_{NL} \underline{\hat{\tilde{u}}} \rightarrow \delta\underline{\hat{u}} \underbrace{\underline{T}^T \underline{\tilde{K}}_{NL} \underline{T}}_{\underline{{}_t^tK}_{NL}} \underline{\hat{u}}$$

where $\underline{{}_t^tK}_{NL}$ represents the non-linear stiffness matrix of the element corresponding to the stationary global coordinates.

the force vector,

$$\delta\underline{\hat{\tilde{u}}}^T \underline{{}_t^t\tilde{F}} \rightarrow \delta\underline{\hat{u}} \underbrace{\underline{T}^T \underline{{}_t^t\tilde{F}}}_{\underline{{}_t^tF}}$$

where $\underline{{}_t^tF}$ is the force vector in the uncurled coordinate frame.

Performing the indicated matrix multiplication gives:

$$
{}^{t}_{t}\underline{K}_{L} = \begin{bmatrix} (\cos^t\theta)^2 & (\cos^t\theta)(\sin^t\theta) & -(\cos^t\theta)^2 & -(\cos^t\theta)(\sin^t\theta) \\ & (\sin^t\theta)^2 & -(\cos^t\theta)(\sin^t\theta) & -(\sin^t\theta)^2 \\ & & (\cos^t\theta)^2 & (\cos^t\theta)(\sin^t\theta) \\ & \textit{Symmetric} & & (\sin^t\theta) \end{bmatrix}
$$

$$
{}^{t}_{t}\underline{K}_{NL} = \frac{{}^{t}P}{L} \begin{bmatrix} 1 & 0 & -1 & 0 \\ & 1 & 0 & -1 \\ & & 1 & 0 \\ & \textit{Symmetric} & & 1 \end{bmatrix}
$$

and $${}^{t}_{t}\underline{F} = {}^{t}P \begin{bmatrix} -\cos^t\theta \\ -\sin^t\theta \\ \cos^t\theta \\ \sin^t\theta \end{bmatrix}$$

The above thus gives us the values we require corresponding to the stationary global coordinates. The following chapter deals with the finite element modeling of a viscoelastic damper element which is to be integrated to the formulation above to give a complete finite element solution of the bundled cable vibration problem. The solution obtained here is then compared to the results obtained from the transcendental eigenvalue problem in chapter 5.

6.1.3 Finite element model of a passive viscoelastic damper element with node connections

Here the finite element model for the passive viscoelastic damper is developed and then it is included in the model of the whole element.

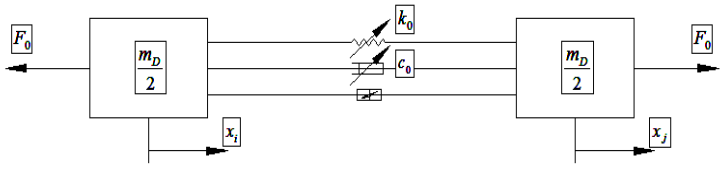

Figure 6.1-5, Lumped mass presentation of a passive viscoelastic damper element

Assuming that the mass of the damper can be equally lumped in both ends, the finite element model for the damper is obtained by applying the Second Newton's Law to the masses shown in figure 6.1-5 as follows:

$$\left\{\begin{array}{l} c_0(\dot{\mathbf{x}}_j - \dot{\mathbf{x}}_i) + k_0(\mathbf{x}_j - \mathbf{x}_i) + \alpha z - \mathbf{F_0} = \dfrac{m_D}{2}\ddot{x}_i \\ c_0(\dot{\mathbf{x}}_i - \dot{\mathbf{x}}_j) + k_0(\mathbf{x}_i - \mathbf{x}_j) - \alpha z + \mathbf{F_0} = \dfrac{m_D}{2}\ddot{x}_j \end{array}\right\} \quad 6.1\text{-}6$$

Writing equation 6.1-6 in the matrix form, we can obtain:

$$\begin{bmatrix} \frac{m_D}{2} & 0 \\ 0 & \frac{m_D}{2} \end{bmatrix}\begin{Bmatrix} \ddot{x}_i \\ \ddot{x}_j \end{Bmatrix} + \begin{bmatrix} c_0 & -c_0 \\ -c_0 & c_0 \end{bmatrix}\begin{Bmatrix} \dot{x}_i \\ \dot{x}_j \end{Bmatrix} + \begin{bmatrix} k_0 & -k_0 \\ -k_0 & k_0 \end{bmatrix}\begin{Bmatrix} x_i \\ x_j \end{Bmatrix} = \begin{bmatrix} 1 & 0 \\ 0 & 1 \end{bmatrix}\begin{Bmatrix} \alpha z \\ -\alpha z \end{Bmatrix} + \begin{bmatrix} 1 & 0 \\ 0 & 1 \end{bmatrix}\begin{Bmatrix} -\mathbf{F_0} \\ \mathbf{F_0} \end{Bmatrix} \quad 6.1\text{-}7$$

Or

$$[\mathbf{M}_{\mathrm{MR}}]\{\ddot{\mathbf{x}}\} + [\mathbf{C}_0]\{\dot{\mathbf{x}}\} + [\mathbf{K}_0]\{\mathbf{x}\} = [\mathbf{I}]\{\mathbf{F}_z\} + [\mathbf{I}]\{\mathbf{F}_0\} \quad 6.1\text{-}8$$

Similarly, the mass and stiffness of the damper can be transformed to global coordinates for assembling purposes. It is noted that the damping coefficient c_0 is significantly larger than the typical structural damping of the bars; thus, the structural damping may be ignored. The global damping matrix $[\mathbf{C}_0]$ of the bar element with damper can also be obtained by transforming the local damping matrix using the rotational matrix as

$$[\mathbf{C}_0]^g = [\mathbf{R}]^T[\mathbf{C}^{(e)}][\mathbf{R}] \quad 6.1\text{-}9$$

which can be properly assembled in the similar way as the stiffness and mass matrices in order to obtain the system damping matrix of the damper bar element. It is noted that the global damping matrix m $[\mathbf{C}_0]^g$ is matrix with time dependent coefficients.

Having FEM for the viscoelastic damper, the FEM for the bar element that contains the damper is proposed. The bar element consists of five individual members as it is shown in figure 6.1-6 below.

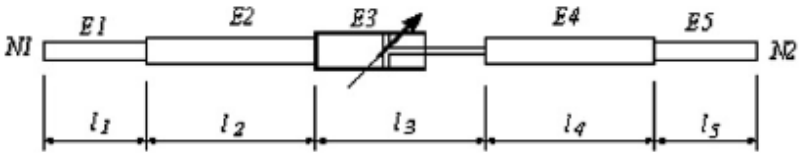

Figure 6.1-6, Finite element for the viscoelastic damper element.

The end elements, E1 and E5, simulates the node and bolt connections and the elements E2 and E4 are the bar members employed to couple the middle element representing the viscoelastic damper to the end connection members.

Considering this, the equivalent stiffness and mass matrices may be written as

$$k_{eq}^{-1} = \frac{k_2k_0k_4k_5 + k_1k_0k_4k_5 + k_1k_2k_4k_5 + k_1k_2k_0k_5 + k_1k_2k_0k_4}{k_1k_2k_0k_4k_5};$$

$$m_{eq} = m_1 + m_2 + m_D + m_4 + m_5. \qquad 6.1\text{-}10$$

Finally the stiffness and mass matrices for the members with the damper are developed. It should be noted that the stiffness matrix for the damper bar element has time dependent coefficients due to inherent non-linearity of the controllable damper. Thus matrix formulation of the structure can be stated as

$$[\mathbf{M}]\{\ddot{\mathbf{x}}(t)\} + [\mathbf{C}(t)]\{\dot{\mathbf{x}}(t)\} + [\mathbf{K}(t)]\{\mathbf{x}(t)\} = \{\mathbf{F}(t)\} \qquad 6.1\text{-}11$$

6.1.4 Solution of the non-linear FEM formulation

When the structure is excited under harmonic excitations and it does not include the damper, the system is linear and equation 6.1-11 can be expressed as

$$[\mathbf{M}]\{\ddot{\mathbf{x}}\} + [\mathbf{C}]\{\dot{\mathbf{x}}\} + [\mathbf{K}]\{\mathbf{x}\} = \mathrm{Im}\{\mathbf{F}\}e^{i\omega t}. \qquad 6.1\text{-}12$$

And the frequency domain solution can be written as

$$\{\mathbf{U}\} = \left(-\omega^2[\mathbf{M}]\right) + i\omega[\mathbf{C}] + [\mathbf{K}]^{-1}\{\mathbf{F}\}. \qquad 6.1\text{-}13$$

When the structure includes the viscoelastic damper, the governing equations are non-linear as stiffness and damping matrices are time dependent. To solve the equations, the Newmark method is applied with an inner iterative process in order to maintain the equilibrium of the forces at each time step. The Newmark method is a single step integration implicit method that attempts to satisfy the differential equation of motion at time $t + \Delta t$ after the solution at time t is found. The following algorithm presents the Newmark method with an inner process to solve the non-linear problem:

(a) Determine at $t = 0$:

$$[\mathbf{M}]_{t=0}, [\mathbf{K}]_{t=0}, [\mathbf{C}]_{t=0}, \{\mathbf{F}\}_{t=0}, \{\mathbf{x}\}_{t=0}, \{\dot{\mathbf{x}}\}_{t=0}.$$

(b) Define Newmark's constants, γ and β, maximum error for the unbalance force, ε, and final time t_f.

(c) Determine the acceleration vector at time $t = 0$:

$$\{\ddot{x}\}_t = [\mathbf{M}]^{-1}\left(\{\mathbf{F}\}_t - [\mathbf{C}]\{\dot{\mathbf{x}}\}_t - [\mathbf{K}]\{\mathbf{x}\}_t\right).$$

(d) Determine the Newmark's constants:

$$b_1 = \frac{1}{\beta\Delta t^2}; \quad b_2 = \frac{1}{\beta\Delta t}; \quad b_3 = \beta - \frac{1}{2}; \quad b_4 = \gamma\Delta t b_1;$$
$$b_5 = 1 + \gamma\Delta t b_2; \quad b_6 = \Delta t(1 + \gamma b_3 - \gamma). \qquad 6.1\text{-}14$$

(e) Compute the effective stiffness matrix and effective load:

$$[\hat{\mathbf{K}}] = b_1[\mathbf{M}] + b_4[\mathbf{C}] + [\mathbf{K}] \qquad 6.1\text{-}15$$
$$\{\hat{\mathbf{F}}\} = \{\mathbf{F}\}_{t+\Delta t} + [\mathbf{M}]\left(b_1\{\mathbf{x}\}_t + b_2\{\dot{\mathbf{x}}\}_t + b_3\{\ddot{\mathbf{x}}\}_t\right) + [\mathbf{C}]\left(b_4\{\mathbf{x}\}_t + b_5\{\dot{\mathbf{x}}\}_t + b_6\{\ddot{\mathbf{x}}\}_t\right) \qquad 6.1\text{-}16$$

(f) Calculate the displacement, velocity and acceleration vectors at iteration $i = 1$:

$$\{\mathbf{x}\}_{t+\Delta t} = [\hat{\mathbf{K}}]^{-1}\{\hat{\mathbf{F}}\},$$
$$\{\dot{\mathbf{x}}\}_{t+\Delta t} = b_4\left(\{\mathbf{x}\}_{t+\Delta t} - \{\mathbf{x}\}_t\right) + b_5\{\dot{\mathbf{x}}\}_t + b_6\{\ddot{\mathbf{x}}\}_t,$$

$$\{\ddot{\mathbf{x}}\}_{t+\Delta t} = b_1(\{\mathbf{x}\}_{t+\Delta t} - \{\mathbf{x}\}_t) + b_2\{\dot{\mathbf{x}}\}_t + b_3\{\ddot{\mathbf{x}}\}_t.$$

(g) Evaluate the unbalance force:

$$\{\delta\mathbf{F}\}^i = \{\mathbf{F}\}_{t+\Delta t} - [\mathbf{M}]\{\ddot{\mathbf{x}}\}^i_{t+\Delta t} - [\mathbf{C}]^i_{t+\Delta t}\{\dot{\mathbf{x}}\}^i_{t+\Delta t} - [K]^i_{t+\Delta t}\{\mathbf{x}\}^i_{t+\Delta t}.$$

If the value of the unbalance force is less than the allowable error ε go to step (k).

(h) Evaluate the effective stiffness matrix at iteration $i = i+1$:

$$[\hat{\mathbf{K}}]^{i+1} = [\mathbf{K}]^i_{t+\Delta t} + b_1[\mathbf{M}] + b_4[\mathbf{C}]^i_{t+\Delta t}.$$

(i) Compute the incremental displacement, velocity and acceleration vectors at $i = i+1$:

$$\{\delta\mathbf{x}\}^{i+1} = [\hat{\mathbf{K}}]^{-1,i+1}\{\delta\mathbf{F}\}^i,$$
$$\{\delta\dot{\mathbf{x}}\}^{i+1} = b_4\{\delta\mathbf{x}\}^{i+1},$$
$$\{\delta\ddot{\mathbf{x}}\}^{i+1} = b_1\{\delta\mathbf{x}\}^{i+1}.$$

(j) Determine the displacement, velocity and acceleration at iteration $i = i+1$:

$$\{\mathbf{x}\}^{i+1}_{t+\Delta t} = \{\delta\mathbf{x}\}^{i+1} + \{\mathbf{x}\}^i_{t+\Delta t},$$
$$\{\dot{\mathbf{x}}\}^{i+1}_{t+\Delta t} = \{\delta\dot{\mathbf{x}}\}^{i+1} + \{\dot{\mathbf{x}}\}^i_{t+\Delta t},$$
$$\{\ddot{\mathbf{x}}\}^{i+1}_{t+\Delta t} = \{\delta\ddot{\mathbf{x}}\}^{i+1} + \{\ddot{\mathbf{x}}\}^i_{t+\Delta t},$$

and then return to step (g).

(k) Go to the next time step $t = t + \Delta t$.

(l) If $t < t_f$ go to step (e), otherwise it is done.

After obtained the output from the above steps, this is manipulated by coming up with a cost function which will enable us to sought the optimal placement of dampers on the structure. This cost function is thus defined as follows:

$$f(t)_{peak} = \sqrt{\sum_{i=1}^{4} \ddot{x}_i^2(t)} \qquad 6.1\text{-}17$$

which is the peak, during the simulation time interval, of a vectorial sum of the accelerations $\ddot{x}_i$ of a single bundle of the structure for a given spacer stiffness. Depending on the number of cables in the bundle the cost function can be altered otherwise. The constraint on the number of dampers is defined as:

$$\sum_{i=1}^{n} \mathbf{n_i} = N \qquad 6.1\text{-}18$$

where $\mathbf{n}$ is the vector of discrete 0/1 design variables and N is the total number of dampers to be placed in the structure.

The objective is to find how many viscoelastic passive dampers, of a given capacity, that are needed to achieve maximum reduction of the cost function when the structure is excited by wind forces, using the genetic algorithm. For each optimization run, having the number of available dampers constrained, optimal placement of dampers is sought. The following section looks into what the whole modeling process constitutes.

6.2 The Modeling process

The model was run in Abaqus using the following modules available in each step; firstly it was creating the part in the PART module, which gives one the ability to vary the length of the model and also to create the partitions were the spacers are attached. The assigning of the property to the model was done using the PROPERTY module, which allows one to define the material behaviors. In this module the general behavior was used, were one defines the density and also the mechanical behavior were one has the option to define the modulus of elasticity and poisson's ratio of the elastically isotropic element was also used.

The model assemblage was made in the ASSEMBLY module. Here the cable element is instanced to form the dual assembly. Spacers were spaced along the span of the cable element using the connectivity type connect-two-points and the value of stiffness obtained by using the Engineering Features, Springs/Dashpots function. The equivalent stiffness and damping were

given for the spacers. Adding these viscoelastic dampers not only increases structural damping but also contributes to the stiffness of the structure. Increase of stiffness may reduce, increase or have negligible impact on the dynamic response of the structure. Zhang *et al.* (1989) concluded in their study that increased stiffness contributed by added dampers does not help to improve dynamic performance of the structure they analysed. In this study, the contribution from the damper to stiffness of the structure have been taken into account in the finite element model by using the Kelvin model of viscoelastic dampers, which consist of a viscous damper in parallel with a linear spring.

The STEP module follows, allowing one to define the steps in which the job is to be run. The first step was of preload the model in the general static procedure using explicit dynamic linear perturbation and then the second step was to extract the frequencies and mode shapes in the Frequency procedure. For both steps the geometric nonlinearities NGLEOM was considered.

The LOAD module followed after this, allowing one to preload the cable and give the required sag. Figure 6.2-1 shows the load being applied to the cables to give the required sag (arrows on the far left). Boundary conditions were assigned to the model. With one end being pinned (Figure 6.2-1, far left hand side) and the other were the preload force was applied being given the following boundary condition; XASSYM (U2=U3=UR1), thus allowing the load to be applied in the U1 direction (Figure 6.2-1, far right hand side).

Figure 6.2-1, A load being applied to the cables.

The model was then meshed in the MESH module by selecting the part instances to be assigned global seeds and giving the global size. Sizes of 0.5m and 1m were used for the different model cases. This global size was chosen on its ability to maintain accuracy in the approximations as well as saving computer time. Figure 6.2-2 shows a typical mesh of 0.5m applied to the system of two conductors on a span of 120m. A further reduction in the global size of the seeds meant

that this would take more computer time but with almost similar results. The truss element was selected as a standard linear element type to mesh the model. The model was then meshed, the mesh verified and this led to the next module.

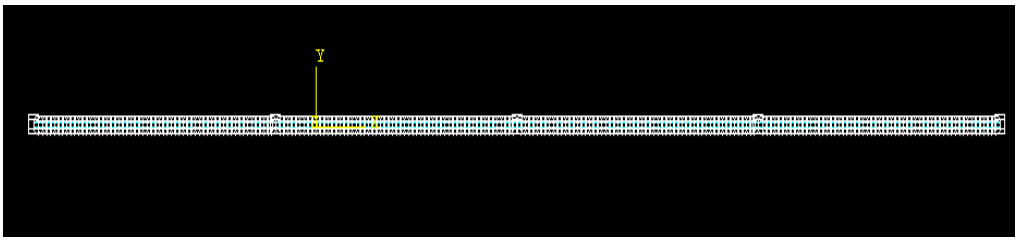

Figure 6.2-2, Cables with a mesh of 0.5m on a span of 120m.

The JOB module, being the next was initiated with the first task being to create the jobs for a full analysis. The capacity of the computer memory to be used was specified and this dependant on the type of machine being used in the analysis. The job is submitted and monitored, the results are obtained, and these are accessible through the VISUALIZATION module. Here one can see the deformed shapes and the plots can be made. Figure 6.2-3 shows a typical presentation of the results as in the visualization module.

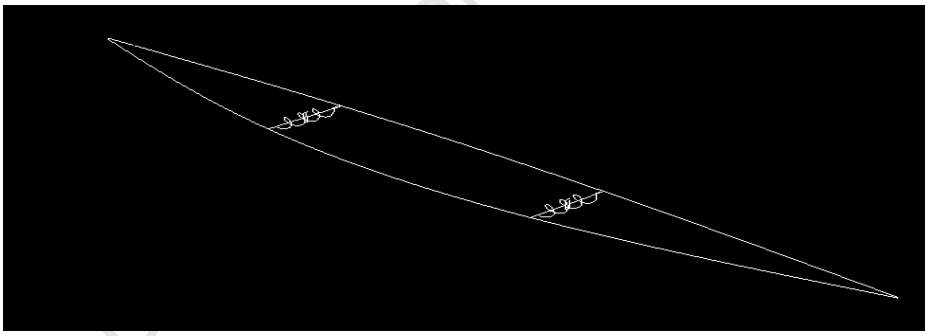

Figure 6.2-3, A dual cable arrangement with two spacers showing the first mode of vibration.

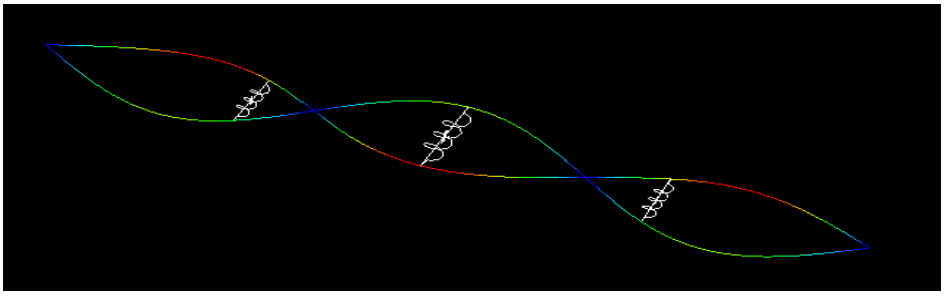

Figure 6.2-4, A dual cable arrangement with three spacers showing the third mode of vibration.

The results for the frequencies and mode shapes can now be tabulated and graphs can be plotted. The software Abaqus offers a function to plot certain graphs but also a user manipulates the results to give the best presentation that one requires.

6.3 Validation of Model

This section spends time in validating the finite element model chosen to represent the problem being studied. Time is spent in the beginning to validate the benchmark model which consists of the undamped system. Further to this the bundled damped system is investigated, here the equations so formulated in Chapter 5 are solved using the mathematical program MATLAB and compared with the results obtained from the finite element program ABAQUS.

6.3.1 Benchmark Model

The benchmark case is based on results obtained by Thomson (1965) in his violin string experiment. These results are compared with the results obtained from ABQUS. The parameters defining the violin string problem are given in table 6.3-1 below.

Table 6.3-1, Violin string parameters.

Cross-sectional area, A	1.979 mm^2
Density, ρ	7801 kg/m^3
Young's modulus, E	20.84 GPa
Tension Force, P	2224 N
Length, L	2.54 m

The results obtained for the free vibration of a violin string modeled by Thomson (1965) and the results obtained by using ABAQUS as well as analytical results from general cable theory (as from Chapter 4) are given in table 6.3-2.

Table 6.3-2, Calibration of Model, violin string problem.

Mode Number	Frequency (Hz)		
	Thomson (1965)	ABAQUS-Results	Analytical (cable theory)
1	74.7	74.5	74.7
2	149	149.02	149.4
3	224	223.5	224.1
4	299	298.04	298.8

The first four mode shapes obtained by using ABAQUS are shown below.

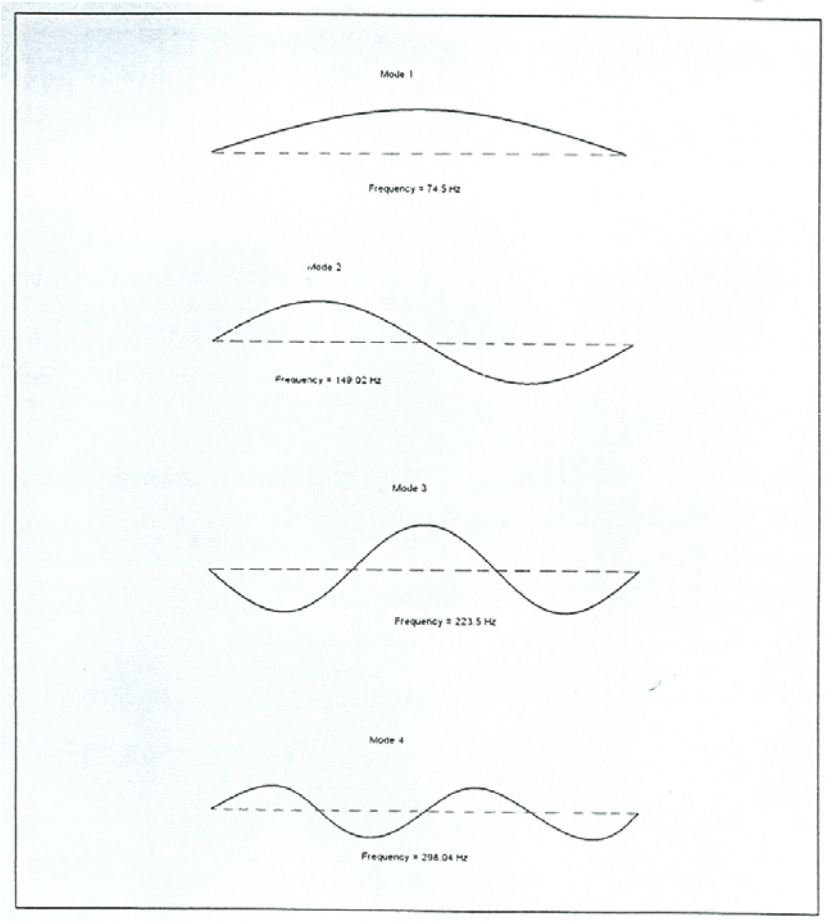

Figure 6.3-1, First four mode shapes as obtained with Abaqus.

The above calibration shows that the proposed model of coming up with natural frequencies is accurate since the results are similar to those obtained by Thomson (1965). However because the introduction of dampers makes the governing equations non-linear, the model is also validated for the bundled system of cables.

6.3.2 Bundled System Validation

The mathematical program Matlab is used to solve the equations formulated earlier in chapter 5. The results obtained are used to validate the values obtained for the same problem using the finite element program Abaqus. To follow is an analysis example showing how the two approaches compare is as far as solving the problem at hand.

6.3.2.1 Cable Properties

The table below shows the conductor properties for the choice of conductor used in the models. This type of conductor is chosen because it is the one adapted by most electricity generation boards and has also by far many advantages than most other conductors. Our local electricity generation body Eskom also has adapted the use of the Aluminium Conductor Steel Reinforced (ACSR) conductors. Attached in Appendix A is a table that shows physical characteristics of the different conductors available and the one eventually chosen for the study. Table 6.3-3 below shows the detailed properties of the cable used in this investigation.

Table 6.3-3, Cable properties (source: ASTM B 232-see Appendix A).

	Conductor
Name	CONDOR
Type	ACSR
Diameter (mm)	27.8
Area (mm^2)	455.03
Modulus of elasticity (GPa)	64.5
Weight per unit length (N/m)	14.94
Mass per unit length (kg/m)	1.524
Initial horizontal tension (kN)	18.8
Rated tensile strength (kN)	125.4

6.3.2.2 Analysis Example

In this example we consider a span made of a bundle of two and four conductors. The conductor bundle spanning a length of 85m is chosen to represents the model. The conductors were separated by a distance of 14 conductor diameters falling in the standard separation specified by most codes of practice. The conductor type as given above is ACSR-CONDOR and the initial tension is 18.8KN which is 15% UTS, the other properties are as shown in table (6.3-3) above. The tension is adjusted to cater for 20%, 25%, 30% and 40% UTS tensions.

Five different cases are considered in the analysis. The conductor is in general considered as having three subspans. The benchmark and most basic case has all three subspans of equal length and then these subspans are varied but with the middle subspan remaining constant.

Table (6.3-4) below gives the summary of all the analysis cases considered.

Table 6.3-4, Summary of the different cases considered.

	Subspan Length, m		
Case	No. 1 (X)	No. 2 (Y)	No. 3 (Z)
1	28.33	28.33	28.33
2	25	28.33	31.67
3	21.67	28.33	35
4	18.34	28.33	38.33
5	15.01	28.33	41.66

Figure (6.3-2) below shows the sketch showing the definition problem.

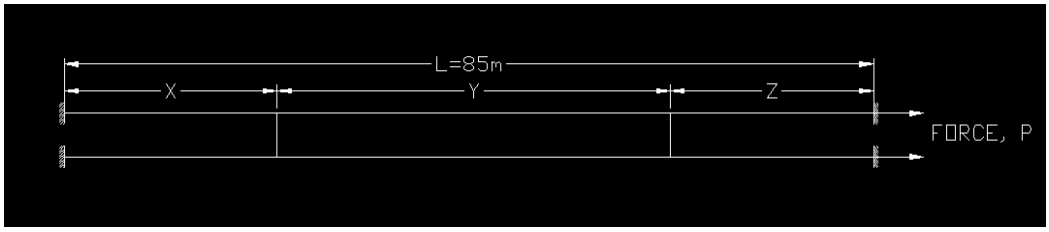

Figure 6.3-2, Definition problem of a system of two conductors.

For each of the cases above the eigenfrequency and eigenvalues were extracted for the first five modes of vibration recorded. The following section deals with the results obtain and the discussions.

6.3.2.3 Results and Discussions

A ratio of the damped to the undamped frequency is taken for each span so that the behavior of each span can be analysed individually and if need for comparison be, this can also be done. For the purpose of this discussion the ratio of the damped to the undamped natural frequency is termed the Response ratio.

From the above analysis one can come up with a variation of frequency and the different mode shapes. Figure (6.3-3) shows this variation at 40% UTS, a significant drop is seen from mode 2 to mode 4 showing a great effect from the spacers.

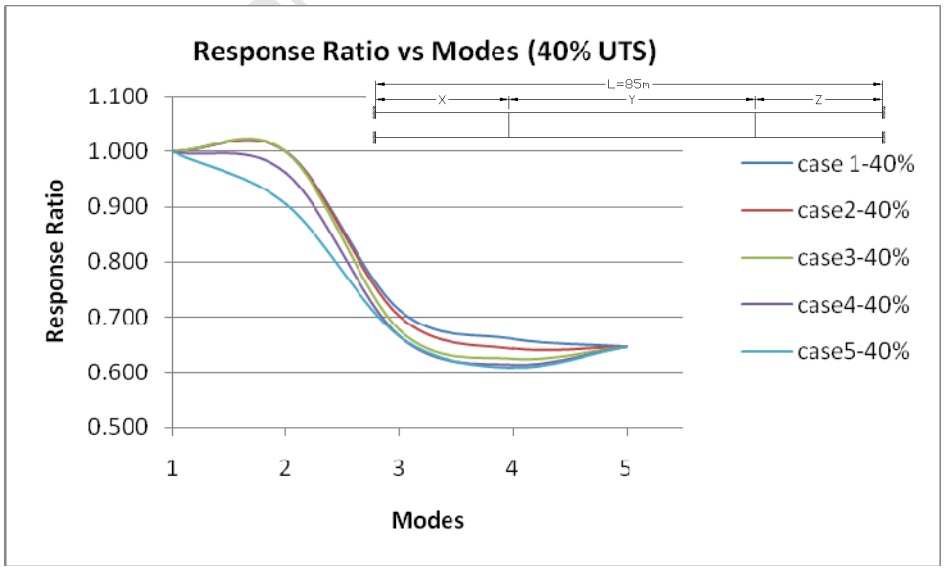

Figure 6.3-3, Response Ratio vs Modes (40% UTS).

The mode shapes are normalized with respect to frequency so that its maximum value is always equal to one. A graph is drawn of the variation of the Response ratio at 20% UTS with the mode shapes and is shown below. The first case shows the ineffectiveness of the spacers as seen by the almost constant graph of case 1.

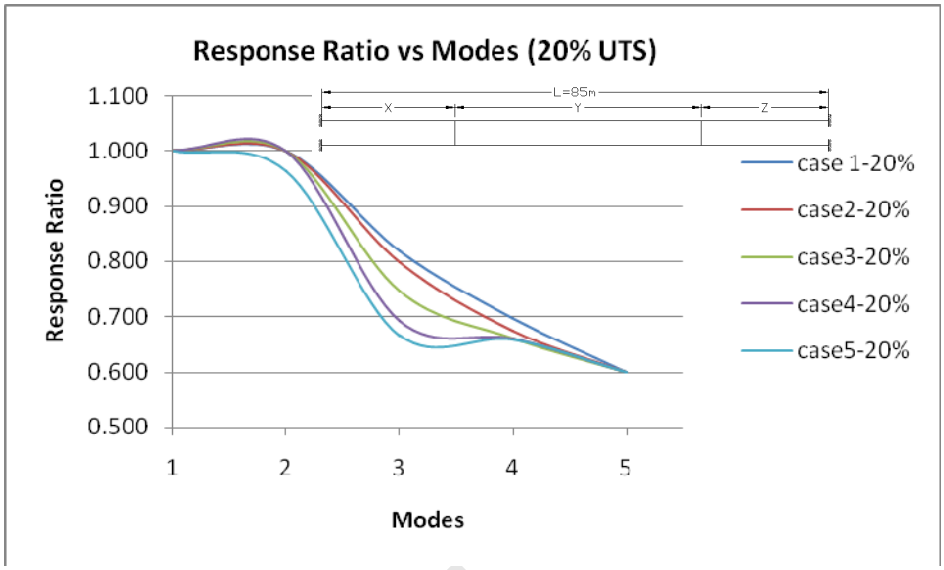

Figure 6.3-4, Response Ratio vs Modes (20% UTS).

As seen in the graphs above the spacer deployment represented by case 1 is by far the most ineffective and great care must be taken to avoid this type of spacer deployment. The figures that follow give a plot of Response ratio against modes for the 15%, 25% and 30% respectively.

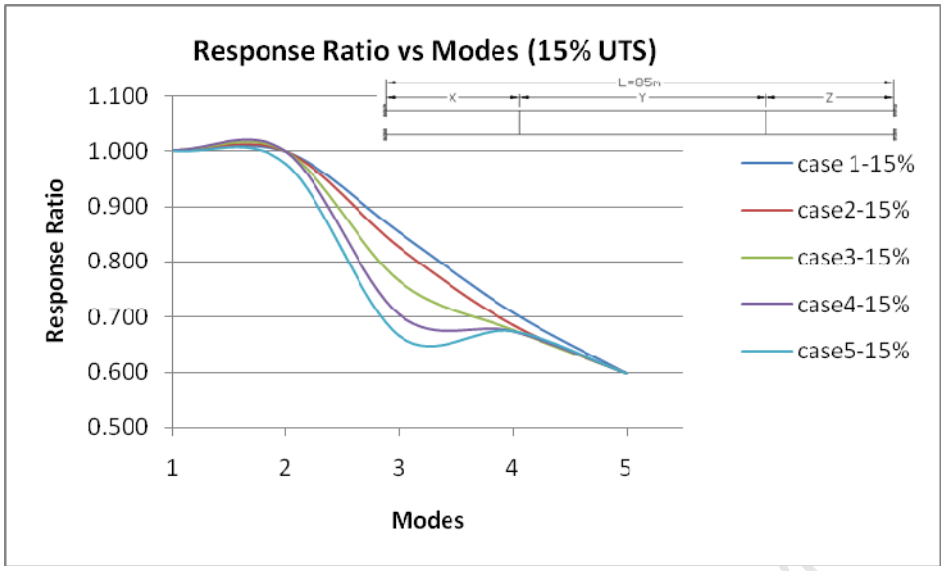

Figure 6.3-5, Response Ratio vs Modes (15% UTS).

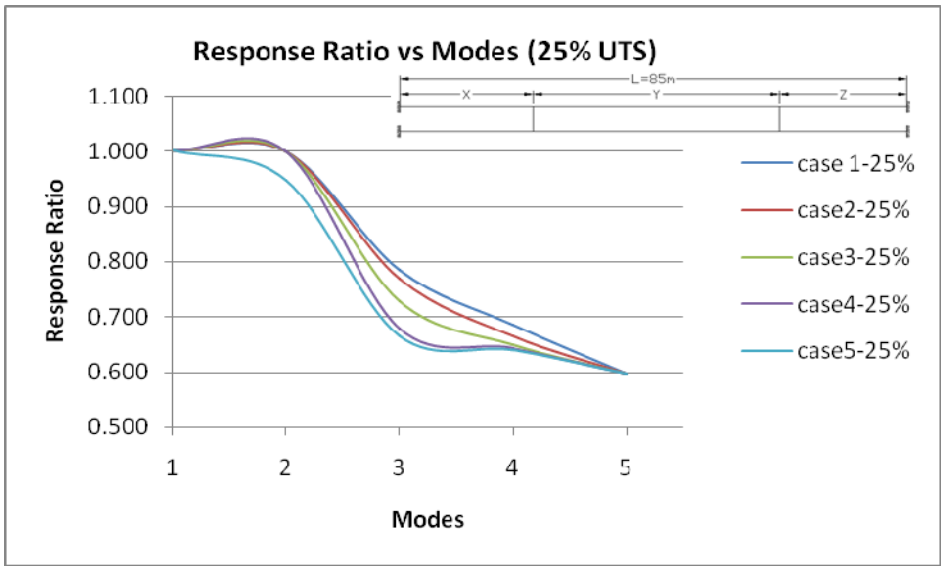

Figure 6.3-6, Response Ratio vs Modes (25% UTS).

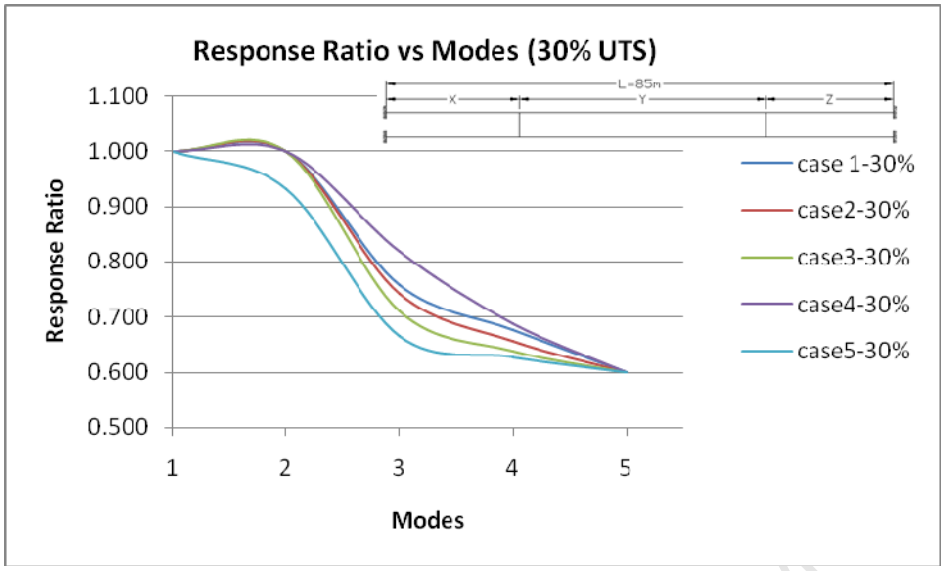

Figure 6.3-7, Response Ratio vs Modes (30% UTS).

Also from these, we see a similar trend as observed in the 20% and 40% UTS plots. These observations agree very well with the findings from literature because this results in the creation of nodes at the position of the spacers and thus render the spacer ineffective in reducing the vibration as observed by (Hearnshaw, D. 1974). It therefore carries some advantage if spacers are placed asymmetrically, thereby removing the possibility of a spacer falling at a node point.

Having establisehed the above we further move on to solve the equations formulated in chapter 5 to obtained the behaviour of the bundled system and compared with the above results obtained fron ABAQUS.

After entering the cable properties into the MATLAB program written NEWMARK_INT (see Appendix A) we go on further to utilise the cost function (equation 6.1-17) to sought the optimal damper placement.

The following inputs are required in the program:

INPUT

Time Vector, Externally Applied Load, Initial Position, Initial Velocity-a function dependant on the wind pressures, System Mass, System Stiffness & System Damping. The outputs are:

OUTPUT

Displacement Response, Velocity & Acceleration

The following table shows the optimisation results for different constraints on number of dampers. These results are compared with the ABAQUS results to complete the bundled conductor problem validation.

Table 6.3-5, Optimisation results for different constraints on number of dampers

Span = 85m	Number of dampers		
	0	1	2
Cost function, run1 (ms^{-2})		0.334537	0.321528
Cost function, run2 (ms^{-2})		0.334537	0.321528
Cost function, run3 (ms^{-2})		0.33487	0.321364
The best cost function (ms^{-2})	0.767	0.33487	0.321364
Reduction in the cost function (%) compare to the case with no dampers (Response ratio)		56.3	**58.1**

The table above shows results which are very useful in as far as obtaining the optimal placement of dampers is obtained. From the graphs shown above figure 6.3-3 to figure 6.3-7, it is quite clear that the response ratio obtained for all cases is minimum at 0.6. This value as a percentage translates to 60 % of the response ratio. Similarly from table 6.3-5 with the same number of dampers it is seen that the reduction in the cost function is found to be 58.1% for the case with two dampers which is quite close to 60% obtained from ABAQUS.

6.3.3 Conclusion

It is essential in every research problem to validated one's model before one embarks on a detailed parametric study. This chapter has shown how the proposed model has been validated by first looking at the benchmark problem comprising the undamped system which has been quite easily validated using the violin string experiment conducted by Thomson (1965).

However the bundled system behaves differently from the assumed theory above and this has been taken into account. The finite element program ABAQUS has been used to come up with different response ratios and these have been plotted out in graphs (see figure 6.3-3 to 6.3-7). These results have been validated using the analytical formulation taken from chapters 5 and 6. The cost functions obtained from this formulation are compared with the case with no dampers to come up with a percentage reduction also termed the response ratio.

The response ratios obtained from the reduction in the cost function are compared with the response ratio obtained from the ABAQUS runs and the results compare so very well. The ratio from the cost function reduction using the same number of dampers is 58.1 % and the response ratio from the ABAQUS plots is found to be 60%.

Taking the above results as a basis for further investigation, a parametric study is conducted to show how these dampers can be optimally placed on various spans of the transmission lines. Chapter 6.4 to 6.8 is a detailed parametric study to show how one can best deploy spacers along the transmission line.

6.4 Parametric Study

For the parametric study to follow, different spans are considered and the number of dampers on these lines are varied. The family of graphs plotted show the results that are achieved from the parametric study. As seen also the tension is varied as 15, 20, 25, 30 & 40 % of UTS for each configuration. The choice of the tension in the cables was done in order to give a reasonable sag to span ratio and is the range recommended in most codes of practice (Cigre, 1999).

The spacer stiffness is also varied in three cases, thus 5kN/m, 10kN/m and 15kN/m, which is the standard values of the readily available dampers (Wang, Q. H., et al 1997). Also an equivalent viscous damping coefficient is applied with the stiffness. Values considered for the damping coefficients are 0.4kNs/m, 0.6kNs/m and 0.8kNs/m respectively. For consistence sake the lower value of stiffness is used with the correspondingly lower value of damping. This is so because the greater the damper stiffness is, the higher the critical velocity is. As a result, the bundled system requires more overall damping and, moreover, a maximum amount of the overall damping is required at or near critical velocity. For each span length, graphs which show how the number of spacers, spacers stiffnesses and the tension vary against the response ratio are produced. The number of dampers are kept odd as much as possible to avoid the additional unwanted minor forces which come up as a result of symmetry, as seen in the analysis example earlier.

Table 6.4-1 below shows the different configuration options adapted.

Table 6.4-1, Parameters considered in the study.

No. of dampers	Span length (m)	Tension (%UTS)	Spacer Stiffnesses (kN/m)	Damping Coefficients (kNs/m)
1,2,3,5	120	15,20,25,30 & 40	5, 10, 15	0.4, 0.6, 0.8
1,2,3,5,7,9	200	15,20,25,30 & 40	5, 10, 15	0.4, 0.6, 0.8
1,2,3,5,7,9,11,13	400	15,20,25,30 & 40	5, 10, 15	0.4, 0.6, 0.8

To follow is the study carried over to the 120m span, 200m and 400m spans.

120m Span

Considering a dual cable system and with dampers placed at a third and two third points we have the following graphs obtained. The tension and stiffness is varied as per table (6.4-1) above.

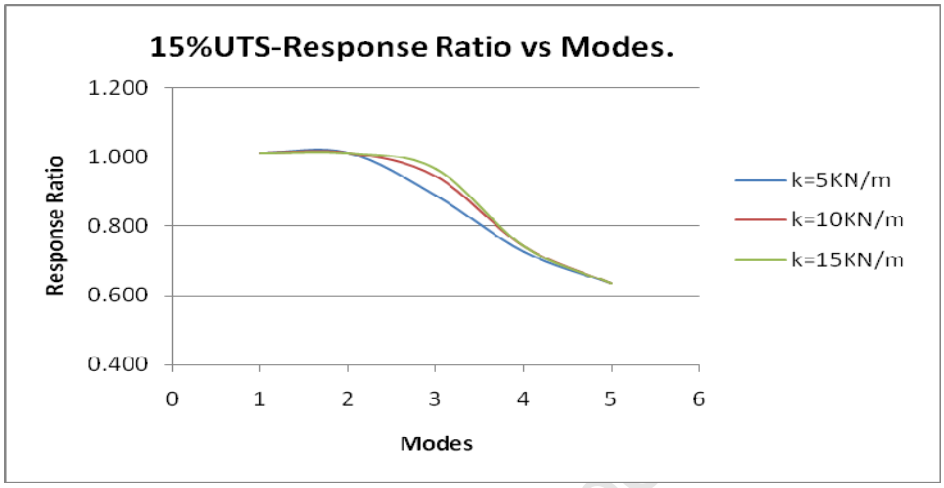

Figure 6.4-1, 15% UTS-Response Ratio vs Modes.

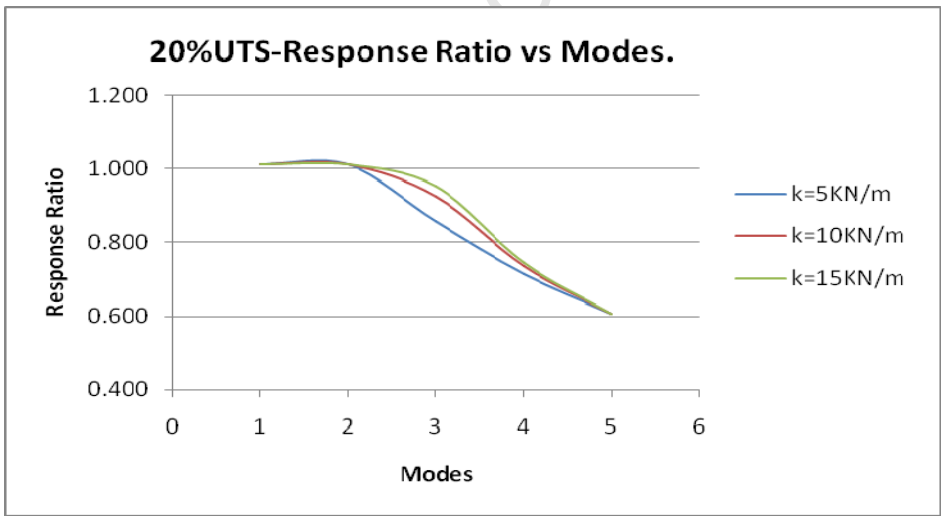

Figure 6.4-2, 20% UTS-Response Ratio vs Modes.

Although the above graphs are for the 15% and the 20% UTS responses only, a similar trend appears in all graphs through to the 40% UTS response. It is seen though that mode 3 and mode 4 give a significant drop in frequencies and these are investigated further, in the figures to follow. Further plots of these modes reveals that as the tension is increased the normalized

frequency increases showing that the difference between the undamped and the damped frequencies is quite significant.

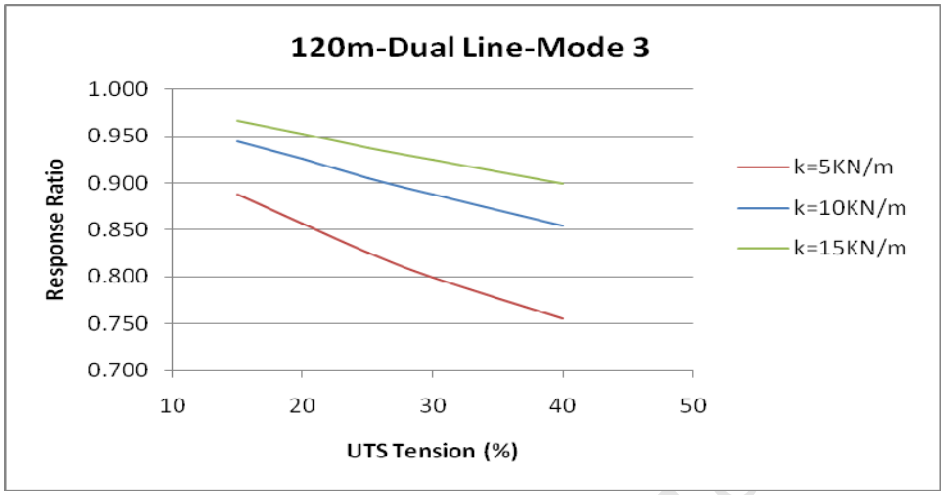

Figure 6.4-3, 120m Dual Line-Mode 3.

In mode 4 the Response ratio even drops further for the maximum UTS tension of 40% and is seen in figure 6.4-4 to be 0.68 for a stiffness of 5kN/m. The figure to follow shows this variation for the fourth mode of vibration.

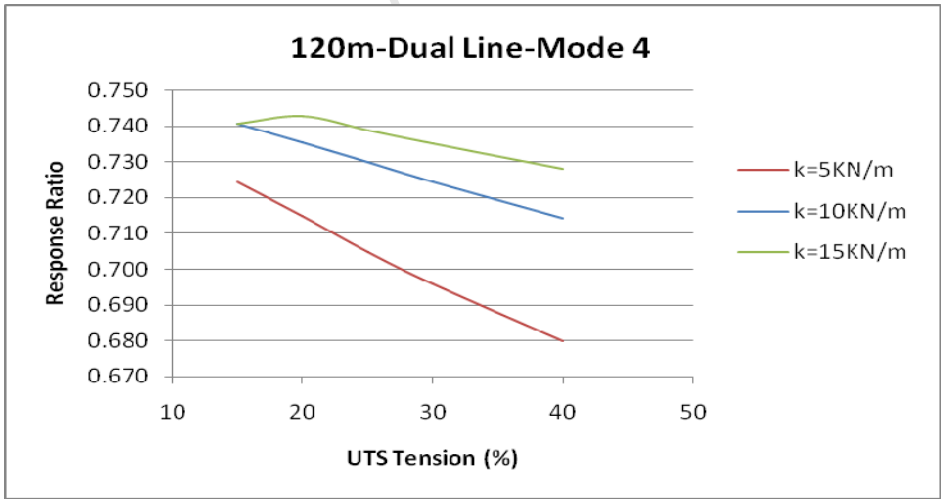

Figure 6.4-4, 120m Dual Line-Mode 4.

The case for the single spacer is also investigated and the resulting graphs plotted. The total family of graphs produced will give a variation of the stiffness, span length, number os spacers

and the applied tension. This will then make it easier for the design engineer to select the particular parameters to vary for a particular span.

Table 6.4-2, shows the modes that change as the stiffness of the spacer was varied. The other modes not shown in the table did not change with a change in stiffness.

Table 6.4-2, 120m-Modes changing with stiffness change.

Span (m)	Number spacers	Tension (%UTS)	Modes changing with a change in stiffness.
120	1	15	2,4
		20,25,30,40	2,5
	2	15	1
		20,25,30,40	3
	3	15,20,25,30,40	4,5
	4	15,20,25,30,40	3
	5	15,20,25,30,40	4,5

200m Span

Considering the 200m span the modes that change as the stiffness of the spacer is varied are given in table 6.4-3 below. These are further explained in the chapter to follow.

Table 6.4-3, 200m-Modes changing with stiffness change.

Span (m)	Number spacers	Tension (%UTS)	Modes changing with a change in stiffness.
200	1	15	2,5
	2	15	3,4,5
		20,25,30,40	3
	3	15,20,25,30,40	4,5
	5	15,20,25,30,40	4,5
	7	15,20,25,30,40	4,5

For the span of 200m it is seen that (table 6.4-3) with only one spacer at the midspan the second and fifth modes are the only ones showing a change in the frequency of excitation whereas the rest of the modes have a constant frequency. Adding one more spacer thus with two spacers equally spaced at third and two third points shows a shift in the mode that changes with change in stiffness. Here it's the third mode only which shows a change in the frequency of excitation due to a change in stiffness. Placing a third spacer equally along the span, thus at quarter points gives a shift in the mode that cahnges with change in stiffness, this time it is the fourth and the fifth mode but with a significant increase in the frequency. This similar trend is also noted when we place a fifth and the seventh spacers onto the system.

Of interest to note is the frequency of vibration which is low for the dually damped system than for the uni-spacer or triple-spacer system showing the effectiveness of adopting this deployment system. An increase in the span tension resulted in an increase in the frequency as expected from theory, but of significance is how the increase in stiffness also increased the frequency of excitation. This shows that careful attention should be given to the selection of the spacers so that the stiffness is in a particular range that gives the design engineer lower vibration frequencies. Values of 5, 10 and 15kN/m used for the rigid type spacers lie in the common range of spacer stiffnesses to choose from.

400m Span

Considering the 400m span the modes that change as the stiffness of the spacer is varied are given in table 6.4-4 below. These are further explained in the chapter to follow.

Table 6.4-4, 400m-Modes changing with stiffness change.

Span (m)	Number spacers	Tension (%UTS)	Modes that change with a change in stiffness.
400	1	15,20,25,30,40	2,5
	2	15,20,25,30,40	3
	3	15,20,25,30,40	4,5
	5	15,20,25,30,40	4,5
	7	15,20,25,30,40	4,5
	9	15,20,25,30,40	4,5
	11	15,20,25,30,40	4,5

As seen earlier for the 200m span, the 400m span presents us with almost the similar behaviour. All the spacer deployment configuration show that the modes that change due to a change in stiffness are the same as the 200m span. However, as expected also the increase in span results in a decrease in the frequency of vibration. Of interest to note however is the shift in the modes that change with the change in stiffness. The least tension thus 15% UTS shows the third, forth and fifth modes changing as a result of change in stiffness in the 200m span but this is not so for the 400m span which only the third mode shows a change.

The table below shows the natural frequencies of the undamped models obtained by using the numerical analysis. These values are compared with the analytical ones and used together with the results of the damped response to give the Response Ratio used to plot the graphs explained in the next chapter.

Table 6.4-5, Comparison of Natural frequencies at 15% UTS.

Modes	Natural Frequencies (15% UTS)					
	Abaqus			Analytical		
	120m	200m	400m	120m	200m	400m
1	0.47	0.28	0.15	0.46	0.28	0.14
2	0.94	0.58	0.29	0.93	0.56	0.28
3	1.40	0.85	0.43	1.39	0.83	0.42
4	1.87	1.13	0.58	1.85	1.11	0.56
5	2.34	1.41	0.71	2.32	1.39	0.69

Table 6.4-6, Comparison of Natural frequencies at 20% UTS.

Modes	Natural Frequencies (20% UTS)					
	Abaqus			Analytical		
	120m	200m	400m	120m	200m	400m
1	0.54	0.32	0.16	0.54	0.32	0.16
2	1.08	0.65	0.32	1.07	0.64	0.32
3	1.62	0.98	0.49	1.61	0.96	0.48
4	2.16	1.30	0.65	2.14	1.28	0.64
5	2.70	1.63	0.82	2.68	1.61	0.80

Table 6.4-7, Comparison of Natural frequencies at 25% UTS.

Modes	Natural Frequencies (25% UTS)					
	Abaqus			Analytical		
	120m	200m	400m	120m	200m	400m
1	0.60	0.36	0.18	0.60	0.36	0.18
2	1.21	0.73	0.37	1.20	0.72	0.36
3	1.81	1.10	0.56	1.80	1.08	0.54
4	2.42	1.46	0.74	2.39	1.44	0.72
5	3.02	1.82	0.92	2.99	1.80	0.90

Table 6.4-8, Comparison of Natural frequencies at 30% UTS.

Modes	Natural Frequencies (30% UTS)					
	Abaqus			Analytical		
	120m	200m	400m	120m	200m	400m
1	0.66	0.39	0.20	0.65	0.39	0.20
2	1.32	0.80	0.40	1.31	0.79	0.39
3	1.98	1.20	0.61	1.96	1.18	0.59
4	2.64	1.59	0.81	2.62	1.57	0.79
5	3.29	1.98	1.00	3.27	1.96	0.98

Table 6.4-9, Comparison of Natural frequencies at 40% UTS.

Modes	Natural Frequencies (40% UTS)					
	Abaqus			Analytical		
	120m	200m	400m	120m	200m	400m
1	0.76	0.45	0.23	0.76	0.45	0.23
2	1.53	0.92	0.47	1.51	0.91	0.45
3	2.29	1.38	0.70	2.27	1.36	0.68
4	3.05	1.84	0.93	3.03	1.82	0.91
5	3.80	2.29	1.16	3.78	2.27	1.14

The above results agree very well with each other and thus this further validates them. Figure 6.4-5 gives a plot of the results obtained for the 120m span for one mode. Since all modes show a similar trend we just consider one mode for the sake of comparison with other published results, say the second mode.

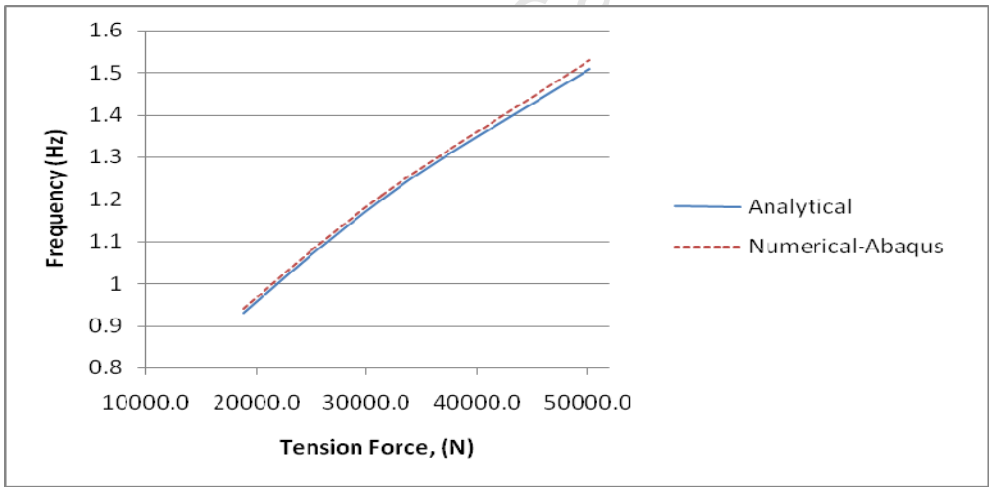

Figure 6.4-5, Comparison of analytical and numerical results.

In work done by Wenjie Wu (2006), a graph drawn of the results obtained in their experiment gives a similar trend in the results obtained in this research and as seen in the figure below there is a strong correlation in the results obtained.

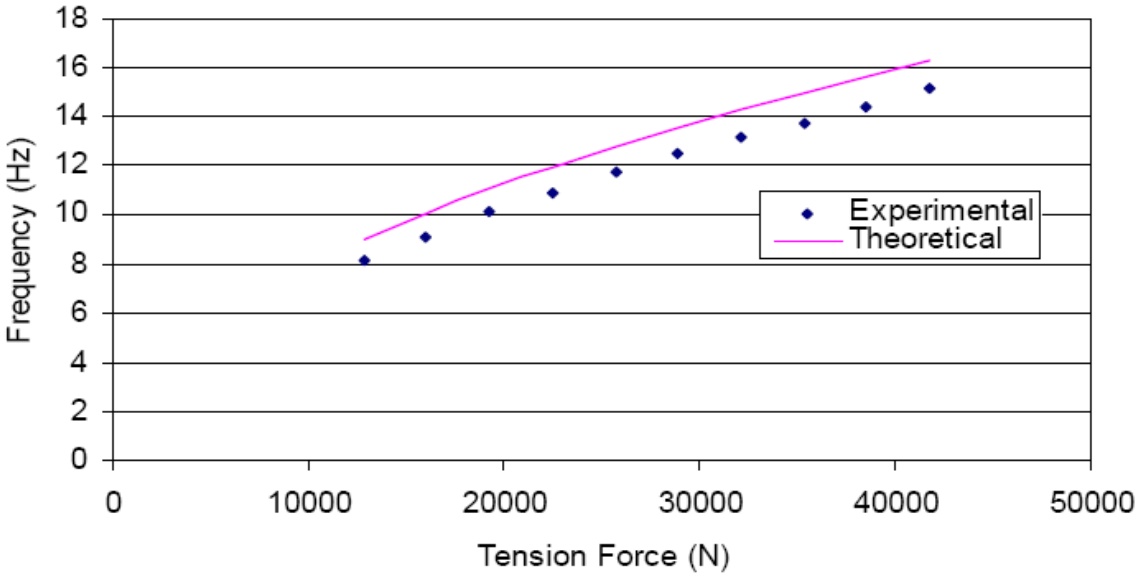

Figure 6.4-6, Comparison of theoretical and experimental results of the cable natural frequencies (Wenji Wu, 2006).

As seen in figure 6.4-6, the fundamental natural frequency was obtained as 8.93 Hz when the cable axial tension force was 16.06 kN. Since the scaling factor used is eight, the frequency of the prototype cable thus corresponds to 1.12Hz, which is within the reasonable range of the actual cable frequency (Tabatabai et al. 1998 in Wenjie Wu, 2006). The above statement then leaves the obtained frequencies in the range of our obtained results.

Similarly running a cost function of the different spans above gives the results tabulated below:

Table 6.4-10, Optimization results for different constraints on number of dampers-120m span.

Span = 120m	Number of dampers				
	0	1	2	3	5
Cost function, run1 (ms^{-2})		0.354534	0.341533	0.318521	0.332523
Cost function, run2 (ms^{-2})		0.354534	0.341533	0.318521	0.332523
Cost function, run3 (ms^{-2})		0.35484	0.341357	0.317845	0.332366
The best cost function (ms^{-2})	0.789068	0.354534	0.341357	0.317845	0.332523
Reduction in the cost function (%) compare to the case with no dampers (Response ratio)		55.07	56.74	**59.72**	57.86

The table above shows the results for the optimal placements found by the genetic algorithm tool. The tool proposes optimal placements in order to reduce the cost function, which is defined as the peak value of vectorial sum of the bundle cable accerations for any given spacer stiffness value. The reduction in the cost function as compared to a case with no spacers is found to be 59.72%. Further plots and discussions are dealt with in Chapter 7.

Table 6.4-11 shows the results of running this genetic algorithm on the 200m span.

Table 6.4-11, Optimization results for different constraints on number of dampers-200m span

Span = 200m	Number of dampers						
	0	1	2	3	5	7	9
Cost function, run1 (ms^{-2})		0.3648	0.3525	0.3225	0.3126	0.3227	0.3263
Cost function, run2 (ms^{-2})		0.3648	0.3525	0.3225	0.3126	0.3227	0.3263
Cost function, run3 (ms^{-2})		0.3648	0.3513	0.3268	0.3124	0.3266	0.3303
The best cost function (ms^{-2})	0.7790	0.3648	0.3513	0.3225	0.3124	0.3227	0.3303
Reduction in the cost function (%) compare to the case with no dampers (Response ratio)		53.17	54.90	58.60	**59.90**	58.57	57.60

It is observed from the table above that the reduction in the cost function is 59.90%. This shows how using 5 spacers on the given span becomes the most efficient system and this is compared with the previous findings from the numerical analysis as we see in the next.

Table 6.4-12 below shows us the optimization results considering the 400m span.

Table 6.4-12, Optimization results for different constraints on number of dampers-400m span

Span = 400m	Number of spacers										
	0	1	2	3	5	7	9	11	13		
Cost function, run1		0.40166	0.39170	0.35835	0.34730	0.33534	0.31291	0.32476	0.36084		
Cost function, run2		0.40166	0.39170	0.35835	0.34730	0.33534	0.31291	0.32476	0.36084		
Cost function, run3		0.40166	0.39039	0.36315	0.34706	0.33344	0.31370	0.32556	0.36173		
The best cost function	0.76875	0.40166	0.39039	0.35835	0.34706	0.33344	0.31291	0.32476	0.36084		
Reduction in the cost function (%) compare to the case with no dampers (Response ratio)		47.75	49.22	53.38	54.85	56.63	**59.32**	57.75	53.06		

From the above table the reduction in the cost function is seen to 59.32%. It also seen from the results above that this reduction occurs when the number of dampers on the transmission line is 9 giving a spacing of 44m on the 400m line.

6.8 Conclusion

It is quite apparent from the results obtained that the use of spacer dampers gives reasonable reductions in conductor vibrations. It is seen however that as the span of the conductors was increased this led to a rather unnoticeable effect of the spacers. From work done by Wenjie Wu (2006), it is seen that the frequency of vibration increases as the tension in the cable increases which was also a similar trend observed with all the different cases. As seen also in section 6.3 the values obtained in this study for the natural frequency were within the range of results obtained by other authors like Simpson, 1965.

The relative positioning of the spacers along the span caused a significant change in the frequencies of vibration and the particular modes excited. From the modes excited, one can observe that placing an even number of spacers equidistantly along the span resulted in the excitation of the odd mode, thus mode three. Also placing an odd number of spacers along the span resulted in the excitation of the first even mode and the second odd mode.

The algorithm to come up with the cost function can be seen to be very useful in obtaining an efficient way to deploy spacers on the transmission line. The results obtained show a similar trend to the numerical results obtained from the numerical analysis. Detailed analyses of these results are discussed in the following chapter.

7.0 DISCUSSION OF RESULTS

Earlier we see that the modes excited due to a change in the stiffness vary according to the number of spacers on the span of the conductors (table 6.7-2 to 6.7-4). This chapter seeks to explain these excited modes and see how they vary with the different spacer configurations. The objective is to be able to specify to the design engineer the most efficient deployment mechanism of these spacers.

7.1 Explaining the excited modes

The figures below show plots of the different cases considered. In figure 7.1-1, one can see that for the same spacer stiffness and with different spans, the normalized frequency is high for the longest span and low in the smallest span. Although this appears to be so, the natural frequency is high for the smaller span than it is for the longer span. This result shows however that the effect of the spacer in reducing vibrations is greatly experienced with the shorter span. However by increasing the number of spacers and keeping the span constant, this behavior changes as seen later in the chapter.

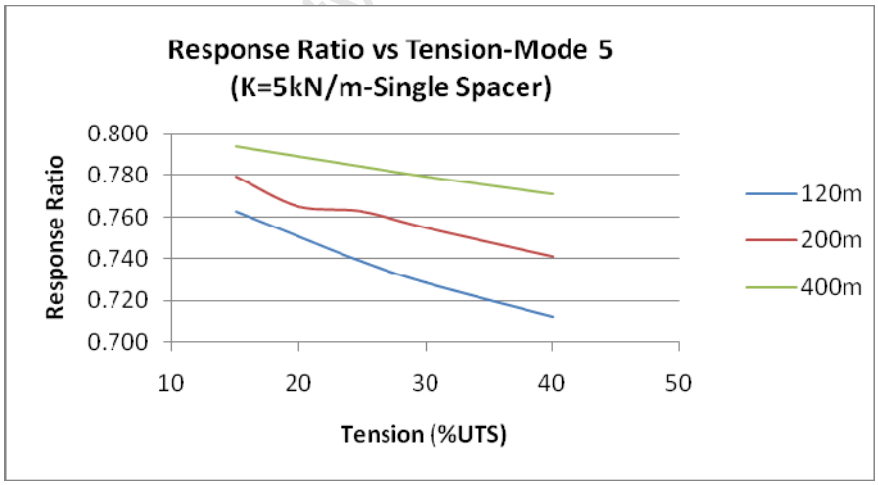

Figure 7.1-1, Plot of Response Ratio vs Tension-Mode 5 (K=5kN/m-Single Spacer).

The observations with the 5kN/m spacer can be extended to the 10kN/m and 15kN/m spacers with the only difference coming in that, as the stiffness of the spacer is increased the effect in reducing the vibration frequency is significantly reduced.

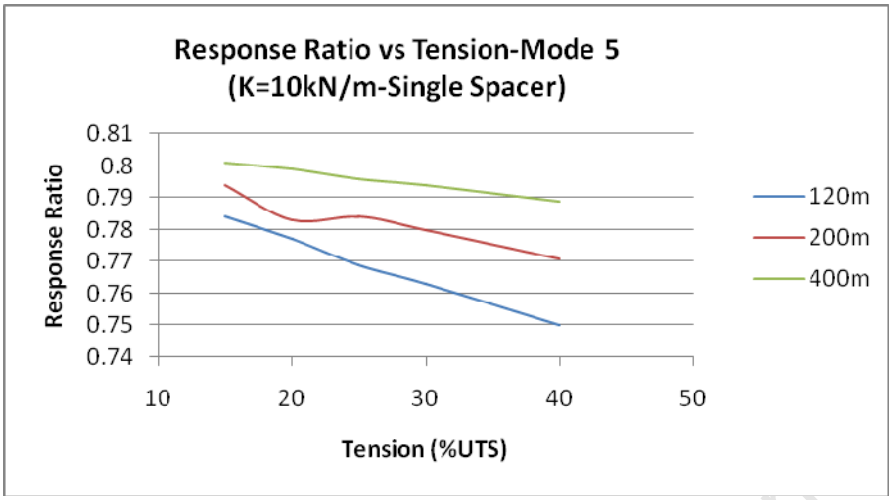

Figure 7.1-2, Plot of Response Ratio vs Tension-Mode 5 (K=10kN/m-Single Spacer).

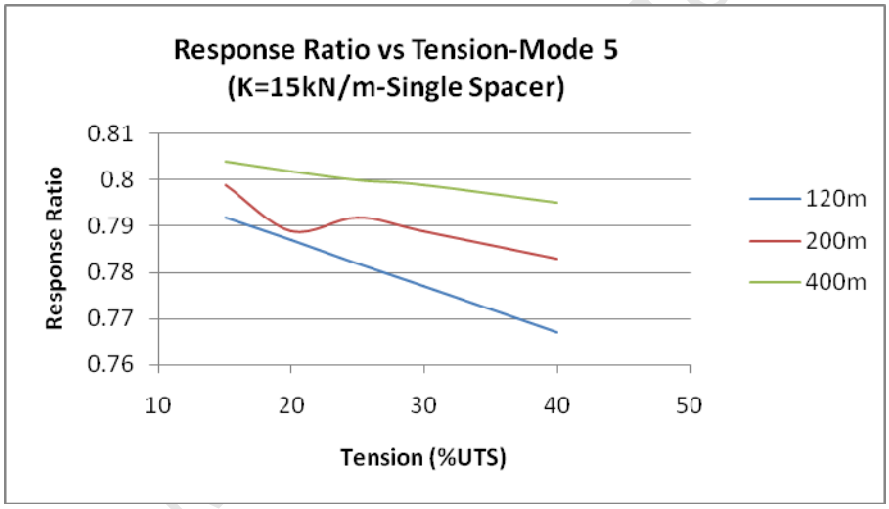

Figure 7.1-3, Plot of Response Ratio vs Tension-Mode 5 (K=15kN/m-Single Spacer).

The above graphs show the behavior of the dual conductor with a single spacer. Here attention is paid to the modes of vibration that are excited during the conductor, thus the fifth mode. Having dealt with the fifth mode of vibration, attention is placed at the second mode of vibration. The following plots now give the behavior of the response ratio to the tension.

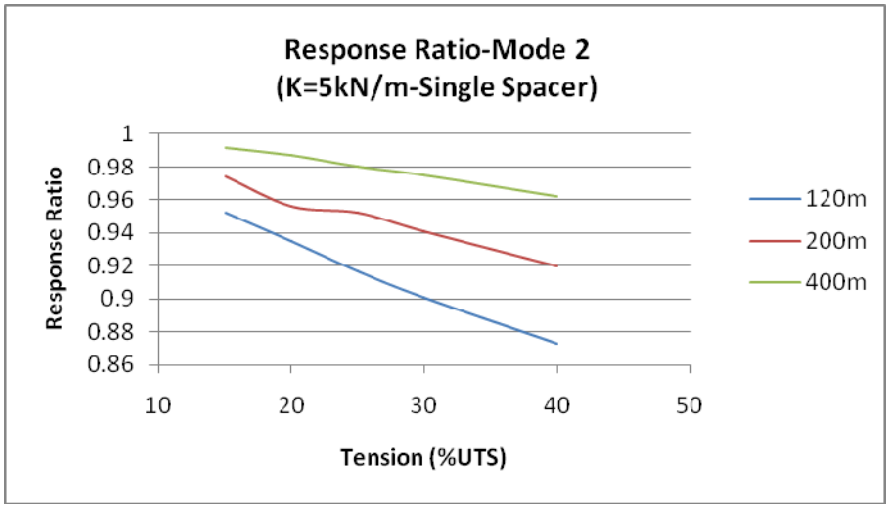

Figure 7.1-4, Plot of Response Ratio vs Tension-Mode 2 (K=5kN/m-Single Spacer).

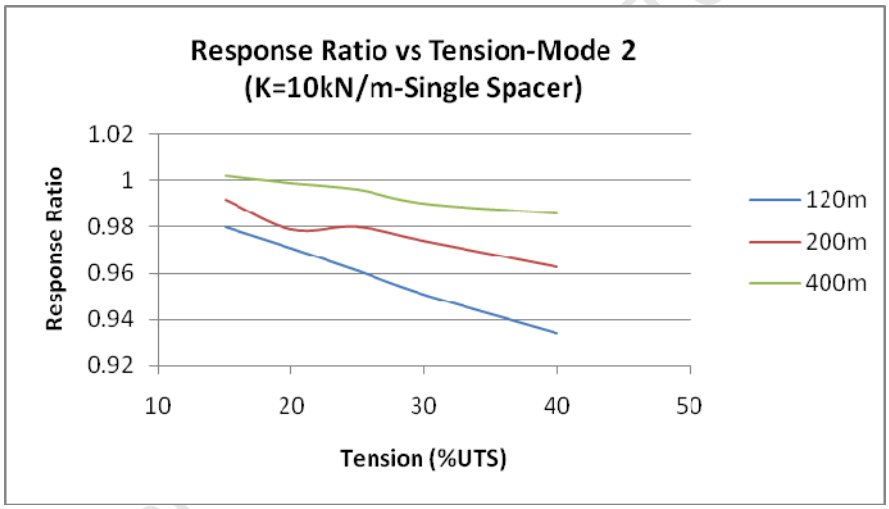

Figure 7.1-5, Plot of Response Ratio vs Tension-Mode 2 (K=10kN/m-Single Spacer).

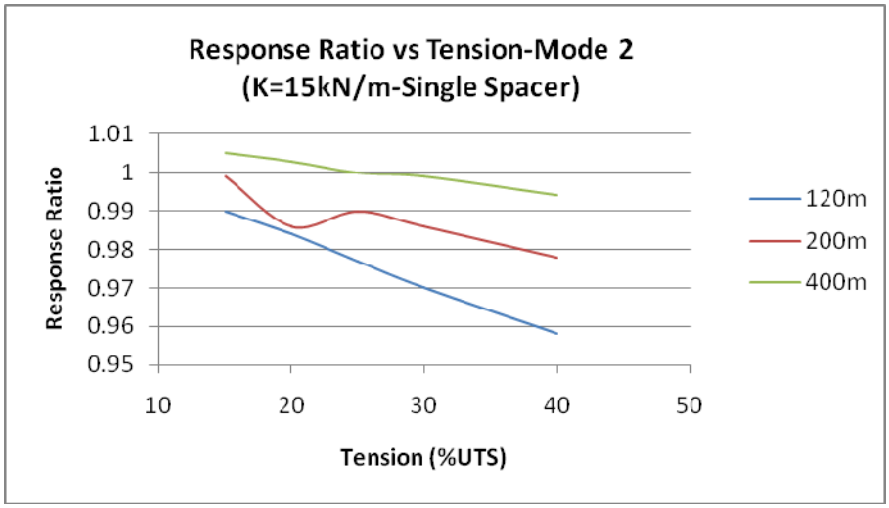

Figure 7.1-6, Plot of Response Ratio vs Tension-Mode 2 (K=15kN/m-Single Spacer).

As seen from the above plots, the same trend as with mode 5 is experienced in the second mode of vibration. However as the span is increased the effect of the spacer is seen to be reduced. This reduction is seen in figure 7.1-6; in the 400m span at a tension of 40 UTS, the Response Ratio is much close to 1.

Figure 7.1-7 shows the appearance of the assembly in the Abaqus output visualization.

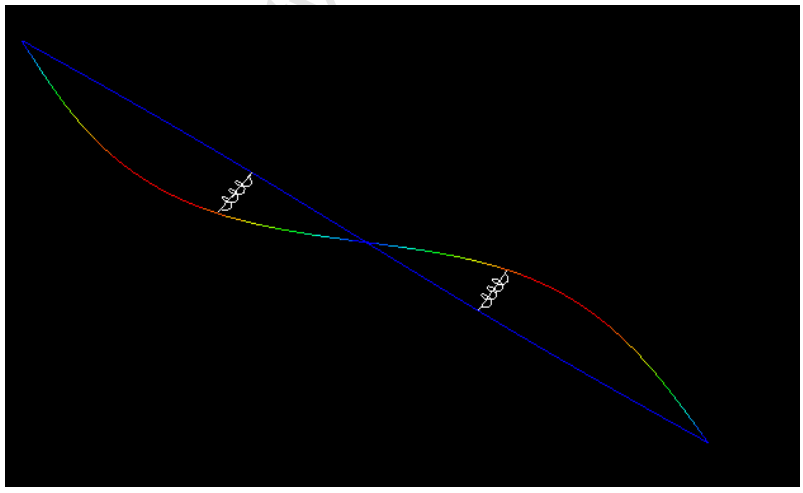

Figure 7.1-7, Two spacers represented in the output visualization-Mode 2 (200m-span).

The following plots consider two spacers along the conductor. Here the third mode is the principal mode that changes due to a change in the spacer stiffness. The following plots enable us to analyse the conductor behavior for this particular mode.

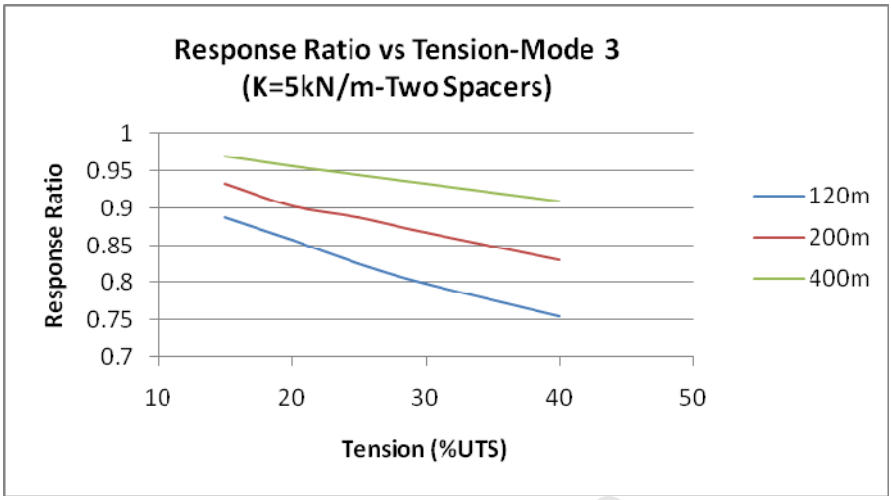

Figure 7.1-8, Plot of Response Ratio vs Tension-Mode 3 (K=5kN/m-Two Spacers).

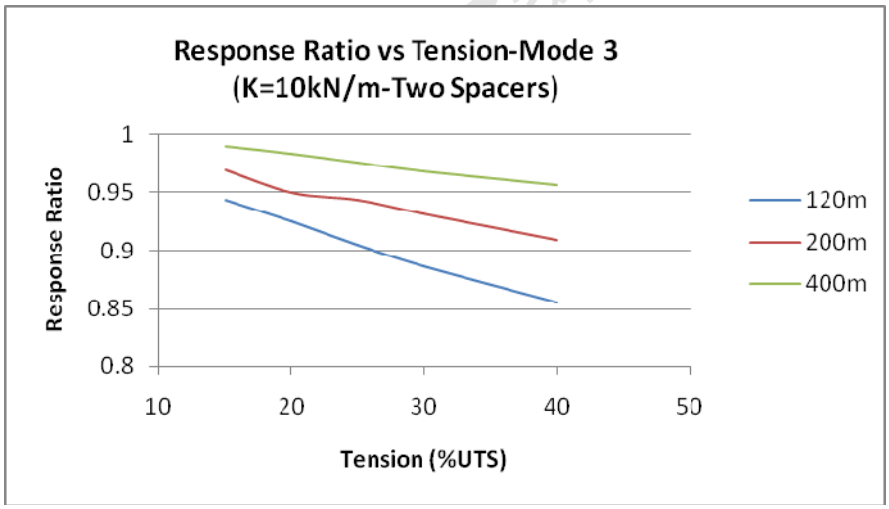

Figure 7.1-9, Plot of Response Ratio vs Tension-Mode 3 (K=10kN/m-Two Spacers).

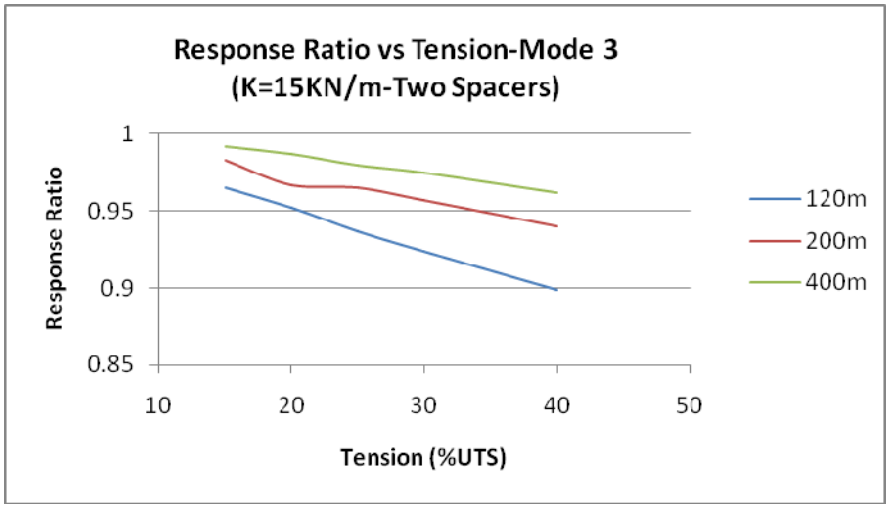

Figure 7.1-10, Plot of Response Ratio vs Tension-Mode 3 (K=15kN/m-Two Spacers).

Figure 7.1-8 to figure 7.1-10 show a similar trend with that obtained for the second and fifth modes of vibration. They seem to show that as the span is increased the effect of the spacers becomes less and less pronounced and also as the stiffness was increased the effectiveness of the spacers became less. After having observed this the number of spacers on the line was increased, and according to the results in table 6.4-10 to 6.4-12 it is seen that the optimal placement is achieved as one significantly increases the spacers.

Placing three spacers along the span results in the following plots: as seen in table 6.6-3, the fourth and fifth modes are the ones which show a change in vibration with the change in stiffness.

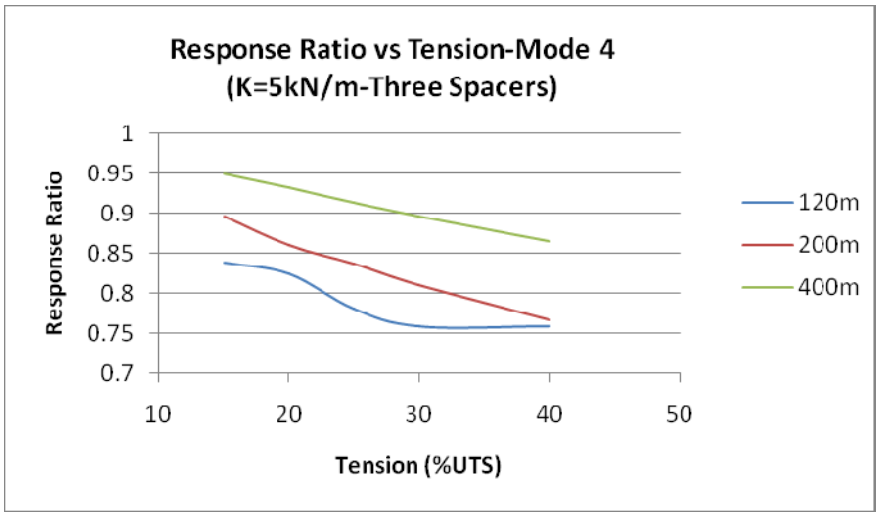

Figure 7.1-11, Plot of Response Ratio vs Tension-Mode 4 (K=5kN/m-Three Spacers).

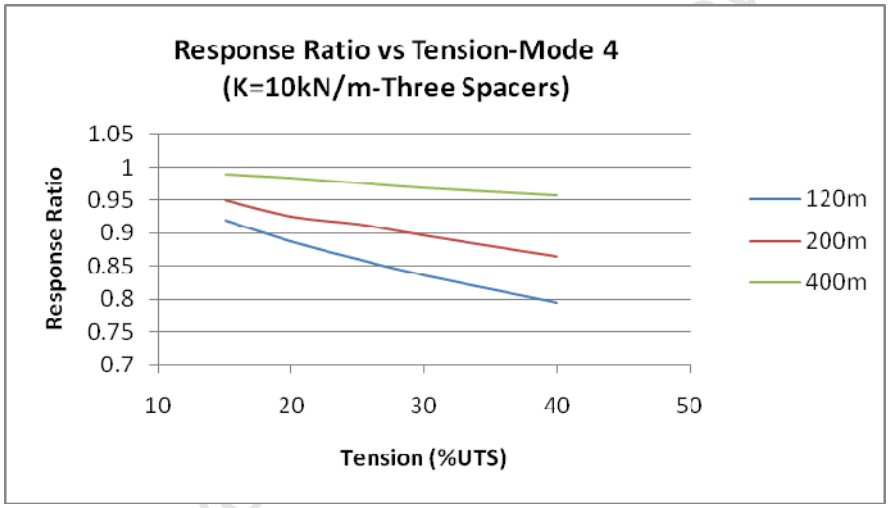

Figure 7.1-12, Plot of Response Ratio vs Tension-Mode 4 (K=10kN/m-Three Spacers).

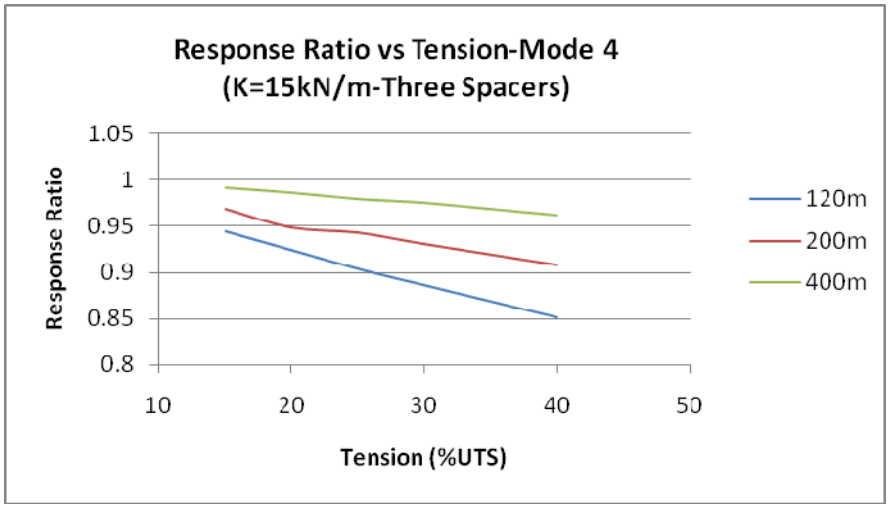

Figure 7.1-13, Plot of Response Ratio vs Tension-Mode 4 (K=15kN/m-Three Spacers).

The above plots (figure 7.1-11 to 7.1-13) show the response ratio plotted against the tension in the conductor. This is only for the fourth mode because the first mode through to the third did not show any change in the frequency as the stiffness was varied.

The following plots show the corresponding behavior for the fifth mode.

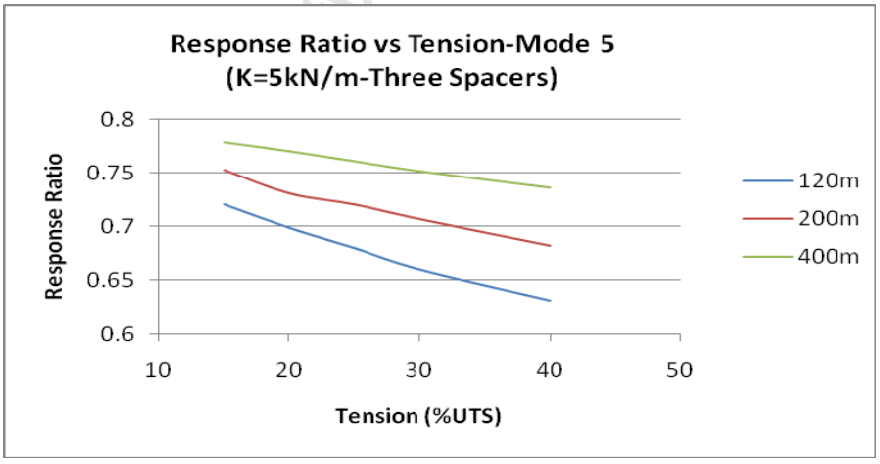

Figure 7.1-14, Plot of Response Ratio vs Tension-Mode 5 (K=5kN/m-Three Spacers).

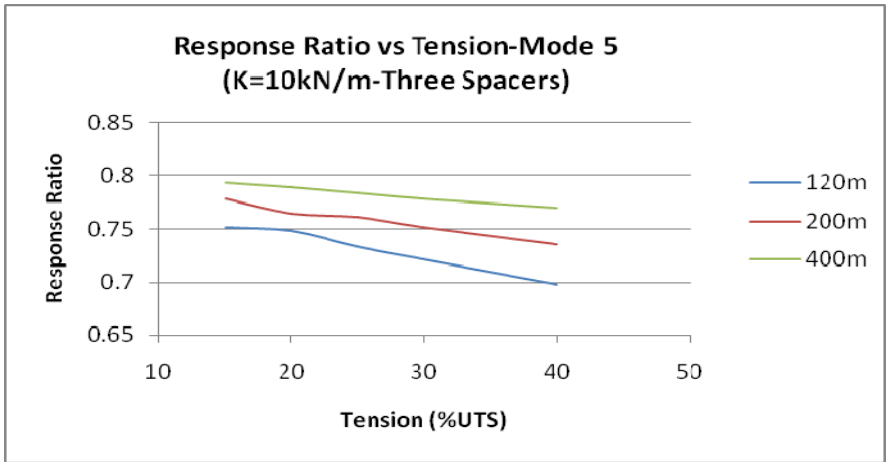

Figure 7.1-15, Plot of Response Ratio vs Tension-Mode 5 (K=10kN/m-Three Spacers).

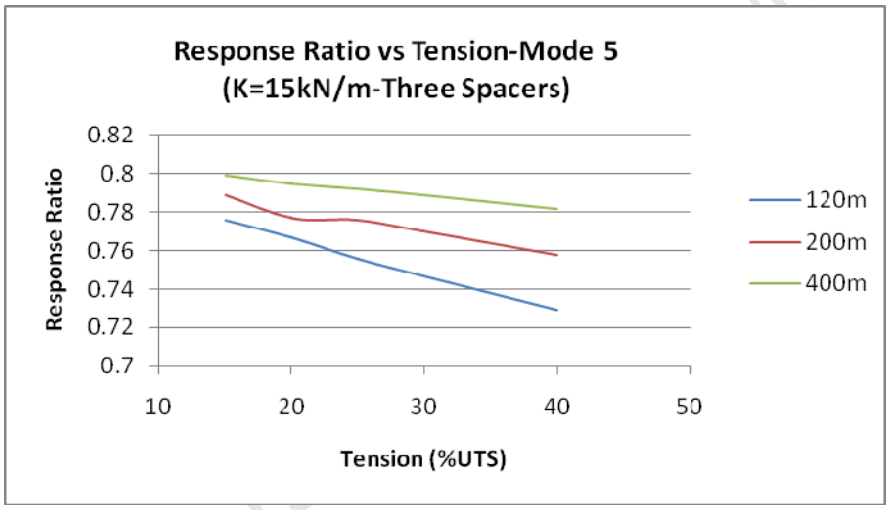

Figure 7.1-16, Plot of Response Ratio vs Tension-Mode 5 (K=15kN/m-Three Spacers).

It is seen however that as the span of the conductors was increased and the number of spacers left unchanged at three this led to a rather unnoticeable effect of the spacers. This led to a further increase in the number of spacers and this eventually resulted in a somewhat optimal placement of dampers as seen in tables 6.4-10 through to 6.4-12. In the table below we see how the spacer stiffness affected the frequency of vibration for each given span.

Table 7.1-1, Frequencies obtained with three spacers @ 20% UTS.

Modes	Frequency (Hz)								
	120m			200m			400m		
	5kN/m	10kN/m	15kN/m	5kN/m	10kN/m	15kN/m	5kN/m	10kN/m	15kN/m
1	0.54	0.54	0.54	0.32	0.32	0.32	0.16	0.16	0.16
2	1.09	1.09	1.09	0.65	0.65	0.65	0.32	0.32	0.32
3	1.63	1.63	1.63	0.98	0.98	0.98	0.49	0.49	0.49
4	1.71	1.91	1.99	1.11	1.20	1.23	0.61	0.62	0.63
5	1.88	2.01	2.06	1.18	1.24	1.26	0.62	0.63	0.64

As seen in the table above, the frequencies of the 400m span representing the fourth and fifth mode are almost the same showing that as the span is increased the effect of the spacers on the frequency of vibration is greatly reduced. This observation however led to the increasing of the spacers and graphs are plotted to show the behavior of the number of spacers to the frequency of the system for the various spans.

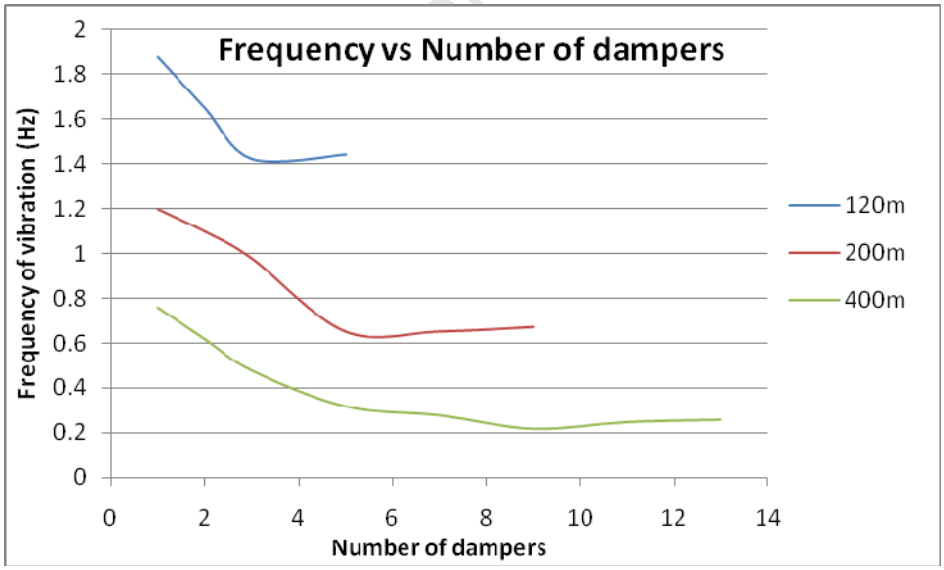

Figure 7.1-17, Plot of frequency against number of dampers (K=5kN/m, C=0.2kNs/m)

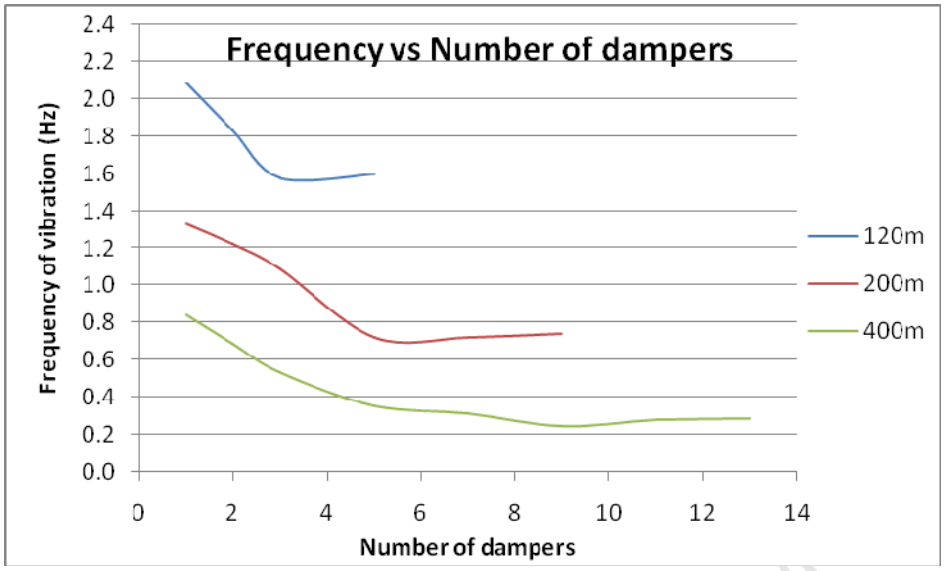

Figure 7.1-18, Plot of frequency against number of dampers (K=10kN/m, C=0.6kNs/m)

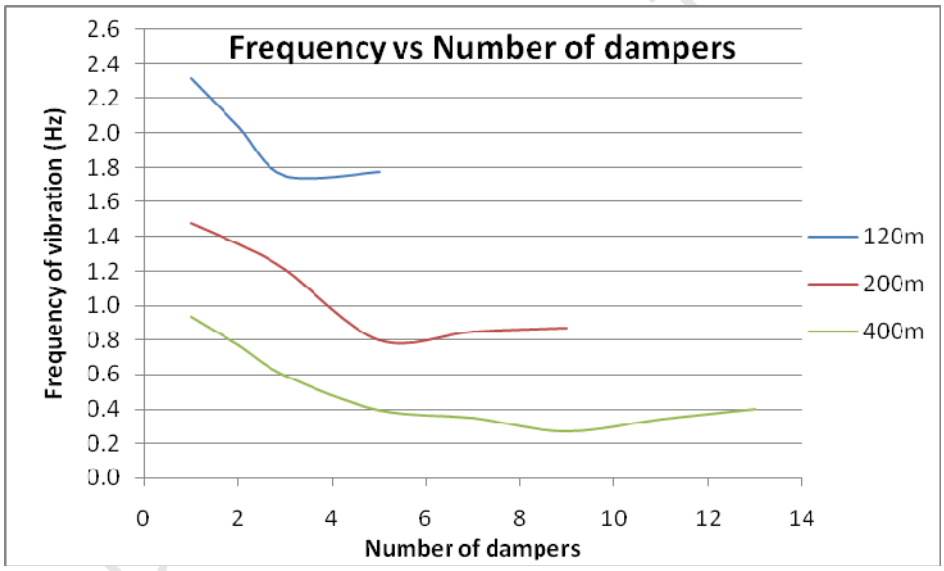

Figure 7.1-19, Plot of frequency against number of dampers (K=15kN/m, C=0.8kNs/m)

The above plots figure 7.1-17 to 7.1-19 show how the frequency of vibration of a particular span varies with the number of dampers placed on the line given the specific damper properties, mainly stiffness and damping coefficient. These results are taken and one has to relate them with the analytical genetic algorithm that we came up with earlier. The brief comparison of the two approaches is done and a conclusion is reached. This conclusion is given in Chapter 7.3 and also in chapter 8.

7.2 Explaining the cost functions

Considering the 120m span it is seen from table 6.4-10 that four different spacers were selected. The first case was the case with no spacers and here the best cost function was found to be $0.789068ms^{-2}$. This cost function was used with the other cost functions obtained by placing 1, 2, 3 and 5 spacers, resulting in the reduction of the cost function. The percentage reduction as compared to the case with no dampers was found to be 55.07%, 56.74%, 59.72% and 57.86% for the 1, 2, 3, and 5 spacers respectively. It is then noted that the best cost function is 59.72%. The trend shown with the placement of the spacers along the line is similar to that seen in figures 7.1-17 through to 7.1-19.

For the 200m span it is observed from table 6.4-11 that selecting six spacers we get a similar trend as that seen for the 120m span. For the 200m span however the best cost function is found to be 59.90%. Results from figure 7.1-17 to figure 7.1-19 gives a comparable basis for these findings. The best cost function is found with five spacers having been placed on the line, this shows a consistence in the distance of separation of these spacers.

Finally looking at the 400m span it is seen from table 6.4-12 that there is a reasonable reduction in the cost function at each addition of a spacer. This is so up to a point when this becomes a minimum and any additional spacer being added becomes redundant. The reduction in the cost function is however found to be 59.32%. As observed for the 120m span and the 200m span, it is quite clear that a similar trend is also seen for the 400m span. Comparing these findings with figure 7.1-17 through to 7.1-19, it is seen that the behavior resulting from the genetic algorithm analysis is similar to that found using the numerical analysis.

7.3 Conclusion

From the results discussed in this chapter it can however be concluded that the stiffness of the spacers plays a vital role in as far as the frequency of the conductors is concerned. This is seen in table 7.1-1 above, it can also be argued that as the stiffness of the spacer is increased, the damping effect of the conductor is reduced, as seen by the reduction in the frequencies.

Placing three spacers along the span did not change the first three vibration modes of the conductors but did affect the fourth and the fifth mode. Also by placing one spacer along the span resulted in the excitation of the second and fifth modes. Contrary to the above observation placing two spacers on the span resulted in the excitation of the third mode only.

Important to note however when the spacers are increased is that their effect is to reduce the frequency up to a point when their effect is negligible and applying any more dampers is ineffective. This fact is seen by plots in figure 7.1-17 to 7.1-19, here the graphs show a reduction in frequencies up to a point where the reduction in frequency becomes unnoticeable

The introduction of the cost function has dealt so much in coming up with an effective tool of optimally placing the spacers. As seen in tables 6.4-10 to 6.4-12, the reduction in the cost function is seen to be about 60% and with this the algorithm becomes very powerful in giving the design engineer a guide to the number of spacers one has to deploy on the transmission line.

The following chapter gives design recommendations and conclusions based on the findings undertaken in this study.

8.0 MAIN CONCLUSION AND DESIGN RECOMMENDATIONS

The first objective was to establish a suitable form of analytical equations to describe the motion of a conductor induced to vibrations. As seen from chapter four and five, expressions were formulated describing the bundled cables vibration problem and the solutions are also given in detail. Establishing the solutions to these expressions met the second objective which was to come up with the relevant solutions that give a description of frequencies and mode shapes of the conductor vibration problem.

The parametric study carried out shows the behavior of spacers along the span and meets the last objective of the study. The previous chapter gave a brief discussion of the results and it is quite apparent from the results obtained that the use of transmission line spacers gives reasonable reductions in conductor vibrations. However, the approach of modeling undertaken gives room for further advancement. Wind as an excitation force can be modeled using computational fluid dynamics and this can be done by using other powerful modeling software.

It is also seen, however that as the span of the conductors was increased this led to a rather lesser effectiveness of the spacers. It is however recommended that the design engineers can however limit the span according to the variation in the level of vibrations of the conductors. Were it is difficult to limit the span, like in river crossings and mountainous areas then one has to increase the spacers on the line accordingly.

The rigid spacer stiffness is a fundamental parameter in the design of the spacers and it is also recommended to change the spacer design and vary the stiffness by also considering the use of flexible spacers or other spacers discussed hereinbefore in the literature.

As seen from the literature, one can also opt to consider including more cables to the bundle, thus the stiffness of the bundle as a whole is increased and thus cable failure is greatly reduced.

Damper placement still remains of fundamental importance in the design of transmission lines as seen in the effect it has on the frequency of vibration of the system of bundled conductors. The introduction of the cost function has helped greatly in coming up with optimally placed spacers.

The reduction of the cost function was seen to be around 60% as compared to the case with no spacers.

In this study the spacers were placed at a spacing ranging from 40m to 60m for the 120m span, from 50m to 100m for the 200m span and from 100m to 200m for the 400m span. According to (Stanford G, 2003) their recommended spacing is 45m for the maximum end span length and 55m for the maximum sub-span length. These ranges compared fairly well with the spacer spacing used in this study. As seen also from the cost function genetic algorithm, the 120m, 200m and 400m spans gave an optimal spacing of 40m, 40m and 44m respectively.

Having met the objectives of the study, it is of paramount importance to make suggestions for future study by highlighting specific areas were this study can be perfected and be best tuned to the relevant industries. The following chapter deals with the recommendations for future work.

9.0 RECOMMENDATIONS FOR FUTURE WORK

It is highly recommended to approach the conductor vibration problem, by also including experimental work. Live electrical transmission line tests can be carried out by placing vibration monitoring devices on the test span. However these are very expensive and time consuming, but with funding available and time not an issue, these live line tests can prove very helpful and reliable in contributing relevant information to the conductor vibration problems.

It is recommended in the future to consider wind tunnel tests, as a means of assessing the wind force acting on the conductors. These also like field tests require a lot of input in terms of funding but can give reliable results to the design engineer and these can also be validated through numerical and analytical models. In this study wind tunnel testing could have been carried out in the vibration research and testing centre at the University of KwaZulu Natal but the testing rig required a couple of modifications to suite the research problem, which also called for much funding and time. It was then impossible to finally carry out these tests due to the issue of time and funding.

Varying a multiple number of parameters can best be solved by numerical analysis (McLure 2003). From the above statement it is recommended to conduct research directed on developing software to specifically deal with the cable vibration problem. Parameters of concern will be conductor type, spacer stiffness/damping value, conductor span, span tensile force, number of conductors in bundle and the support boundary conditions. The above parameters can thus be designed to act as direct input into the cable vibration analysis software.

In as far as the cost function genetic algorithm is concerned, it will be best to have other genetic algorithms to compare with and this can be developed in further research. Also improved computer modeling is of structural joint connections based on hysteresis tests is an area to pursue further.

REFERENCES:

1. ADINA R&D Inc. (2000). *Automatic Dynamic Incremental Nonlinear Analysis* (ADINA) Theory and Modeling Guide 2000. Report ARD 00-7, Watertown, MA.
2. Bartoli, G., Cluni. F, Gusella, V., and Procino. L. (2006). *Dynamics of cable under wind action: Wind tunnel experimental analysis*. Journal of Wind Engineering and Industrial Aerodynamics 9, pp 259-273.
3. Bate, E. & Callow, J. (1934). *The quantitative determination of the energy involved in the vibration of cylinders in an air stream*. Transactions IEE (Australia) XV, 149-162.
4. Bathe K.J. (1996). *Finite element procedures*. Upper Saddle River, NJ: Prentice-Hall.
5. Belloli, M., Collina, A., and Resta, F. (2006). *Cables vibration due to wind*, Politecnico di Milano O.I.T.A.F. SEMINAR Grenoble 27 April 2006.
6. Berggren, L. (1992). *Energy take-out from a wave energy device*. Report series A:23, Department of Hydraulics, Chalmers University of Technology, Goteborg, Sweden.
7. Bishop, R. E. D. and Johnson, D. C. (1960). *The Mechanics of vibration*. Cambridge: Cambridge University Press.
8. Bjerkan, L and Lillevik, O. (2004). *Measurements on Aeolian Vibrations on a 3km Fjord crossing with fibre-optic bragg grating sensors*, SINTEF, Trondheim, Norway
9. Blevins, R. D. (1977). *Flow-Induced* V*ibrations*. New York: Van Nostrand Reinhold.
10. Boyce, W. E. and DiPrima, R.C. (1997). *Elementary differential equations and boundary value problems.* New York, Wiley Publishers.
11. Brika, D. and Laneville, A. (1993). *Vortex-induced vibrations of a long flexible circular cylinder*. Journal of Fluid Mechanics 250, 481-508.
12. Carrier, G. F. (1949). *Quarterly Journal of Applied Mathematics*, 7:97-101.
13. Chikwedu, S. C., and Kevorkian, J. (1972). *Journal of Applied Mathematics*. Society of Industrial and Applied Mathematics, 22:235-258.
14. CiGRE. (1999). *Guidelines to fittings for optical cables to transmission lines*. Technical Procedures. Cigre SC22.
15. Claren, R. and Diana, G. (1969). *Mathematical Analysis of Transmission line Vibration*. IEEE Transactions on power apparatus and systems, Vol PAS-88, No. 12.
16. Clough, R.W., and Penzien, J. (1975). *Dynamics of structures*. McGraw Hill, NY.

17. Davenport A.G and Loredo Souza A.M. (1998). *The effects of high winds on transmission lines.* Journal of Wind Engineering and Industrial Aerodynamics, 74-76, 987-994.
18. Diana, G. and Falco, M. (1971). *On the forces transmitted to a vibrating cylinder by a blowing fluid*. Meccanica 6, 9-22.
19. EPRI (Electric Power Research Institute). (1979). *Transmission line reference book; wind induced conductor motion*. Project 792, Palo Alto, California.
20. Farquharson,F. B. and McHugh, R. E. (1956). *Wind tunnel investigation of conductor vibration with use of rigid models*. Transactions AIEE, Power Apparatus and Systems 75, 871-878.
21. Hagedorn, P. (1982). *On the Computation of Damped Wind Excited Vibrations of Overhead Transmision Lines.* Journal of Sound and Vibration, **83**(2), pp 253-271.
22. Hagedorn, P., M. Schafer, S. Meynen, H. Verma (2004). *On the numerical simulation of vortex-induced vibrations of oscillating conductors.*
23. Hardy, C. (1990). *Analysis of self-damping characteristics of stranded cables in transverse vibrations*. CSME Mechanical Engineering Forum.
24. Hearnshaw, D. (1974). *Spacer dampers performance-a function of in-span positioning*. IEE Transactions. PAS, v. 93 no.5, 1298-1309.
25. Inman, D. J. (2001). Enginering Vibration. 2nd Edition, Upper Saddle River, NJ: Prentice Hall International.
26. Irvine, H. M., and Caughey, T. K. (1974). *The Linear theory of free vibrations of a suspended cable.* Proceedings of the royal society of London, series A, vol 341, 229-315.
27. Irvine, H. M., and Griffin, J. H. (1976). *On the Dynamic response of a Suspended Cable*. International Journal of Earthquake Engineering structural Dynamics, **4**:389-402.
28. Irvine, H. M. (1978). *Free Vibrations of Inclined Cables*. ASCE, Journal of the structural division, vol 104, No ST2, pp343-347.
29. Irvine, H. M. (1981). *Cable Structures*. MIT Press, Cambridge.
30. Jamaleddine A, McClure G, Rousselet J, Beauchemin R. (1993). *Simulation of ice-shedding on electrical transmission lines using ADINA.* Computer Structures, 47(4/5):523–536.
31. Kanev, S., F. Weber, and Verhaegen, M. (2006). *Experimental validation of o finite-element model updating procedure*. Journal of Sound and Vibration 300, pp 394-413.

32. Lapointe M. (2002). *Dynamic analysis of a power line subjected to longitudinal loads*, ME thesis, McGill University, Montreal, Canada.
33. Macdonald, R., Pon, C. J., Havard, D. G. and Currie, I. G. (1989). *Aeolian vibration excitation of Bundle Conductors*, Volumes I and II. Canadian Electrical Association Report, Montreal, Canada.
34. McClure G. (1989). *Dynamic correlations in transmission lines, as a means of transport and breaking of cables*. PhD thesis, Electrical Polytechnic of Montreal, Montreal, Canada.
35. McClure G, Lapointe, M. (2003). *Modeling the structural dynamic response of overhead transmission lines* Computers and Structures **81,** 825–834.
36. Meirovitch, L. (1975). *Elements of Vibration Analysis*. New York: McGrawHill, Chapter 10.
37. MIT Video Course. (1986). *Finite Element Procedures for Solids and Structures-Nonlinear Analysis. The two-noded truss element-Updated Lagrangian Formulation*, tape 8. Massachusetts Institute of Technology, Center for Advanced Engineering Study.
38. Mocks Lotar. (1984). *Damping of high-voltage overhead line conductor vibrations*, Berlin: VDE VERLAG.ETZ Report; 15e.
39. Nefzger, J. (1933) *Disturbances from mechanical vibrations of conductor lines and remedy methods.* CIGRE Report No. 126.
40. Palm III. (2006). *Mechanical Vibrations*, University of Rhode Island. John Wiley and Sons, Inc
41. Parkinson, G. V., Feng, C. C. and Ferguson, N. (1968). *Mechanisms of vortex-excited oscillation of bluff cylinders*. *Symposium on Wind Effects on Buildings and Structures*, Loughborough University of Technology, Paper No. 27.1.
42. Pugsley, A.G. (1949). *On the Natural Frequency of Suspension chains.* Quarterly Journal of Mechanics and Applied Mathematics. Vol 2, Part 4, pp 412-418.
43. Ramberg, S. E., and Griffin, O. M. (1977). *Proceeding of the Journal of Structural Division*. ASCE, 103:2079-2092.
44. Roshan Fekr. M. and McClure G. (1998). *Numerical modelling of the dynamic response of ice-shedding on electrical transmission lines*. Atmos Res, 46:1–11.
45. Routh, E. J. (1955). *Advanced Dynamics of rigid bodies*, Dover, NY, 6th edition.

46. Sarpkaya, T. (1979). *Vortex-induced oscillations: a selective review*. Journal of Applied Mechanics **46**, 241-258.
47. Saxon, D. S., and Cahn, A. S. (1953) *Modes of vibration of a suspended chain*. Quarterly Journal of Mechanical Applied Mathematics. Vol 6:273-285.
48. Simpson, A. (1972). *Determination of the natural frequencies of multiconductor overhead transmission lines.* Journal of Sound and Vibration **20** (4), 417-449.
49. Simpson, A and Sembi P.S. (1984). *On the use of exact modal analysis techniques in the design of damping devices for multi-conductor overhead power lines, Part 1: The Control of Aeolian Vibration*, Journal of Sound and Vibration **97** (3), 357-385.
50. Stanford, G., Naidoo, A., Hill, B., and Mavhungu, N. (2003). Eskom Distribution Standard Part 6: *Sub-Transmission Lines*; Section 4: Vibration Dampers.
51. Starossek, U. (1994). *Cable Dynamics-A Review*. Structural Engineering International, vol 3/94.
52. Steidel, Jr., R. F. (1989). *An Introduction to Mechanical vibrations*, 3rd Edition. New York: John Wiley & Sons.
53. Stockbridge, G. H. (1925). *Overcoming Vibration in Transmission Cables*. Electrical World, vol. **86** issue 26, pages 1304-1305.
54. Strouhal, V., UG. (1878). *A special kind of sound excitement*. Journal of Physics and Chemistry, NewSeries, Vol. 5, 216-251.
55. Szabo, I. (1979). *History of mechanical Principles*. Birkhauser Publishing Company, 2nd edition.
56. Tabatabai, H., Mehrabi, A. B. (1999). *Tuned Dampers and Cable Fillers for Suppression of Bridge Stay Cable Vibrations*. IDEA program final report, Construction Technology Laboratories, Inc., Skokie, IL.
57. Thomson, W.T. (1965). *Vibration and Applications*. Prentice-Hall Englewood Cliffs, NJ.
58. Vecchiarelli, J., Currie, I. G., and Havard, D. G. (1998). *Computational analysis of aelian conductor vibration with a stockbridge-type damper*, Journal of Fluids and Structures (2000) **14,** 489-509 Department of Mechanical and Industrial Engineering, University of Toronto.
59. Wang, H.Q., Miao, J.H., Luo, J. H., Huang, F., and Wang, L. G. (1997). *The free vibration of long-span transmission line conductors with dampers*. Journal of Sound and Vibration 208(4), pp 501-516.

60. Wenjie, Wu. (2006). *Theoretical and experimental study on cable vibration reduction with TMD-MR damper*. Doctor of philosophy dissertation. Graduate Faculty of the Lousiana State University and Agricultural and Mechanical College.
61. Zetterholm D. (1960). *Vibration of conductors in overhead transmission lines.* Broderna Lagerstrom AB, Stockholm.
62. Zhang, H., Soong, T., Mahmoodi, P. (1989), "*Seismic response of steel frame structures with added viscoelastic dampers*", Earthquake Engineering and Structural Dynamics, No.18, pp.389-96.

APPENDIX A

INPUT FILES

1. ABAQUS
2. MATLAB
3. EXCELL FILES
4. CONDUCTOR PROPERTIES

1. ABAQUS INPUT FILE

Abaqus Input File For 120m Undamped Span.

```
*Heading
 Natural Frequencies for 120m span @ 15% UTS.
** Job name: Natural-Frequencies Model name: Model-1
*Preprint, echo=NO, model=NO, history=NO, contact=NO
**
** PARTS
**
*Part, name="ASCR Conductor"
*End Part
**
**
** ASSEMBLY
**
*Assembly, name=Assembly
**
*Instance, name="ASCR Conductor-1", part="ASCR Conductor"
*Node
      1,        -30.,          5.,          0.
      2,       -29.5,          5.,          0.
      3,        -29.,          5.,          0.
      4,       -28.5,          5.,          0.
      .
      .
      .
    238,        88.5,          5.,          0.
    239,         89.,          5.,          0.
    240,        89.5,          5.,          0.
    241,         90.,          5.,          0.
*Element, type=T3D2
 1,  1,  2
 2,  2,  3
 3,  3,  4
 4,  4,  5
 .
 .
 .
238, 238, 239
239, 239, 240
240, 240, 241
*Nset, nset=_PickedSet2, internal, generate
  1,  241,    1
*Elset, elset=_PickedSet2, internal, generate
  1,  240,    1
** Region: (Truss Element:Picked)
*Elset, elset=_PickedSet2, internal, generate
```

```
  1,  240,    1
** Section: Truss Element
*Solid Section, elset=_PickedSet2, material="Aluminium Steel Reinforced"
0.00045503,
*End Instance
**
*Instance, name="ASCR Conductor-2", part="ASCR Conductor"
        0.,          0.,         0.42
*Node
      1,        -30.,          5.,          0.
      2,       -29.5,          5.,          0.
      3,        -29.,          5.,          0.
      4,       -28.5,          5.,          0.
      5,        -28.,          5.,          0.
      6,       -27.5,          5.,          0.
      .
      .
      .
    238,        88.5,          5.,          0.
    239,         89.,          5.,          0.
    240,        89.5,          5.,          0.
    241,         90.,          5.,          0.
*Element, type=T3D2
 1,  1,  2
 2,  2,  3
 3,  3,  4
 .
 .
 .
238, 238, 239
239, 239, 240
240, 240, 241
*Nset, nset=_PickedSet2, internal, generate
  1,  241,    1
*Elset, elset=_PickedSet2, internal, generate
  1,  240,    1
** Region: (Truss Element:Picked)
*Elset, elset=_PickedSet2, internal, generate
  1,  240,    1
** Section: Truss Element
*Solid Section, elset=_PickedSet2, material="Aluminium Steel Reinforced"
0.00045503,
*End Instance
**
*Nset, nset=_PickedSet7, internal, instance="ASCR Conductor-1"
 241,
*Nset, nset=_PickedSet7, internal, instance="ASCR Conductor-2"
 241,
```

```
*Nset, nset=_PickedSet8, internal, instance="ASCR Conductor-1"
 1,
*Nset, nset=_PickedSet8, internal, instance="ASCR Conductor-2"
 1,
*Nset, nset=_PickedSet9, internal, instance="ASCR Conductor-1"
 241,
*Nset, nset=_PickedSet9, internal, instance="ASCR Conductor-2"
 241,
*End Assembly
**
** MATERIALS
**
*Material, name="Aluminium Steel Reinforced"
*Density
 3344.32,
*Elastic
 6.45e+11, 0.33
** ----------------------------------------------------------------
**
** STEP: Apply a Preload
**
*Step, name="Apply a Preload", nlgeom=YES
Apply a Preload to get the required sag.
*Static
1., 1., 1e-05, 1.
**
** BOUNDARY CONDITIONS
**
** Name: BC-1 Type: Symmetry/Antisymmetry/Encastre
*Boundary
_PickedSet8, PINNED
** Name: BC-2 Type: Symmetry/Antisymmetry/Encastre
*Boundary
_PickedSet9, XASYMM
**
** LOADS
**
** Name: Preload   Type: Concentrated force
*Cload
_PickedSet7, 1, 18800.
**
** OUTPUT REQUESTS
**
*Restart, write, frequency=0
**
** FIELD OUTPUT: F-Output-1
**
*Output, field, variable=PRESELECT
```

```
**
** HISTORY OUTPUT: H-Output-1
**
*Output, history, variable=PRESELECT
*End Step
** ----------------------------------------------------------------
**
** STEP: Extract Frequencies
**
*Step, name="Extract Frequencies", perturbation
Extract the required Frequencies and Mode Shapes
*Frequency, eigensolver=Lanczos, acoustic coupling=on, normalization=displacement, number
interval=1, bias=1.
, , 2., , ,
**
** OUTPUT REQUESTS
**
*Restart, write, frequency=0
**
** FIELD OUTPUT: F-Output-2
**
*Output, field, variable=PRESELECT
*End Step
```


Abaqus Input File For 120m Damped Span with two spacers of 10kN/m Stiffness.

```
*Heading
 Natural Frequencies for 120m span @ 15% UTS with two Spacers of 10kN/m Stiffness.
** Job name: Natural-Frequencies Model name: Model-1
*Preprint, echo=NO, model=NO, history=NO, contact=NO
**
** PARTS
**
*Part, name="ASCR Conductor"
*End Part
**
**
** ASSEMBLY
**
*Assembly, name=Assembly
**
*Instance, name="ASCR Conductor-1", part="ASCR Conductor"
*Node
     1,        -30.,          5.,          0.
     2,   9.99600029,          5.,          0.
     3,   49.9980011,          5.,          0.
```

```
      .
            .
            .
   238,   87.9999008,          5.,          0.
   239,   88.4999237,          5.,          0.
   240,   88.9999466,          5.,          0.
   241,   89.4999771,          5.,          0.
*Element, type=T3D2
 1,  1,  5
 2,  5,  6
 3,  6,  7
 .
 .
 .
238, 239, 240
239, 240, 241
240, 241,   4
*Nset, nset=_PickedSet2, internal, generate
  1,  241,    1
*Elset, elset=_PickedSet2, internal, generate
  1,  240,    1
** Region: (Truss Element:Picked)
*Elset, elset=_PickedSet2, internal, generate
  1,  240,    1
** Section: Truss Element
*Solid Section, elset=_PickedSet2, material="Aluminium Steel Reinforced"
0.00045503,
*End Instance
**
*Instance, name="ASCR Conductor-2", part="ASCR Conductor"
        0.,          0.,         0.42
*Node
      1,        -30.,          5.,          0.
      2,   9.99600029,          5.,          0.
      3,   49.9980011,          5.,          0.
      .
            .
            .
   238,   87.9999008,          5.,          0.
   239,   88.4999237,          5.,          0.
   240,   88.9999466,          5.,          0.
   241,   89.4999771,          5.,          0.
*Element, type=T3D2
 1,  1,  5
 2,  5,  6
 3,  6,  7
 .
 .
```

```
.
238, 239, 240
239, 240, 241
240, 241,   4
*Nset, nset=_PickedSet2, internal, generate
  1,  241,    1
*Elset, elset=_PickedSet2, internal, generate
  1,  240,    1
** Region: (Truss Element:Picked)
*Elset, elset=_PickedSet2, internal, generate
  1,  240,    1
** Section: Truss Element
*Solid Section, elset=_PickedSet2, material="Aluminium Steel Reinforced"
0.00045503,
*End Instance
**
*Nset, nset=_PickedSet7, internal, instance="ASCR Conductor-1"
 4,
*Nset, nset=_PickedSet7, internal, instance="ASCR Conductor-2"
 4,
*Nset, nset=_PickedSet8, internal, instance="ASCR Conductor-1"
 1,
*Nset, nset=_PickedSet8, internal, instance="ASCR Conductor-2"
 1,
*Nset, nset=_PickedSet9, internal, instance="ASCR Conductor-1"
 4,
*Nset, nset=_PickedSet9, internal, instance="ASCR Conductor-2"
 4,
*Element, type=SpringA, elset=Springs/Dashpots-1-spring
1, "ASCR Conductor-2".2, "ASCR Conductor-1".2
*Spring, elset=Springs/Dashpots-1-spring

10000.
*Element, type=SpringA, elset=Springs/Dashpots-2-spring
2, "ASCR Conductor-2".3, "ASCR Conductor-1".3
*Spring, elset=Springs/Dashpots-2-spring

10000.
*End Assembly
**
** MATERIALS
**
*Material, name="Aluminium Steel Reinforced"
*Density
 3344.32,
*Elastic
 6.45e+11, 0.33
** ----------------------------------------------------------------
```

```
**
** STEP: Apply a Preload
**
*Step, name="Apply a Preload", nlgeom=YES
Apply a Preload to get the required sag.
*Static
1., 1., 1e-05, 1.
**
** BOUNDARY CONDITIONS
**
** Name: BC-1 Type: Symmetry/Antisymmetry/Encastre
*Boundary
_PickedSet8, PINNED
** Name: BC-2 Type: Symmetry/Antisymmetry/Encastre
*Boundary
_PickedSet9, XASYMM
**
** LOADS
**
** Name: Preload   Type: Concentrated force
*Cload
_PickedSet7, 1, 18800.
**
** OUTPUT REQUESTS
**
*Restart, write, frequency=0
**
** FIELD OUTPUT: F-Output-1
**
*Output, field, variable=PRESELECT
**
** HISTORY OUTPUT: H-Output-1
**
*Output, history, variable=PRESELECT
*End Step
** ----------------------------------------------------------------
**
** STEP: Extract Frequencies
**
*Step, name="Extract Frequencies", perturbation
Extract the required Frequencies and Mode Shapes
*Frequency, eigensolver=Lanczos, acoustic coupling=on, normalization=displacement, number
interval=1, bias=1.
, , 2., , ,
**
** OUTPUT REQUESTS
**
*Restart, write, frequency=0
```

```
**
** FIELD OUTPUT: F-Output-2
**
*Output, field, variable=PRESELECT
*End Step
```

2. MATLAB INPUT FILE

```
function [u, udot, u2dot] = newmark_int(t, p,u0 ,udot0 ,m ,k ,xi ,varargin)
%Newmark's Direct Integration Method
%-------------------------------------------------------------------------
% Integrates a 1-DOF system with mass "m", spring stiffness "k" and damping
% coefficient "xi", when subjected to an external load P(t).
% Returns the displacement, velocity and acceleration of the system with
% respect to an inertial frame of reference.
%
% SYNTAX
%       [u, udot, u2dot] = newmark_int(t,p,u0,udot0,m,k,xi,varargin)
%
% INPUT
%       [t] :       Time Vector             [n,1]
%       [p] :       Externally Applied Load [n,1]
%       [u0]:       Initial Position        [1,1]
%       [udot0]:    Initial Velocity        [1,1]
%       [m]:        System Mass             [1,1]
%       [k]:        System Stiffness        [1,1]
%       [xi]:       System Damping          [1,1]
%       [varargin]: Options
%
% OUTPUT
%       [u]:        Displacement Response   [n,1]
%       [udot]:     Velocity                [n,1]
%       [u2dot]:    Acceleration            [n,1]
%
%  N = number of time steps
%
% The options include changing the value of the "gamma" and "beta"
% coefficient which appear in the formulation of the method. By default
% these values are set to gamma = 1/2 and alpha = 1/4.
%
% EXAMPLE
% To change newmark's coefficients, say to gamma = 1/3 and alpha = 1/5,
% the syntax is:
%       [u, udot, u2dot] = newmark_int(t,p,u0,udot0,m,k,xi, 1/3, 1/5)
%
% if nargin == 7
   disp('Using default values:');
   disp('    gamma = 1/2');
   disp('    beta  = 1/4');
   gam = 1/2;
   beta = 1/4;
else
   if nargin == 9
      beta = varargin{1};
      gam = varargin{2};
```

```
    else
        error('Incorrect number of imput arguments');
    end
end
wn = sqrt(k/m);
wd = 2*xi*wn;

dt = t(2) - t(1);
c = 2*xi*wn*m;

kgor = k + gam/(beta*dt)*c + m/(beta*dt^2);
a = m/(beta*dt) + gam*c/beta;
b = 0.5*m/beta + dt*(0.5*gam/beta - 1)*c;

dp = diff(p);
u = zeros(length(t),1); udot = u; u2dor = u;
u(1) = u0;
udot(1) = udot0;
u2dot(1) = 1/m*(p(1)-k*u0-c*udot0);

for i = 1:(length(t)-1)
    deltaP = dp(i) + a*udot(i) + b*u2dot(i);
    du_i = deltaP/kgor;
    dudot_i = gam/(beta*dt)*du_i - gam/beta*udot(i) + dt*(1-0.5*gam/beta)*u2dot(i);
    du2dot_i = 1/(beta*dt^2)*du_i - 1/(beta*dt)*udot(i) - 0.5/beta*u2dot(i);
    u(i+1) = du_i + u(i);
    udot(i+1) = dudot_i + udot(i);
    u2dot(i+1) = du2dot_i + u2dot(i);
end
```